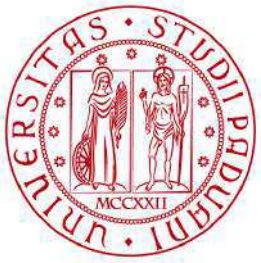

UNIVERSITÀ
DEGLI STUDI
DI PADOVA

Università degli Studi di Padova

Department of Industrial Engineering

Ph. D. COURSE in Industrial Engineering
CURRICULUM: Thermo-mechanical Energy Engineering
XXX Series

An Aerodynamic Method to Design Low-speed Axial Fans with Imposed Diameter and Rotor speed

Coordinator: Prof. Paolo Colombo
Supervisor: eng. Massimo Masi
Co-Supervisor: Prof. Andrea Lazzaretto

Ph.D. stundent: Stefano Castegnaro

Ricordati, quando commenti l'acque, d'allegar prima la esperienza e poi la ragione.

— Leonardo Da Vinci

ABSTRACT

This dissertation treats the aerodynamic design of low-speed axial fans for industrial applications, considering dimensional and/or rotor-speed constraints as eventual additional design requirements.

In the last years, the complexity of the design task and the number of related tools have increased exponentially in turbomachinery, with industrial axial-flow fans making no exception. Recent automated design softwares and optimization routines provide highly efficient fan designs. Regardless of the effectiveness of these computer-based methods however, the variables that mostly affect fan performance and efficiency are still related to the basic primary design choices, as the selection of the axial fan configuration, for instance.

In spite of a long history of axial fans, some basic questions on the aerodynamic design of these machines still do not have a clear and definitive answer in the technical literature. In particular, two major design issues have been identified:

a) the lack of quantitative indications that guide the designer into the selection of the axial fan configuration, among rotor-only, rotor-straightener, preswirler-rotor, and multistage machine;

b) the lack of quantitative information that guide the fan designer into the choice of the suitable span-wise aerodynamic loading distribution (i.e., the design vortex criterion) for the required operation in case of rotor-only axial fans.

According to these needs, a research has been conducted into several aspects of the aerodynamic design of low-speed axial fans. A data-base of fan performance and efficiencies has been collected to provide maps that can guide fan designers into the primary design choices reported at items *a)* and *b)*. The construction of this data-base required the collection of fan data from the available literature and from a dedicated experimental campaign. Most of the fans that have been tested on two ISO 5801 inlet-chamber test rigs are specifically-designed rotor-only prototypes. Therefore, an effective aerodynamic design method has been developed for this widely used type of machine (i.e., for rotor-only axial fans). The method is based on the information resulting from the fan data-base, as well as on a preliminary mean-line performance and efficiency estimation procedure. The *local* (i.e., the velocity field) and *global* (i.e., performance and efficiency) behavior of the resulting geometries have been verified by means of a CFD (Computational Fluid Dynamic) model, before the manufacturing of the prototypes. CFD simulations are run on a simplified model that is particularly appropriate for the industrial requirements of rapidity and accuracy of results. All the necessary information to perform satisfactorily the aerodynamic design

of a rotor-only fan are provided. Most of these indications can be directly extended to design also machines with fixed bladings.

The main results of the investigation are graphs that summarize axial fan performance around the well-known Cordier curve, identifying: *i)* suitable operating areas for each fan configuration, and *ii)* suitable vortex-criteria operating areas in case of rotor-only fans. Theoretical explanations are provided at support of the observed trends. Such information represent simple and quantitative aids to guide fan designers into the primary design choices. In particular, the data show that vane-axial and contra-rotating fans operate at lower specific speeds and diameters with respect to rotor-only ones. Thus, a Cordier-line diagram specific for Rotor-only axial fans relies at higher specific diameters with respect to vane-axial machines. Whether the rotor-only configuration is the only one permitted (for instance due to dimensional constraints), *Forced*-vortex rotors (i.e., with aerodynamic loading distributions that increase towards the blade tip) represent a suitable solution for operations at low specific speeds, relatively large flow-rates and pressure rises. However, the fan efficiency of forced-vortex rotor-only fans is lower than that of rotor-straightener machines operating at the same pressure-rise, making the forced-vortex design solution appropriate in presence of constraints on both the fan axial length, the fan diameter and the rotor speed (for instance, the fans installed on air-conditioner external units).

The scope of the work is providing an aerodynamic design methodology for industrial axial fans. The information reported in this work can be useful for fan designers and manufacturers, as well as for anyone interested in the field of mechanical ventilation.

CONTENTS

LIST OF SYMBOLS

D fan diameter (equal to the casing internal diameter) [m]

v air velocity within a duct; generic velocity [m/s]

q_v volumetric flow-rate [m^3/s]

q heat transfer [$\frac{J}{kg}$]

s blade spacing, $\frac{2\pi \cdot r}{nr_{bl}}$

nr_{bl} number of blades

C_L blade element lift coefficient

C_l isolated airfoil lift coefficient

p_s air static pressure, [Pa]

p_t air total pressure (according to ISO 5801 standard), $p_s + \frac{1}{2}\rho v_m^2$ computed considering the axial velocity pressure only, [Pa]

p_{tt} total pressure (according to the usual fluid-dynamic convention), $p_s + \frac{1}{2}\rho\|\vec{v}\|^2$

Δp_{tt} total-to-total pressure rise, $p_{tt2} - p_{tt1}$ [Pa]

$\Delta p_{tt_{th}}$ inviscid total-to-total pressure rise, [Pa]

Δp_s static pressure rise, $p_{s2} - p_{s1}$, [Pa]

p_f fan pressure (according to ISO 5801 standard), $p_{t2} - p_{t1}$ (with p_t computed considering the axial velocity pressure only), [Pa]

p_{sf} fan static pressure (according to ISO 5801) also named total-to-static pressure, $p_f - p_{df}$ [Pa]

p_{df} fan dynamic pressure (also named fan velocity pressure), $\frac{1}{2}\rho(\frac{q_v}{\frac{\pi D^2}{4}})^2$. p_{df} is computed at the fan exit section, [Pa]

m mass, [kg]

$\dot{m}$ mass of air per second, [kg/s]

r radius, [m]

R fan radius (equal to the duct internal radius), [m]

w generic velocity relative to the blade (within the fan annulus), [m/s]

c generic absolute velocity (within the fan annulus), [m/s]

u generic blade velocity, [m/s]

U blade tip speed (assuming $tc = 0$), ωR [m/s]

c_u swirl velocity in the annulus, [m/s]

v_m, v_a air velocity within a duct or at the fan exit (according to ISO 5801) $\frac{q_v}{\frac{\pi D^2}{4}}$ [m/s]

$y+$ wall dimensionless distance

k,b generic constants

n rotor speed [rpm]

bs blade span [m]

Re Reynolds number

tc tip clearance [m]

tc^* dimensionless tip clearance [m]

rc^* dimensionless root clearance [m]

ch chord length [m]

rc root clearance [m]

T_a shaft torque, [Nm]

T_r impeller torque, [Nm]

F generic force [N]

Re_c Reynolds number based on the chord lenght, $\frac{\rho \cdot w_m \cdot ch}{\mu}$

Re_D Reynolds number based on the fan diameter, $\frac{\rho \cdot (\omega \cdot R) \cdot D}{\mu}$

W work [J];

t time [s].

Greek symbols

α angle of attack with respect to the chord, [°]

β flow angle relative to the blade

$\in$ from set theory: an element belonging to a set

ν hub-to-tip ratio, $\frac{d_h}{D}$

δ specific diameter (computed with the fan pressure p_f)

σ specific speed (computed with the fan pressure p_f)

Δ generic variation

Γ aerodynamic circulation, $s \cdot (c_{u1} - c_{u2})$ $[m^2/s]$

γ sweep angle, $[^\circ]$

ϵ swirl coefficient $\frac{c_u}{c_a}$; coefficient for a finite number of blades (according to Eck, 1964)

η_f fan efficiency (also commonly named *fan mechanical efficiency* or *fan total efficiency*), $\frac{q_v \cdot p_f}{T \cdot \omega}$

ρ mass density $[kg/m^3]$

σ_{bl} blade solidity, $\frac{n r_{bl} \cdot ch}{2\pi \cdot r}$; also specific speed

ξ, stagger angle (angle between the blade element chord and the fan axis) $[^\circ]$

ϕ_p blade positioning angle, $90^\circ - \xi$

Ψ Pressure coefficient

Φ Flow coefficient

Λ Annulus flow coefficient

ω rotational speed $[rad/s]$

μ dynamic viscosity $[Pa \cdot s]$

θ flow deflection, $\beta_1 - \beta_2$, $[^\circ]$

Abbreviations

BE Blade Element

RO rotor-only

RS rotor-straightener

PR preswirler-rotor

PRS preswirler-rotor-straightener

CR contra-rotating

DP Design point

BEP Best Efficiency point

AV arbitrary vortex

FV free vortex, $c_u = \frac{k}{r}$

CS constant swirl, $c_u = const$

RB rigid body, $c_u = k \cdot r$

NFV Non-free-vortex

Subscripts

c refers to the chord (also chamber)

r refers to the blade root

1 rotor inlet

2 rotor outlet

atm atmospheric

cam camber

f referring to the fan pressure (ISO 5801 standard)

sf referring to the fan static pressure (ISO 5801 standard)

fan any parameter referring to the fan

rot any parameter referring to the rotor

r root

ew ending wall of the rig chamber

in fan inlet section

out fan outlet section

n natural (i.e., occurring even in absence of a specific component)

u refers to the tangential direction

a refers to the axial direction

d dynamic

rad refers to the radial direction

m mean, alternatively meridional

MS refers to the mid-span radius

tip refers to the tip radius

h refers to the hub radius

loss losses

Tc Tail-cone

tc due to the tip clearance

th theoric (i.e., inviscid)

tt total-to-total, fluid-dynamic convention (not ISO)

Superscripts

’ first assumed value within an iterative computation

$\overline{x}$ mass-flow averaged parameter

1 INTRODUCTION

This dissertation is aimed toward providing fan designers an aerodynamic procedure to design low-speed single-stage axial fans for industrial applications. Design indications that were not available in previous works on the subject have been included.

Low-speed fans are historically considered "*the stepchild of technology*"[1], and "*the poor relation of turbomachinery*"[2]. With respect to other turbomachines, the aerodynamic research on low-speed fans received minor attention; moreover, it is mainly performed by the industries, thus involving a limited dissemination [1]. As a consequence of this habit, the fan market presents an heterogeneous picture, spanning from accurate aerodynamic design with high efficiency to basic low-efficiency designs. At the same time however, fans also represent the most diffused (i.e., numerous) gas-treating turbomachine and are consequently responsible for a relevant use of energy. In 2011 the consumption of electrical energy related to fans (driven by motors with an electric input power between 125 W and 500 kW) was estimated to be 344 Twh in Europe [3] ($\simeq$ 2% of the overall consumption of the European Union [4]) and is expected to rise up to 560 TWh within 2020 [3]. Some authors, however, suggest that the percentage of energy consumption related to all the fans is higher ($\simeq$ 23% according to Cermak [5]). In front of this massive use of energy and with the increasing attention to environmental problems, in the last years European and American authorities introduced Regulations [3, 6] to impose minimum efficiencies for the machines commercialized within their countries. In Europe these limits have been increased in 2015 [3] and are expected to rise even further in 2020 [7]. These regulations are imposing fan manufacturers a renovation of their offer towards higher efficiency products. Consequently, there is a real current industrial need for effective aerodynamic design methods, to produce fans that operate at high efficiency.

In spite of a long history of aerodynamic design methods for axial fans (first references date back to $\simeq$ 1920 [8, 9]), some inconsistencies and *"grey areas"* on some design aspects were found after performing a comparative study of the most known references on the subject [10]. These *"grey areas"*, together with others reported in the following, indicate that a definitive and comprehensive method of axial-flow fan design is still not available; the geometrical differences among fans featuring the same application are a first evidence of this lack of a unified design method. Some emblematic examples are presented in Fig. 1, for both giant-diameter (D $>$ 3 m) and small-diameter machines: it is evident that even a slight difference on the efficiency between the two giant fans of Fig. 1 translates into a relevant saving/waste of electrical energy and CO_2 emission. This energy-inefficient habit of choos-

Figure 1: Use of different Fan Geometries for similar applications. Only one fan will feature the higher efficiency and, accordingly, the minimum electrical consumption and CO_2 emission.

ing different machines for the same application is well documented (see e.g., [11, pp.12;16]). The information contained within this dissertation represent a contribution toward a energy-efficient design criterion for axial fans that might avoid these inefficient situations.

1.1 BACKGROUND ON AERODYNAMIC DESIGN METHODS.

This is a short paragraph that summarizes the evolution of the aerodynamic design methods for axial fans, from the beginning to the current years. The design developments that share common features have been grouped for years (e.g., 1937-53); this is an arbitrary classification however, and others might be eventually considered.

1920-30. Pioneers Design: from Aeronautical Propellers to Fans. According to Cory [11, p. 5], the first axial fan appeared in 1827 in Paiseley, Scotland for mining operations. At that time there were not yet reliable aerodynamic theories of lift [12]; it is thus likely that the first machines were produced by an empirical *trial and error* procedure. As a matter of fact, first publications dealing with aerodynamic design theories for axial fans appeared only a century later (*circa* 1920-30, [8, 9, 13]). These pioneering methods were based on the *Blade Element Theory*, which assumes that each Blade Element BE (i.e., a section of the blade along the span) behaves like an airfoil

of known lift and drag performance, and were descending from the design of aeronautical propellers. At that period, most of the Axial fans were low-pressure low hub-to-tip ratio machines, thus supporting the direct analogy with airplane propellers. Although there were cases of high-pressure fans with relevant hub-to-tip ratios (see e.g., [11, p. 9]), generally, centrifugal machines were chosen at those time in case of applications requiring relevant pressures [11] . However, the main aerodynamic differences between those low-pressure axial machines and the aeronautical propellers were the ducted operation, which avoids the *vena contracta* [9], and the induced system of tip vortices [8].

The *Blade Element Theory* still represents nowadays the backbone of any aerodynamic design method.

1937-53. The development of Design Theories specific for Axial Fans. Except at very low pressure-rise, axial fan geometries considerably differ from aeronautical propellers. Therefore, design methods were specifically developed during the ~ 1940-50's to account for the aerodynamic peculiarities of fans. For the design of the drive system of a new wind tunnel in Göttingen, in 1937 Ruden [14] performed an extensive theoretical and experimental investigation on aerodynamic axial fan design. Ruden treated arguments as the use of fixed vanes, blade interference effects and blade loading distributions different than the usual free-vortex one. Being probably the first researcher that accounted for radial flow motions within the blade passages with the definition of an approximate radial equilibrium equation, Ruden tested four rotor-stator configurations with hub-to-tip ratio ν=0.5; the best solution achieved a medium pressure rise with high efficiency ($\eta \simeq 90\%$). On the other side of the ocean, in 1942 the American NACA was investigating similar aspects (solidity, fixed vanes and the blade section) in a more empirical manner with the works of Bell [15] and Bell & DeKoster [16]. The fans under investigation were featuring ν=0.69 and were intended for airplane engine-cooling purposes. In 1947 NACA's investigations achieved a theoretical approach with the works of Kahane [17, 18]. The theoretical findings of Ruden [14] and Kahane [17] suggested that the use of a fixed row of blades before the rotor (*preswirler* configuration) can relevantly increase the fan pressure rise. Both the authors provided also empirical correlations to estimate the losses of fan performance due to the increase of the tip clearance [14, 18]. It is remarkable noticing that these design innovations were provided by military investigations, as claimed later by Eck [1]. The Blade Element theory continued to be the base of blading design and was applied into designing one of the first aeronautical multi-stage axial compressors [19]. In 1953 Cordier presented the Diagram that took his name [20], collecting the performance of "*optimum*" fans and pumps in terms of specific speed and diameter. This diagram identifies the operational range pertaining to each machine configuration (i.e., axial or centrifugal) [21, p. 16] and represents a milestone in the field of low-speed turbomachinery design.

1956-80. Achieving the maturity of Analytic Design Method and the Introduction of Computers During the 50's, Marcinowsky performed an extensive investigation on Axial fan aerodynamics [22]. However, the international dissemination of Marcinowsky's results was likely limited by the use of German as language for the publication. Most of fan researchers, indeed, accessed part of the findings by Marcinowsky almost 20 years later, through the acclaimed english version of Eck's book on Fan Design [1]. Among the several findings, Marcinowsky verified the applicability of a theoretic equation to identify the fan hub-to-tip ratio ν for a given fan duty. The equation is based on the *Strscheletzky* criterion [1, p. 266] and equalizes the hub diameter with the size of the dead-air core downwind of the rotor. According to Bamberger [23, p.16], the findings by Marcinowsky are still highly relevant nowadays.

During these years the literature on fan design registered the inclusion of two relevant works of international dissemination: Eck in 1956 (the original german version of [1]) and Wallis in 1961 [24] published their books on fan Design. The methods proposed by these two authors were based on solid aerodynamic backgrounds and became the backbone of the major analytic design methods. In parallel however, the fan industry carried on (and still carries on nowadays) a practical *trial and error* approach [25, p.4.1], thanks to the relative easiness and rapidity of fan prototype testing. With the refinement of the design methods, axial fans gained market to centrifugal machines [11, 24]. Due to the increase of the blade solidity for higher pressure rise purposes, design methods based on cascade data appeared for high solidity rotors [24]: rather than using the lift and drag coefficients of a singular (isolated) airfoil, designers could use deflection and pressure loss data obtained from cascade data (e.g., [26]).

Although sharing the same basic aerodynamic phenomena, during the years the axial fan design discipline separated almost completely from the propulsive propeller one. Nonetheless, an attempt toward a unified design and analysis method for ducted fans and propellers was proposed by Borst [27] in 1978. Borst's method is based on the blade element theory and on the vortex theory to determine three-dimensional effects, allowing the estimation of the stage axial thrust and torque. The method showed good agreement against experimental results on a helicopter ducted tail rotor and an axial compressor.

In the second half of the XX century the advent of computers revolutionized engineering calculations and the axial fan discipline was not an exception. The first automated method of solving the axial fan design exercise was proposed by Myles et al [28] at the *NEL* in England. The automated approach was based on NACA-65 cascade data by Herrig et al [26] and provided the blading geometry after that the required fan duty were given as inputs. The method, however, was restricted to rotor-stator configurations with a free-vortex loading distribution. In 1968 Katsanis [29] proposed a fortran-based routine to solve the inviscid flow through a blade-to-blade

passage for turbomachinery applications; this work represents one of the precursor of today's Computational Fluid Dynamics CFD.

1987-2010. Analytic Design and CFD Optimization. With the advent of *Computational Fluid Dynamics* CFD in the last years of the XX century, computers became a primary tool in turbomachinery design. Numeric simulations are used to perform local analysis and to optimize the machine geometry that results from the analytical design method, thanks to the degree of detail allowed that would be difficult to achieve experimentally [30]. A second advantage is clearly the saving that can be obtained avoiding excessive experimental evaluations (for instance in case of comparison of numerous geometries). Differently from the aeronautic industry however, industrial fan designers and manufacturers took years before embracing these numerical tools [31] as their use was only justified for special cases (Smith, in [32]). The use of CFD, however, was important in the development of non-radial-stacking line theories (see e.g., [33]) and has now became a current industrial standard [2].

2011-Current days. State of the art and Recent developments. The current consolidated custom is performing the preliminary design task on the basis of theoretical and empirical knowledge, and then optimizing the geometry by means of CFD analysis or on prototype evaluation (e.g., [2, 34]). These are also the fundamentals on which automated design softwares are based (see e.g., [35]). At the same time, the academies developed different through-flow computer-based methods to evaluate new Rotor-only fan designs (e.g., [36, 37]). On the other hand, there is the industrial habit of modifying existing machines in order to meet new requirements, thus avoiding the risks related to completely new designs [38].

The current evolution trend in turbomachinery design appears the computer-based multidisciplinary optimization technique. The avant-gard of aerodynamic design of axial fans is represented by optimization routines based on numerical methods as *neural-networks* [23]: this computer-based approach iteratively compares several different geometries achieving the requirements, lastly providing the optimized one (e.g., the most energy-efficient). Bamberger [23] collected the numerical results into design charts that have been validated against three rotor-only axial fans.

1.2 DISSERTATION OBJECTIVES AND METHODS

UNSOLVED ISSUES AND PROPOSED APPROACH The complexity of the design exercise has increased over the years. Along with this complexity, the skills required to the fan designer have been increasing as well: while first designers were pure aerodynamicists (with a solid engineering background to account for structural, noise and vibrational issues) nowadays the task has been spread over several disciplines, requiring a deep knowledge and

comprehension of both physical phenomena and of complex virtual tools (e.g., CFD codes, programming skills, etc.). Nonetheless, in their simplicity, the classic analytic methods remain the most immediate link between the understanding of the physical aerodynamic phenomena and the fan geometries, that lastly represent the target of the design task. The comprehension of the physics behind the phenomenon is the basis of any efficient design exercise.

In spite of the increasing design complexity, it is felt that some basic lacks and "*grey areas*" still persist in the literature on fan design. In particular, after a comprehensive study of the fan literature, two basic questions still appear without a quantitative answer:

i) The selection of the suitable axial fan configuration (i.e., layout) related to the given requirement;

ii) The selection of the suitable aerodynamic loading distribution along the blade-span for a given fan duty.

Both these aspects have to be considered when a given fan duty is required, especially in presence of dimensional and operational constraints on the fan diameter and rotor speed. Many authors during the years faced with the questions *i)* and *ii)*, and this work does not have the presumption of providing definitive answers about. In particular, the indications presented herein regarding item *ii)* are limited to the Rotor-Only Configuration (i.e., a fan without fixed bladings). Nonetheless, the information collected on *i)* and *ii)* items have been organized in form of a design method that provides innovative aspects with respect to those available so far. In particular, it is believed that a comprehensive fan design approach shall be based on the three following points:

a) be physically-based and of easy comprehension;

b) be easy to implement (i.e., does not require the designer to acquire specific skills other than being able of solving the basic design equations);

c) present a comprehensive database of fan operation, with the dual aim of presenting the usable axial fan range and validating the indications provided within the design method.

METHODS AND DESIGN VARIABLES During the research, investigations have been performed both on global (i.e., fan performance and efficiency) and local (e.g., blade design) aspects of axial-flow fans (see Tab. 1). Fan performance and efficiency do not depend on blading effectiveness only, but are the result of the overall interaction between the airflow and the machine [39]. All the variables within Tab. 1 contribute to the fan pressure rise and efficiency (in terms of the dimensionless quantities Ψ and η), although with different magnitudes (+ signs in Tab. 1).

The investigation relied on three approaches simultaneously used:

- A review of the existing fan literature; this review has been fundamental to collect and analyze previously existing design indications and rules, as well as to extrapolate numerous experimental data that enabled the partial construction of the fan performance databases.

- Global and local evaluation of new geometries with the use of CFD simulations. This approach has been used as an intermediate passage to evaluate the fan behavior, between the analytic mean-line performance estimation and the experimental verification.

- Experimental tests on two ISO 5801 inlet-chamber test rigs to verify the estimated fan performance of new designs, as well as to test available geometries that contributed to the completion of the performance database. The larger test rig ($D_{max} = 0.8$ m) has been specifically designed and constructed.

The design method proposed in this work is a step-wise approach that can be summarized as follows:

I For a given fan diameter D and rotational speed n, the fan overall layout is selected to accomplish the required duty, in terms of flow-rate q_v and fan pressure p_f. This step is performed using the fan performance database, whose indications are corroborated by an analytic inviscid formulation of the Euler Equation.

II Whether the rotor-only configuration is selected (mandatorily or because it is suitably efficient), the vortex criterion is selected on the basis of a second fan performance data-base. Afterward, a mean-line computation provides an estimation of fan performance and efficiency. This estimation is based on analytic and empirical equations that can be easily implemented in a simple MATLAB®code.

III The design of the rotor-only fan is performed, accounting both for global (i.e., the vortex distribution criterion) and local design variables.

After treating all the possible axial fan configurations in I, steps II and III are limited to the Rotor-only layout. This restriction is justified by considering that the rotor-only is the most used industrial configuration, due to its simplicity and cheapness. In second instance, the higher degrees of freedom allowed by the absence of components as stator vanes and tail-cone results into a more complex and varied flow-field at the fan exit. Consequently, most of the literature does not treat exhaustively this axial fan layout, although being the mostly diffused one. Nonetheless, the information presented in this work can be easily integrated with indications on stator vane design from the literature (e.g., [1, 40]), to provide the basis of a comprehensive design procedure that involves any kind of axial fan configuration.

Table 1: Design Variables for fans with imposed D and n, and how they affect fan performance. Effects on the fan characteristics have been classified as follows: ++++ the variable determines substantially different curves both in shape and magnitude; +++ the variable changes the magnitudes of the curves and the shape to a minor extent; ++ minor changes in magnitude and shape; + marginal effect on the characteristic curves. Investigated variables are marked with *Yes* (Y) , according to three degrees of analysis: ✓ indications obtained from the literature; ✓✓ Indications from the literature and analytic or numeric evaluation; ✓✓✓ Indications from the literature, numeric evaluation and experimental testing. For not-investigated variables (marked with N) references are suggested, whether available.

Role	Variable	Effects		Analyzed	Indic.
		Ψ	η	Y/N	
Global	Hub-to-tip ratio ν	++++	++++	Y	✓
Global	Fan Configuration (*RO;RS;PR;PRS*)	++++	++++	Y	✓✓✓
Global	Reynolds number	++	++	Y	✓✓✓
Layout	Nose-fairing	+	+	Y	✓
Layout	Tail-cone	++	++	N	[40]
Layout	Motor position (foreword or aftword)	++	++	N	—
Layout	Hub shape	++	++	N	[40]
Layout	Casing length	+	+	N	—
Layout	Casing shape	++	++	N	—
Layout	Rotor distance from duct inlet	++	++	N	[1]
Blading	Rotor tip clearance tc	+++	+++	Y	✓✓✓
Blading	Rotor hub clearance hc	+++	+++	Y	✓✓✓
Blading	Tip end plates	+	+	N	[41, 42]
Blading	Span-wise Loading distribution	+++	+++	Y	✓✓✓
Blading	number of blades nr_b	++	+++	Y	✓
Blading	Design lift coeff. C_L	+++	+++	Y	✓✓✓
Blading	Solidity distr. $\sigma(r)$	+++	+++	Y	✓✓✓
Blading	Isolated/cascade design	++	++	Y	✓✓✓
Blading	Stagger Angle computation	++	++	Y	✓✓✓
Blading	Stacking line shape	++	++	Y	✓✓✓
Blading	Blade roughness	+	+	N	—
Blading	Airfoil	++	++	Y	✓✓
Blading	Blade attach. system	+	+	N	—
Airfoil	camber-line type	++	++	N	[23, 43]
Airfoil	max camber position $\frac{y_c}{c}$	++	++	N	[23, 43]
Airfoil	thickness distribution $\frac{y_c}{c}$	+	++	Y	✓✓
Airfoil	max thickness position $\frac{x_t h}{c}$	+	+	N	[23, 43]
Airfoil	LE radius	++	++	N	[40, 43]
Airfoil	TE radius	++	+++	Y	✓✓✓

1.3 DISSERTATION STRUCTURE

The aerodynamic basics of the operation of the axial fan are presented in Chapt. 2. Chapter 2 is fundamental to acquire familiarity with the design subject and related issues, as well as with the performance and efficiency parameters used in this dissertation. Furthermore, two analytic models that describe the axial-fan operation on the basis of fundamental equations are presented. In Chapt. 3 the numerical and experimental methods of analysis and performance assessment are presented. The heart of the Dissertation is then presented in Chapt. 4, where the selection of the axial fan configuration and of the most suitable rotor-only vortex distribution are treated. Performance data-sets of existing machines are collected into summary graphs, in terms of pressure and flow coefficients (Ψ and Φ) and of specific speed and diameter (σ and δ), that can guide the design selection. Observed trends are explained in relation to theoretical basis. Chapter 5 provides the information on which the rotor-only design is based, from the correlations used for the performance and efficiency estimation to the indications to perform satisfactorily the machine design. At last, in Chapter 6 the entire design method is presented in a suitable schematic form. To help the reader, a specific bibliography is dedicated to each Chapter and reported at the end of each one.

This dissertation would like to represent a step toward a definitive aerodynamic design method for axial fans of any configuration. The information presented herein can be used directly to design a required machine or, eventually, as a preliminary step before a refined computer-based optimization.

BIBLIOGRAPHY

[1] Bruno Eck. "Fans". In: *1st English ed., Pergamon Press, Oxford* (1973), pp. 139–153.

[2] Eleftherios Andreadis. *Design of a low speed vaneaxial fan*. MS Thesis,Cranfield, UK University of Higher Education. 2011.

[3] EC. "COMMISSION REGULATION (EU) No 327/2011 of 30 March 2011 implementing Directive 2009/125/EC of the European Parliament and of the Council with regard to ecodesign requirements for fans driven by motors with an electric input power between 125 W and 500 kW". In: *Official Journal of the European Union* (2011).

[4] *Eurostat Webpage*. http://ec.europa.eu/eurostat/statistics-explained/index.php/Consumption_of_energy. Accessed: 2017-07-08.

[5] PEng John Cermak PhD. "Select fans using fan total pressure to save energy". In: *ASHRAE Journal* 53.7 (2011), p. 44.

[6] ASHRAE. "Energy standard for buildings except low-rise residential buildings". In: *ASHRAE/IESNA Standard* 90.1 (1999).

[7] Marcos González Álvarez. *ECODESIGN REQUIREMENTS FOR FANS Current Situation and Future Developments*. Keynote at FAN 2015 Conference. Apr. 2015.

[8] Enrico Pistolesi. *Il problema dell'elica intubata e le sue applicazioni.* 11. Tipografia editrice cav. F. Mariotti, 1924.

[9] Hermann Glauert. *The elements of aerofoil and airscrew theory*. Cambridge University Press, 1926.

[10] Stefano Castegnaro. "A Critical Analysis of the Differences Among Design Methods for Low-Speed Axial Fans". In: *ASME Turbo Expo 2017: Turbomachinery Technical Conference and Exposition*. American Society of Mechanical Engineers. 2017, V001T09A008–V001T09A008.

[11] William Cory. *Fans and ventilation: a practical guide*. Elsevier, 2010.

[12] Theodore Von Kármán. *Aerodynamics: selected topics in the light of their historical development*. Courier Corporation, 2004.

[13] Curt Keller. "Axialgebläse vom Standpunkt der Tragflügeltheorie". PhD thesis. 1934.

[14] P Ruden. "Investigation of single stage axial fans". In: *NACA TM* 1062 (1944).

[15] E Barton Bell. "Test of Single-Stage Axial-Flow Fan". In: *NACA Rep.* 729 (1942).

[16] E Barton Bell and Lucas J Dekoster. "The Effect of Solidity, Blade Section, and Contravane Angle on the Characteristics of an Axial-Flow Fan". In: *NACA Wartime Report* L-304 (1942).

[17] A Kahane. "Charts of pressure rise obtainable with airfoil-type axial-flow cooling fans". In: *NACA TN* 1199 (1947).

[18] A Kahane. "Investigation of axial-flow fan and compressor rotors designed for three-dimensional flow". In: *NACA TN* 1652 (1947).

[19] John T Sinnette, Oscar W Schey, and J Austin King. "Performance of NACA Eight-Stage Axial-Flow Compressor Designed on the Basis of Airfoil Theory". In: (1943).

[20] Otto Cordier. "Ähnlichkeitsbedingungen für Strömungsmaschinen". In: *BWK Bd* 6 (1953).

[21] RI Lewis. *Turbomachinery performance analysis*. Butterworth-Heinemann, 1996.

[22] Heinz Marcinowski. "" Optimalprobleme bei Axialventilatoren". PhD thesis. Technischen Hochsehule, 1956.

[23] Konrad Bamberger. "Aerodyamic Optimization of Low-Pressure Axial Fans". PhD Thesis. Siegen, Ger: University of Siegen, 2015.

[24] R Allan Wallis. *Axial Flow Fans: design and practice*. Academic Press, 1961.

[25] Frank Bleier. *Fan Handbook: selection, application, and design*. McGraw-Hill Professional, 1998.

[26] L Joseph Herrig et al. "Systematic two-dimensional cascade tests of NACA 65-series compressor blades at low speeds". In: *NACA Rep* 1368 (1958).

[27] Henry V Borst. "A new blade element method for calculating the performance of high and intermediate solidity axial flow fans". In: (1978).

[28] DJ Myles, RW Bain, and GHL Buxton. *The Design of Axial Flow Fans by Computer. Part 2*. 1965.

[29] T Katsanis. "Computer Program for Calculating Velocities and Streamlines on a Blade-to-Blade Stream Surface of Revolution". In: *NACA TN* 4529 (1968).

[30] JH Horlock and JD Denton. "A review of some early design practice using computational fluid dynamics and a current perspective". In: *Transactions of the ASME-T-Journal of Turbomachinery* 127.1 (2005), pp. 5–13.

[31] RJ Downie, MC Thompson, and RA Wallis. "An engineering approach to blade designs for low to medium pressure rise rotor-only axial fans". In: *Experimental thermal and fluid science* 6.4 (1993), pp. 376–401.

[32] Institution of Mechanical Engineers (Great Britain). Fluid Machinery Committee. *Industrial Fans - Aerodynamic Design: Papers Presented at a Seminar Organized by the Fluid Machinery Committee of the Power Industries Division of the Institution of Mechanical Engineers and Held ...on 9 April 1987*. IMechE seminar. Mechanical Engineering Publications for the Institution of Mechanical Engineers, 1987. ISBN: 9780852986387. URL: https://books.google.it/books?id=8RXFQgAACAAJ.

[33] MG Beiler and TH Carolus. "Computation and measurement of the flow in axial flow fans with skewed blades". In: *Transactions-american society of mechanical engineers journal of turbomachinery* 121 (1999), pp. 59–66.

[34] Szu Hsien Liu, Rong Fung Huang, and Li Ju Chen. "Performance and inter-blade flow of axial flow fans with different blade angles of attack". In: *Journal of the Chinese Institute of Engineers* 34.1 (2011), pp. 141–153.

[35] *CFturbo®*. https://en.cfturbo.com/fileadmin/content/down/CFturbo_Flyer_A4_160112.pdf. Accessed: 2017-10-27.

[36] Thomas H Carolus and Ralf Starzmann. "An aerodynamic design methodology for low pressure axial fans with integrated airfoil polar prediction". In: *ASME 2011 Turbo Expo: Turbine Technical Conference and Exposition*. American Society of Mechanical Engineers. 2011, pp. 335–342.

[37] Francois G Louw et al. "The design of an axial flow fan for application in large air-cooled heat exchangers". In: *ASME Paper No. GT2012-69733* (2012).

[38] Tommaso Bonanni et al. "Derivative Design of Axial Fan Range: From Academia to Industry". In: *ASME Turbo Expo 2016: Turbomachinery Technical Conference and Exposition*. American Society of Mechanical Engineers. 2016, V006T07A006–V006T07A006.

[39] R. A. Wallis. "Definition and determination of fan duties". In: *Journal of the Institution of Heating & Ventilating Engineers* (May 1964), pp. 49–59.

[40] R Allan Wallis. *Axial flow fans and ducts*. Krieger, 1993.

[41] Michael B Wilkinson and J Sybrand. "The effect of fan tip configuration on air-cooled condenser axial flow fan performance". In: *Proceedings of FAN 2015 Conference. France* (2015).

[42] Alessandro Corsini, Franco Rispoli, and A Geoff Sheard. "Development of improved blade tip endplate concepts for low-noise operation in industrial fans". In: *Proceedings of the Institution of Mechanical Engineers, Part A: Journal of Power and Energy* 221.5 (2007), pp. 669–681.

[43] ADS Carter. "Blade Profiles for Axial-Flow Fans, Pumps, Compressors, Etc." In: *Proceedings of the Institution of Mechanical Engineers* 175.1 (1961), pp. 775–806.

2 AXIAL FAN PERFORMANCE, GEOMETRIES AND PARAMETERS

In this Chapter, the axial-flow fan is introduced starting from a comprehensive definition, the physical principles underneath its operation and the possible geometries. Several authors complain a diffused confusion related to the interpretation and use of the fan performance parameters and efficiency, in particular connected with the use of the *fan static pressure* p_{sf} and related efficiency [1–5]. Therefore, this Chapter is an attempt of organizing the material and information on axial fan operation and performance in an ordered, simple and clear form.

In the first paragraph a specific definition for axial fans is introduced, followed by a description of the fan performance and geometries and a theoretical model of fan operation; the parameters used to assess fan performance are introduced as well. Two theoretical models of an installation category provided in the Standards are then presented: the first is a *1-D* actuator disk model, whereas the second model exploits the mechanical energy equation. The dimensionless parameters herein used are then introduced, together with the typical axial-fan performance range according to the established literature. At last, the radial equilibrium and the loading-factor equations are included.

All the parameters used in this work are defined in the *List of Symbols*; the reader is invited to get familiar with them before proceeding further.

2.1 AXIAL FANS: PRINCIPLES AND DEFINITIONS

In this paragraph a comprehensive definition of an Axial fan is introduced and presented. According to the ISO Standard Vocabulary [6], a fan (of any type) is:

> *"[a] rotary-bladed machine that receives mechanical energy and utilizes it by means of one or more impellers fitted with blades to maintain a continuous flow of air or other gas passing through it and whose work per unit mass does not normally exceed 25 kJ/kg."*

This definition can be subdivided into three logical parts:

1. the first sentence *"rotary-bladed machine that receives mechanical energy and utilizes it by means of one or more impellers fitted with blades.."* provides a description of the machine;

2. the second *"..to maintain a continuous flow of air or other gas passing through it.."* presents the fan duty;

2. the third *"..and whose work per unit mass does not normally exceed 25 kJ/kg"*. provides a customary limit to distinguish fans from turbocompressors.

The ISO Vocabulary then categorizes fans according to: *i) installation* (A free inlet-free outlet (with a partition in between); B free inlet-ducted outlet; C ducted inlet-free outlet; D ducted inlet-ducted outlet; E free inlet-free outlet, without partition); *ii) function* (ducted, partition, jet, circulating and air curtain); *iii)* the fluid path (e.g., axial, centrifugal, mixed); and *iv) operating conditions* (i.e., the operational environment; for instance, hot-gases or smoke, wet-gases, etc.).

For an axial fan the following definition is reported [6, p. 4]:

> *"fan in which the air enters and leaves the impeller along essentially cylindrical surfaces coaxial with the fan."*

Although pertaining to different *installations* or *functions*, the physical principle underneath the operation of an axial fan remains the same: a pressure difference is created between the upstream and downstream side of the rotor by the relative motion of the blades with respect to the airflow (see Fig. 2). This is the physical principle lying underneath the operation of the *Airscrew* and is part of the aerofoil theory according to Glauert [7].

The pressure rise provided by the rotor is generated by the aerodynamic force on the blades, which deflects the airflow velocity (the relative w and the absolute one c, according to the frame of reference). The pressure rise achievable by deflecting the airstream at constant radius (as is barely the case of axial turbomachines) is lower with respect to the case in which the radial position of the flow increases along the blade channel (as for centrifugal machines). Furthermore, in axial machines the magnitude of the upstream-downstream pressure difference is lower for a pressure-rise rotor rather than for a turbine. This behavior is due to the boundary layer tendency to detach from the blade surface in presence of an increasing pressure along the air path. According to the previous limitations and to the low rotor speeds involved, axial fans are generally classified as *low-pressure* machines [6, p. 10] (fan pressure at maximum efficiency $p_f \leqslant 2\,\mathrm{kPa}$ or, equivalently, $\frac{p_f}{\rho} \leqslant 1.67\,\mathrm{kJ/kg}$ for standard air). [1]

A general definition, similar to the one provided for any fan, was not found in the literature for axial machines. Thus, the definition provided at the beginning of the paragraph has been modified in light of the previous indications (relevant modifications with respect to the original sentence have been highlighted). The suggested definition of an axial fan is:

> *"a rotary-bladed machine* ***co-axial with the flow*** *that receives mechanical energy and utilizes it by means of one or more impellers fitted with blades* ***to receive a flow of air*** *(or other gas)* ***with a predominant axial direction*** *and* ***to send it forward along its path*** *in a continuous manner, whose work per unit mass* ***is provided by the***

1 Axial fans are then, in turn, subdivided into low-, medium-, and high-pressure machines according to the hub-to-tip ratio [6, p. 10]; see also Chapt. 5.

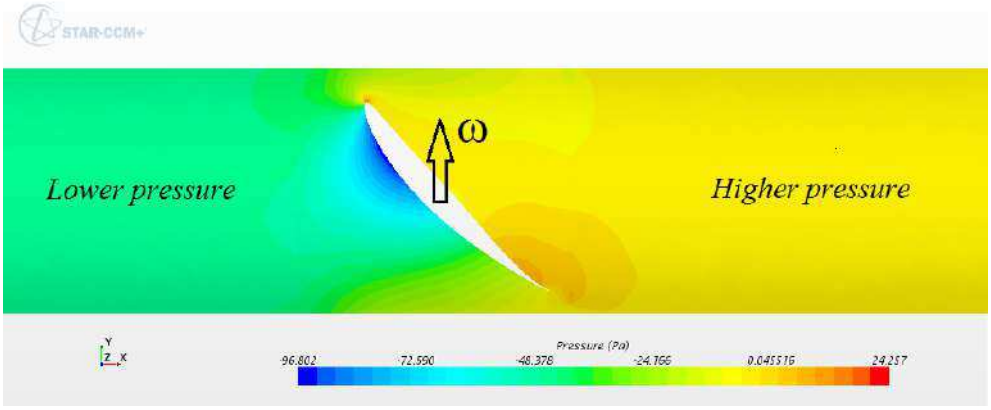

Figure 2: Static pressure distribution on a cylindric surface around a generic axial fan blade section. The upstream-downstream pressure difference is created by the aerodynamic force on the rotor blades.

> ***aerodynamic force on the blades*** *and does not normally exceed* ***1.67 kJ/kg****."*

In particular, the substantial difference introduced relies in the words *"to send it* ***forward****"*, to remark a flow direction that is a fundamental operational principle of the fan, as will be seen in the following paragraphs.

2.2 AXIAL FANS: PERFORMANCE AND GEOMETRIES

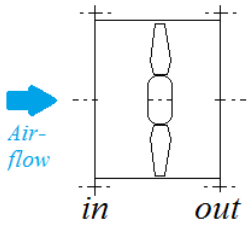

Figure 3: Sketch of a generic Ducted Axial fan.

In Fig. 3 a sketch of a generic axial-flow fan is presented to introduce the definition of fan unit. The *basic axial fan unit* is here defined according to Wallis [1, 8] as:

> *"that indivisible part of the equipment contained between the inlet and outlet flanges of the fan casing, inclusive of the centre bodies such as nose and tail fairing."*

The inlet and outlet flanges are indicated as *in* and *out* sections in Fig. 3. According to [8], whether a diffuser is attached at the fan outlet, the system shall be considered a *fan assembly* and not a fan unit anymore. This

difference is important to distinguish the performance of the assembly from those of the unit.[2] In particular, for an axial-flow fan the *unit* is composed of a straight cylindrical duct that includes the rotor, the eventual stator bladings, the prime mover (e.g., electrical motor, pulley, etc.) and, eventually, the nose-cone and tail-fairing, and whose flanges (sections *in* and *out*) are connected to the airway. Not all the previous components are necessary for the fan to work; however, the *fan unit* performance will vary according to their presence or not.

This paragraph is subdivided into the following sequential four parts:

- Fan duty
- Matching Fan and System
- Standard Performance Parameters
- Geometries and Components

Fan Duty

The primary duty of a fan is sending the required airflow q_v from a position to another within a given air system. The air system can be as simple as a hole through a partition which separates two environments, or can be rather complex as, for instance, an airway for mining purposes. In nature, a mass of air would not move from its stationary position (except for natural convection e.g., due to thermal gradients). Once an airflow is put into motion within a duct in fact, losses due to friction and recirculation decrease the energy (total pressure) of the moving air, providing resistance to the motion. To overcome this resistance, the axial fan supplies energy to the airflow *to send it forward* along the duct, equalizing the total pressure losses that the air encounters along the path. The well-know Euler equation for turbo-machinery (Eq. 1) quantifies the transfer of mechanical energy to the air. The total-to-total pressure rise for the generic streamline is:

$$\Delta p_{tt} = \eta_{tt} \cdot \rho \cdot (u_2 c_{u2} - u_1 c_{u1}) \tag{1}$$

where u is the blade speed, c_u is the air tangential absolute velocity at the rotor outlet (subscript 2) and inlet (subscript 1), and η_{tt} the energy conversion efficiency. For axial-flow machines the airflow generally develops

2 Fan performance at the test bench should be referred exclusively to fan units. Unfortunately, there has been a diffused industrial custom in testing axial fans with a diffuser attached [8], thus providing fan assembly performance.

on cylindrical surfaces of constant radius r.[3] Accordingly, for streamlines elaborated by axial machines Eq. 1 is written as:

$$\Delta p_{tt} = \eta_{tt} \cdot \rho \cdot \omega r \cdot (c_{u2} - c_{u1}) \tag{2}$$

$$\tag{3}$$

where $u = \omega \cdot r$ is the blade speed at the generic radius.

Matching Fan and System

The energy diagram for a generic air distribution system is represented in Fig. 4a): the fan increases the air energy to compensate the total pressure losses experienced by the airflow, thus enabling the required q_v to complete its path along the airway. This occurrence is called *matching* between the system losses curve and the fan characteristic (see Fig. 4b)). The matching between fan and system should be performed with the lowest energy use (i.e., with the highest efficiency). Accordingly, it is required that: *a)* for the required operation the most efficient fan shall be selected (in terms of type and size, generally), and *b)* the matching between system and fan characteristic shall occur close to the fan best efficiency point (*BEP*). American Standards, for example, require that any duty of the ventilation system does not differ from the one at best efficiency more than 10-15% [10]

AIR TOTAL PRESSURE In incompressible conditions, the air total pressure at a point of the flow field is the sum of a static and dynamic term:

$$p_{tt} = p_s + \frac{1}{2}\rho \mid \vec{v} \mid^2 \tag{4}$$

$$= p_s + p_d \tag{5}$$

where $\vec{v}$ is the local air velocity vector and p_d is the related dynamic pressure. However, *Caveat lector*, the fluid-dynamic total pressure p_{tt} differs from the air total pressure p_t defined by the ISO 5801 Standard [11], where the dynamic term is conventionally computed exclusively on the axial velocity, as will be shown in the following.

STATIC AND DYNAMIC PRESSURE According to the Bernoulli principle, the dynamic pressure term can be ideally converted into the static one and vice-versa. However, converting the dynamic pressure into static is not as easy as the opposite transformation, because of the total pressure losses typically occurring in diverging flows (these losses, again, are related to the boundary layer detaching tendency in presence of a positive pressure gradient). This is likely the reason why Brendel [9] refers to the static component as *potential* energy; although incorrect from the point of view of the theory, it expresses

3 This is rigorously true exclusively for machines that feature free-vortex blading. Nonetheless, the radial motion experienced by the flow within the blade passage of non-free vortex machines is generally of reduced entity and can be neglected for the aim of the present paragraph.

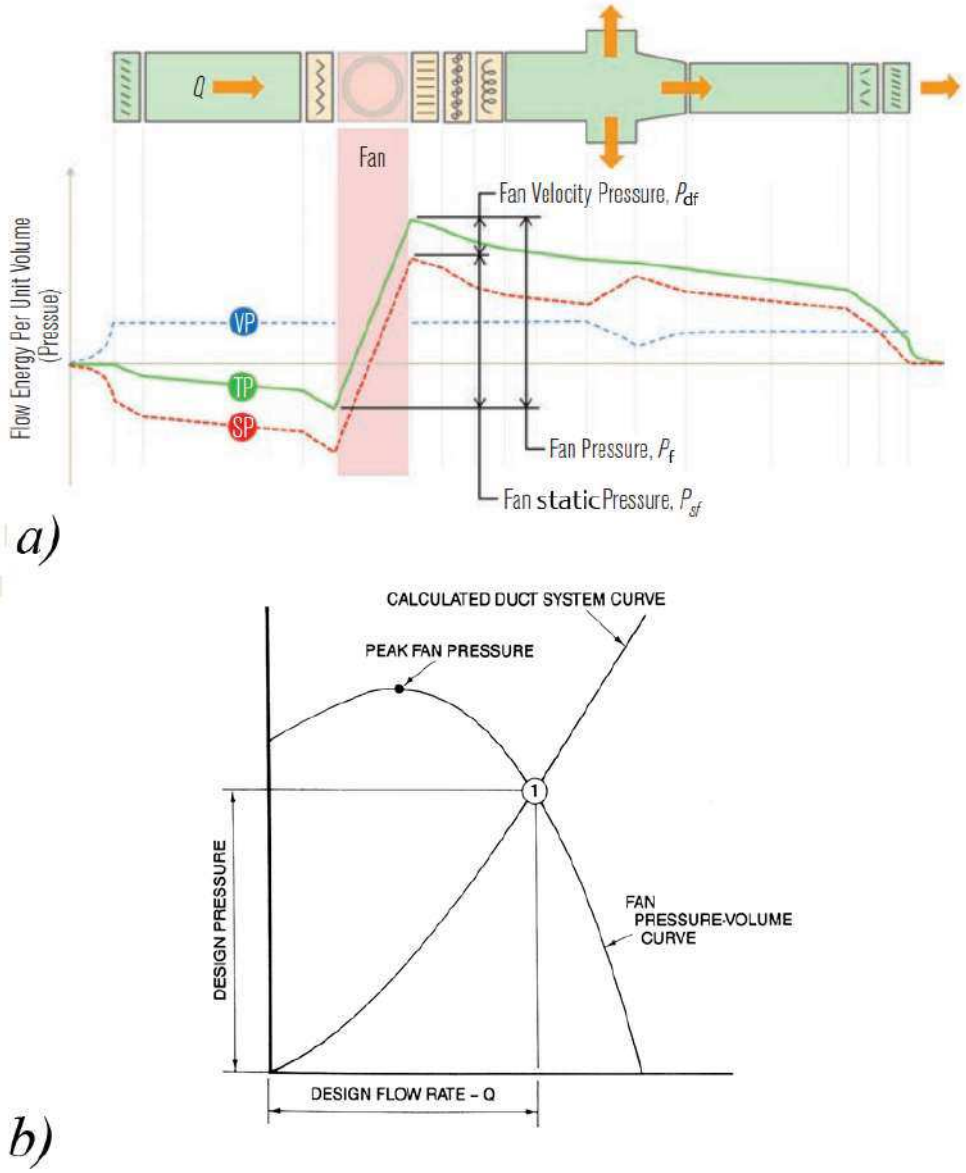

Figure 4: a) Energy diagram for a generic air distribution system (adapted from [9]; b) Matching between system curve and fan characteristic.

the industrially diffused feeling that the static pressure is the precious part of the air energy.

AIR VELOCITIES IN A DUCT Three velocity components exist in a *3-D* space. For mechanical ventilation purposes however, the unique velocity component conventionally considered useful within a duct is the mean longitudinal (i.e., axial) one[4], which is defined by the ISO Standard [11] as

$$v_{m_x} = \frac{q_{v_x}}{\pi \frac{D_x^2}{4}} \tag{6}$$

where x refers to the generic duct section along the airway. The radial and tangential velocity components are thus neglected. The swirl velocities, in particular, are not directly useful to overcome the duct resistance (i.e., to send forward the airflow) [12, p. 5] as their energy would be dissipated into heat (refer to the interesting case described by Bleier [13, p. 1.11], for instance). On the other hand, radial motions immediately disappear to cope with the radial equilibrium (see Par. 2.6). In particular, when x refers to the fan outlet section *out*, $v_{m_{out}}$ is called *fan outlet velocity* and the related dynamic pressure is named *fan velocity pressure*.

THE PRESSURE RISE OF THE AXIAL-FLOW FAN The fan rotor increases the air total pressure acting on the airflow in an active and reactive manner, according to its degree of reaction [14]. However, the tangential velocity v_u (i.e., the active part of the energy delivered to the fluid) is ineffective in overcoming the duct resistance if it is not converted into static pressure with a straightener. Being the axial velocity $v_a = v_{m_{out}}$ within the fan casing constrained by the continuity equation (for fans with equal inlet and outlet diameter, as is generally the case of axial machines), the ventilation-effective total pressure rise Δp_{tt} through the fan unit equals the static-to-static pressure rise Δp_s [12, p. 187],[15, p. 34] (see the pressure trends of Fig.s 4 and 5). It is fair to notice that the static-to-static pressure rise through the fan Δp_s is different from the *fan static pressure* p_{sf} defined in [11] and introduced in Par. 2.2 .

SIMPLE MODELING OF FAN-SYSTEM OPERATION A simple way of providing a physical look at the operational matching between the fan and the system in which the machine is installed is considering the closed circuits of Fig. 5. Once the fan is started and brought to the nominal speed, the air contained inside the air system is accelerated from rest ($v = 0$) to a velocity $v_a = \frac{q_v}{\pi \frac{D^2}{4}}$ (at the *in* and *out* sections), where D is the fan casing diameter. The fan operation (at nominal speed) uniquely identifies this flow-rate q_v as the volume of air per second that experiences a loss of total pressure along the path equal to the pressure rise delivered by the machine. When these two effects are balanced the air acceleration stops and a stationary constant airflow condition is reached. This is, for instance, the working principle of a

4 See, for instance, the 2017 version of the ISO 5801 Standard, Annex G, p.110

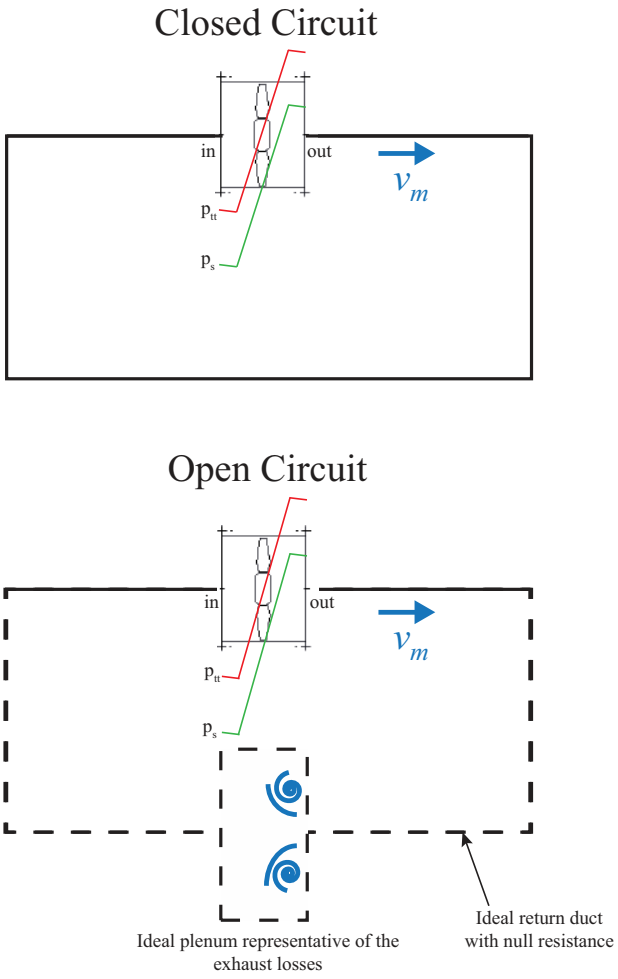

Figure 5: Fan-System Matching: all the systems can be modeled as an ideal closed circuit.

closed wind tunnel: the losses dissipate energy (pressure) into heat, increasing the air temperature; internal heat-exchangers are commonly installed inside the tunnel to cool down the airflow [16].

The closed circuit configuration provides a simple manner for the theoretical explanation of the fan operation: as all fans operate in the atmosphere, any air system can be modeled as a closed circuit, with an eventual *virtual* duct with no resistance connecting the airway exhaust with the inlet of the same system. Some authors (e.g., [1] and the European Regulation 327 [17] as well) make a distinction between *in-line* and *exhaust* fans to assess fan performance: *in-line* fans are those machines that operate in ducted-ducted conditions (e.g., a fan within a closed wind tunnel), while *exhaust* fans deliver the airflow directly to an open environment with no useful work downstream. The use of the fan pressure p_f is recommended for the in-line case and the fan static pressure p_{sf} for the exhaust one [1, 17] (see the following section for the definition of p_f and p_{sf}). Because of the continuity of the medium (air) however, there are no conceptual differences between the two installations: an open system (exhaust case) can be modeled as a closed system (in-line case) with an ideal return duct of null resistance (see Fig.5) but including the discharge to a large plenum that dissipates the fan velocity pressure p_{df} with an abrupt expansion. Accordingly, the operation of the fan running at the nominal speed, again, will identify a particular airflow q_v flowing through the system.

Standard Performance Parameters

Unless otherwise specified, the dimensional performance parameters used in this work are coherent with the ISO 5801 standard [11]. In particular, the fan pressure p_f is computed as the difference between the air total pressure at fan outlet and inlet:

$$p_f = p_{t_{out}} - p_{t_{in}} \tag{7}$$

where, *caveat*, the total pressure at the fan outlet $p_{t_{out}}$ is conventionally computed as sum of the local static pressure p_{s2} and the average component of the axial dynamic pressure. As anticipated, this last is generally called *fan velocity pressure* [15] and is defined at the fan outlet section as:

$$\begin{aligned} p_{df} &= \frac{1}{2}\rho v_{a_{out}}^2 \\ &= \frac{1}{2}\rho\left(\frac{4q_v}{\pi D^2}\right)^2 \end{aligned} \tag{8}$$

As reported previously, the energy related to eventual swirl motions is neglected. It is fair noticing that with an axial fan p_{df} is uniquely defined by the design flow rate q_v and the axial fan size D selection. The fan pressure p_f is the parameter used to asses the performance of in-line fans, while for

exhaust units a third parameter called *fan static pressure* p_{sf} is used [1], with p_{sf} defined as:

$$\begin{aligned} p_{sf} &= p_f - p_{df} \\ &= (p_{t_{out}} - p_{t_{in}}) - \frac{1}{2}\rho v_{a_{out}}^2 \end{aligned} \tag{9}$$

The fan static pressure p_{sf} represents the air total losses before entering a fan unit that delivers directly to the atmosphere (*exhaust* units). It is the correct parameter to asses the performance of exhaust fans, as no useful work is delivered downstream of the fan unit [1, 8, 12]. However, the use of the word static is a misnomer [12, p. 4], as p_{sf} does not represent the static pressure rise through the fan (i.e, $\Delta p_s \neq p_{sf}$). To eliminate this ambiguity, authors used different names for p_{sf}, as *fan inlet total pressure* FITP [12] or the commonly used total-to-static pressure (e.g., [18]). However, such *static* misnomer generated several misunderstandings and installation errors during the years, as reported in [2–4, 8, 19]

According to the parameter used, *fan efficiency* η_s and *fan static efficiency* η_{sf} are defined as:

$$\eta_f = \frac{p_f \cdot q_v}{T_r \cdot \omega} \tag{10}$$

$$\eta_{sf} = \frac{p_{sf} \cdot q_v}{T_r \cdot \omega} \tag{11}$$

where the impeller torque T_r is only due to aerodynamic actions.

Most of Rotor-only axial units are tested according to the exhaust configuration (A category, [11]); accordingly, their performance are usually presented in terms of p_{sf}. However, as these Rotor-only units are largely employed in the in-line configuration as well, the conversion to fan pressure is obtained as:

$$p_f = p_{sf} + p_{df} \tag{12}$$

being aware that Eq. 12 can be used only in presence of a good-quality flow at the fan outlet [12, p. 346]. The assumption underneath Eq. 12 is the equivalence of the results obtained from different test bench categories (e.g., $p_{f_A} = p_{f_B}$) [20]. According to Eck [21, p. 266] however, there is a considerable amount of natural conversion of swirl into static pressure for free-discharging rotational flows; Marcinowsky suggests that 15-25% of the swirl dynamic pressure is converted into p_s by natural diffusion [18, p. 19]. Therefore, the fan pressure p_f computed with Eq. 12 might be slightly larger than if it were directly measured in a B-type (free-inlet-ducted outlet) or D-type (ducted-inlet-ducted outlet) test rig. Although the new ISO 5801 Standard [22, p. 15] acknowledges the issue, no quantifications are reported or known to the author, however.

Geometries and Components

Single-stage axial fans can feature markedly different geometries: two solutions of opposite complexity (i.e., the simplest and the most complex, re-

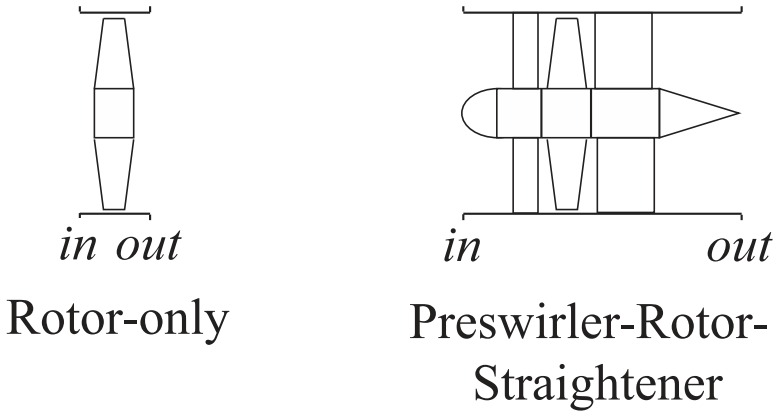

Figure 6: Ducted axial fan geometries of different complexity: the Rotor-only is the simplest single-stage solution (also named Tube-axial fan), while the Preswirler-Rotor-Straightener (with nose and tail-cone) is the most complex. Axial fans with fixed blade are generically referred as Vane-Axial machines.

spectively) are represented in Fig. 4. The casing identifies the longitudinal length of the fan. Contra-Rotating (*CR*) fans may be even more complex than the P-R-S layout; however, the *CR* machine is a particular case of compact multistage unit (not a single-stage one) [12, p. 309]. Therefore, four single-stage axial fan layouts are identified and presented in terms of increasing design complexity:

RO Rotor-Only layout: the unique aerodynamic components are the fan casing and the rotor (i.e., hub and blades). An inlet spinner and a tail-cone can eventually be installed. This layout is industrially known as *Tube-Axial Fan* [13] and is extensively used for its intrinsic simplicity and cheapness [1]. Maximum efficiencies η_f around 75% are achievable by this layout [13, 15].[5]. Common values for actual small-to-medium size applications range around 60-70% [23].

RS Rotor-Straightener layout: the rotor is followed downstream by a stator blading that convert the swirl energy into static pressure. This type of axial-fans are widely diffused [14, p. 24] and provides the highest efficiencies [12, p. 265], up to $\eta_f = 87\%$ according to [15, p. 46].

PR Preswirler-Rotor layout: in this configuration the stator is in front of the rotor. The preswirler accelerates the airflow towards the tangential direction, thus providing an additional velocity at the rotor entrance with respect to the *RO* and *RS* cases. *PR* fans are generally used for applications requiring higher pressure rises than Rotor-straighteners

5 The fan manufacturer Flakt-Woods claims a maximum efficiency of 77% for their best Rotor-only machine (see http://www.flaktwoods.it/products/air-movement-/ventilation-fans/axial-fans/jm-aerofoil-)

[p. 24][14], as well as in cases in which the axial length of the unit is limited [12, p. 306].

PRS Preswirler-Rotor-Straightener: this layout is quite rare and their use restricted to special installations. A case presented by Wallis [12, p. 306] required this blading layout because of a limited rotor speed (for acoustic reasons) and, consequently, needed a relevant flow deflection Δc_u. Another PRS fan is showed in Fig. 7.

Figure 7: A PRS fan installed in a steel production plant in Italy, for conglomerate cooling purpose before entering the furnace (reproduced by courtesy of Boldrocchi Spa).

Axial fans with fixed blading (rear or forward) are generally known as *Vane-Axial Fans* [13]. Vane-axial fans are generally able of higher pressure rise (and efficiency) than tube-axial fans of similar dimensions; however, the axial length of the machine unavoidably increases.

A rotor-only fan can properly operate as well: the air will find *its own efficient way* flowing through the fan. If the tail-cone is absent, the dead-air zone that creates downstream of the hub works as a low-efficient tail-cone while the residual swirl component is dissipated into heat after some fan diameters (except for a small case-dependent amount that is naturally converted into static pressure). However, the airflow losses related to the absence of the straightener and the tail-cone will lower the fan performance and the efficiency. A fair nose-cone or spinner is required to ensure good inlet flow conditions to the fan blading (see for instance [24]).

2.3 FUNDAMENTAL EQUATION MODELS FOR THE AXIAL FAN

2.3.1 An actuator disk model for the axial-fan-inlet-chamber case

It is of interest introducing a simple 1-D model to analyze the actual performance of an axial fan during a test. The model has been developed on the basis of the Actuator Disk Model (*ADM*) reported by Glauert in [7, p. 201], with the initial aim of relating the fan operation with the Standard parameters (Par. 2.2) resulting from the experimental tests. The basic idea of the force F_{fan} by which the fan acts on the fluid to *send it forward* along the airway is described and derived. The *ADM* is usually employed in the classic literature to describe the operational principle of the propulsive propeller (e.g., for aeronautical applications). Differently from the unducted-propeller case however, the physical domain here considered (see Fig. 9) resembles the one of an inlet-chamber rig for axial fan testing [11]; a rig of this type is showed in Fig. 8 and will be described in Chap. 3. The chamber walls

Figure 8: The medium-size inlet-chamber fan testing rig installed at the Laboratorio di Macchine Aerauliche e Termiche in Padova, Italy. The fan under test is positioned at the chamber exit (right side of the picture).

separate the incoming airflow, which will be elaborated by the fan under test, from the surrounding ambient. Thus, the air parameters (pressure and temperature) can be measured inside the chamber; the incoming airflow is measured as well with a suitable instrument (e.g., a venturi-nozzle) installed upstream of the chamber (refer to Chap. 3 and to the ISO Standard [11, p. 107] for a comprehensive description of the rig configuration). Before being elaborated by the fan under test, the airflow inside the chamber is almost at rest because of the relatively large cross-section dimensions. The fan then accelerates the air, discharging it directly to the surrounding atmosphere. The ideal domain is presented in Fig. 9a), together with the energy diagrams in Fig. 9b) and with the actions (i.e., forces, pressures and shear

stresses) on the control-volume in Fig. 9c). Only for this Paragraph, the sections of the fan and of the airway have been numbered according to Fig. 9a), differently from the rest of the Dissertation.

Hypothesis

The hypothesis underneath this simple model are:

- The fan is a vane-axial fan working at the optimum condition in which there is no tangential velocity at the blading exit (i.e., absence of swirl). Accordingly, there is no swirl dissipation downstream of the blading (section 4 of Fig. 9a) and the airflow discharged to the Atmosphere is purely axial.[6]
- The physical system is axial-symmetric: the actions along the transversal axes (y and z) are perfectly balanced. Thus, only the actions along the x direction are considered.
- Wall friction losses inside the inlet chamber and inside the fan duct casing are low and neglected in the analytic model. However, the energy diagram of Fig. 9b) rigorously accounts for them as well.
- The static pressure at the fan duct outlet (section 5) is equal to the atmospheric pressure. This is a reasonable assumption in absence of radial and tangential motion of the fluid.
- Velocities are assumed to be homogeneous at each section of the airway. Accordingly, the wall boundary layers are assumed to be infinitesimal.

Airflow path

Along its left-to-right path, the airflow goes through the following environments (refer to Fig. 9*a) and* b)):

c-0 **Chamber** This is the rig chamber. Inside, the airflow is homogeneous and the air velocity is very low ($\simeq 2-3\,m/s$). Accordingly, total and static pressure (p_{tt} and p_s, respectively) differ by few Pascals [Pa]. The friction wall losses are low as well and neglected accordingly.

0-1 **Bell-mouth** The duct bell-mouth is part of the duct system (not of the fan) and is fundamental to provide good inlet flow conditions to the fan. The air is smoothly accelerated from the chamber conditions to the velocity within the fan casing. The static pressure falls down to p_1 according to the acceleration of the airflow (see the p_{ew} trends in Fig. 9). Some total pressure losses occur due to the wall friction; however these are very low for a flow contraction [15] and are thus neglected. As axial fans normally feature an equal diameter at the fan entrance and exit,

6 The first hypothesis simplifies the analytical treatment; Otherwise, the pressure distribution related to the swirl should be taken into account (See Betz A., *The theory of the Screw Propeller*, NACA TN No. 83)

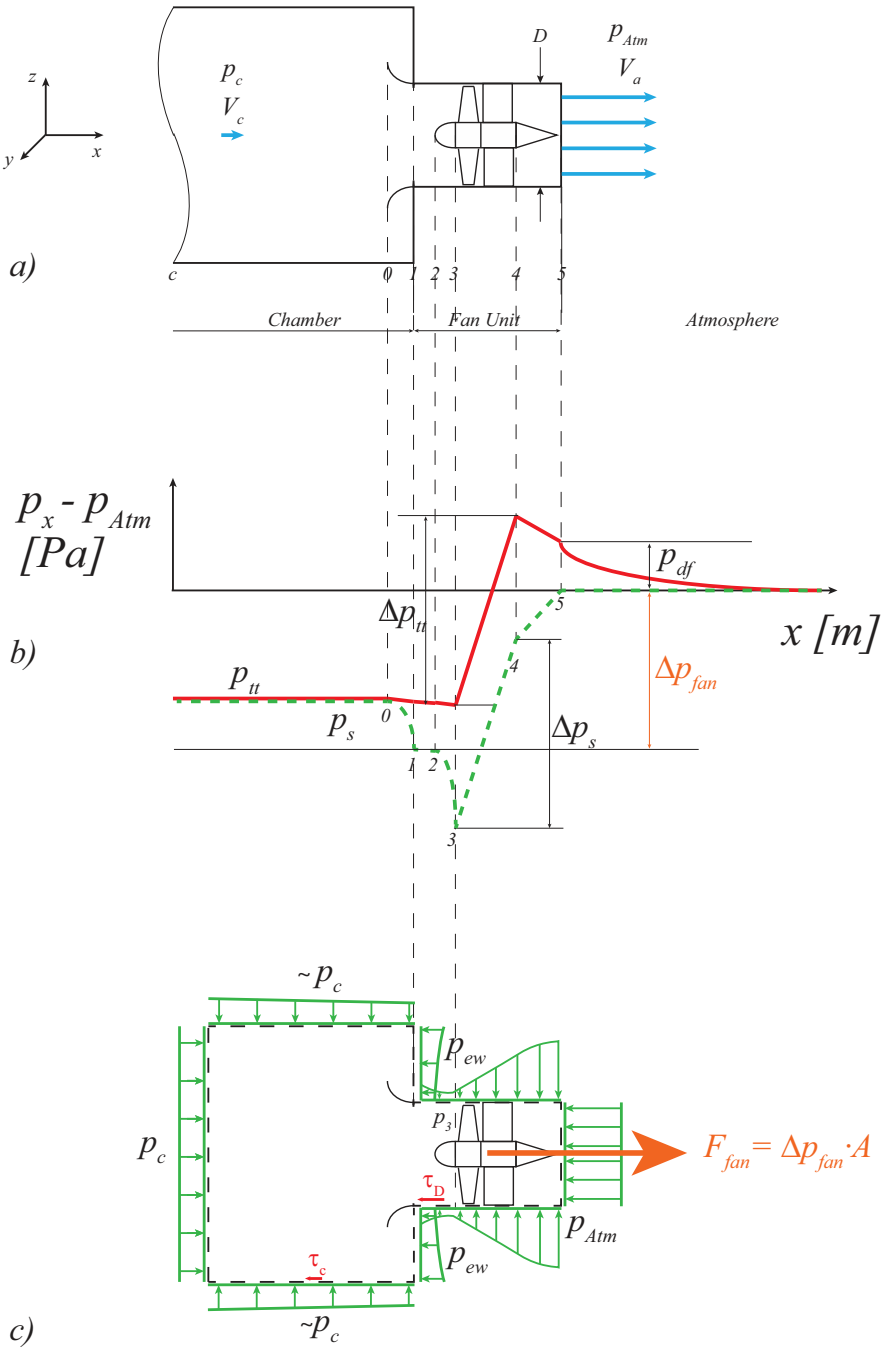

Figure 9: Actuator Disk Model: the solid red line represents the total pressure while the green dashed one the static pressure; the difference between the two is the dynamic pressure (line not reported for sake of graphical clearness).

the dynamic pressure within the duct immediately downstream of the bell-month is equal to the *fan dynamic pressure* p_{df}

$$p_{df} = \frac{1}{2}\rho\left(\frac{q_v}{\pi\frac{D^2}{4}}\right)^2 = \frac{1}{2}\rho\left(\frac{q_v}{A}\right)^2 \tag{13}$$

$$= \frac{1}{2}\rho v_a^2 \tag{14}$$

1-2 **Duct Casing** A short (eventually absent) portion of cylindrical duct ensures regular inlet flow condition [21, p. 301].

2-3 **Nose-cone** Before entering the blading passage, the airflow velocity is further increased according to the change of cross section (from cylindrical to annular); the static pressure decreases down to p_3.

3-4 **Fan Blading** The airflow energy is increased while passing through the rotor; for modeling purposes however, it is convenient considering jointly the rotor and the stator blading. Regardless of how much energy has been supplied to the fluid in active and reactive form (i.e., the rotor degree of reaction) in fact, at the blading exit (section 4) all the mechanical energy received by the fluid for ventilation purpose has taken the form of static pressure. This is accomplished by the action of the straightener in a Rotor-Straightener fan. Thus, at section 4 the flow velocity is completely axial and, according to the continuity equation, equal to the velocity at section 3.

4-5 **Tail-cone** At this point, the airflow is slowed from the annulus velocity to the duct one. Depending on the tail-cone diffuser efficiency, the axial dynamic pressure within the annulus is partly converted into static pressure. Being a relatively short diverging passage, some total pressure losses are experienced by the fluid; moreover, a wake downstream of the fan hub is generated. Accordingly, the total pressure decreases between 4 and 5 sections and the static pressure recovery is lower than the previous variation between 2 and 3. The hub wake is assumed to be expired right at the exit of the fan, at section 5; this is not representative of the reality, as the wake expires some fan diameters downstream of section 5. However, this simplification allows to assume a uniform flow velocity v_a at the fan outlet.

5-Atm **Jet Discharge** The airflow is finally discharged to the atmospheric ambient: under the hypothesis of no radial and swirl velocities, at section 5 the static pressure can be considered equal to the atmospheric pressure $p_{s5} = p_{Atm}$. The airflow additional energy with respect to the surrounding air is identified by the fan velocity pressure p_{df} that is gradually dissipated by turbulent and viscosity effects some diameters downstream. Notice that a diffuser connected to the fan outlet flange (section 5) would reduce this loss and, consequently, increase the static pressure rise of the *fan assembly* (not of the fan unit).

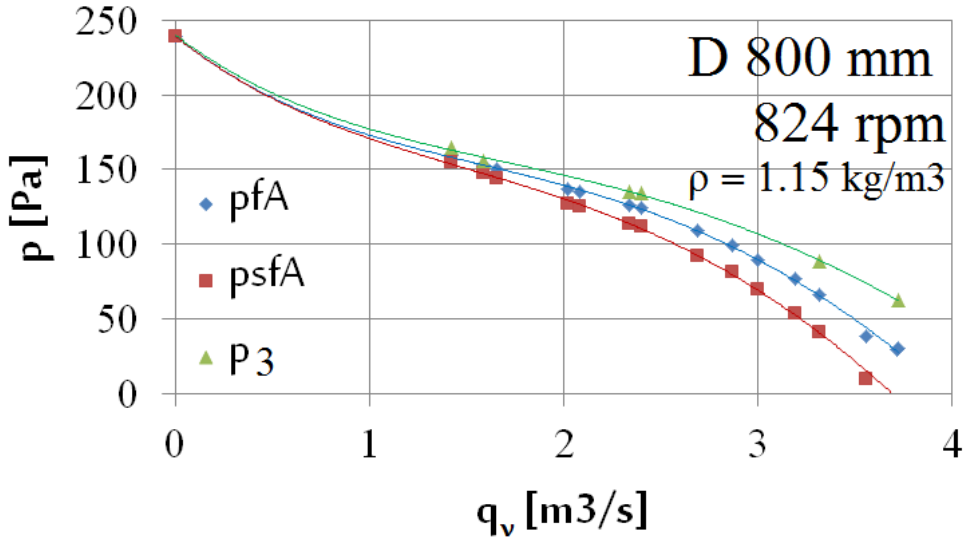

Figure 10: Fan characteristic curves compared with static pressure measurements at the preswirler entrance. This fan has been tested at the University of Padova on the Large-size rig (see Chapt. 3).

Figure 10 reports the experimental characteristic curves of a 800 mm, $\nu = 0.4$, preswirler-rotor fan. Together with the Standard fan pressure p_f and fan static pressure p_{sf} curves, the modulus of the static pressure p_3, which is measured immediately upstream of the preswirler, is reported as well.

Analytic model

A longitudinal force must be applied by the fan on the airflow to send the air (or gas) continuously along its path of the airway. This axial force, applied by the fan on the fluid, is given by the following:

$$F_{fan} = \Delta p_{fan} \cdot A \tag{15}$$

$$= \Delta p_{fan} \cdot \pi \frac{D^2}{4} \tag{16}$$

where Δp_{fan} is the static pressure difference between sections 1 and 5 (the fan unit flanges) and A is the fan disk area. The force F_{fan} could be easily measured connecting a load cell (mounted longitudinally along the duct axis) to a fan that can freely slide along the x direction. It is remarkable that the first NACA tests on axial fans were presenting a similar rig solution [25]. Once F_{fan} is measured, Δp_{fan} can be easily obtained:

$$\Delta p_{fan} = \frac{F_{fan}}{A} \tag{17}$$

Focusing on the control volume of Fig. 9c), the principle of the conservation of momentum can be applied along the longitudinal x direction to the

flowing system under stationary conditions (i.e., $\frac{d..}{dt} = 0$) in the form that follows:

$$\sum F_x = \dot{m} \cdot \Delta v_x \tag{18}$$

under the hypothesis of homogeneous velocities at the two sides (entrance and exit) of the volume. The LHS term represents all the actions that are applied on the fluid system. Considering all the terms contained within the control volume, from left to right we obtain:

$$p_c \cdot A_c - \tau_c \cdot A_{wall_c} - p_{ew} \cdot (A_c - A) + F_{fan} - \tau_D \cdot A_{wall_D} - p_{Atm} \cdot A = \dot{m} \cdot \Delta v_x \tag{19}$$

where the term τ represents the wall frictional stresses, A_c is the chamber cross-section area, p_c is the static pressure inside the chamber, and p_{ew} is the static pressure at the end-wall of the chamber. The term p_{ew} actually represents the integral average over an unknown pressure distribution along the ending wall surface, whose trend is qualitatively reported in Fig. 9c). Neglecting the wall friction terms and writing $F_{ew} = p_{ew} \cdot (Ac - A)$ we obtain:

$$p_c \cdot A_c - F_{ew} + F_{fan} - p_{Atm} \cdot A = \dot{m} \cdot (v_5 - v_c) \tag{20}$$

The end-wall term F_{ew} must be written in an explicit form. The flow in

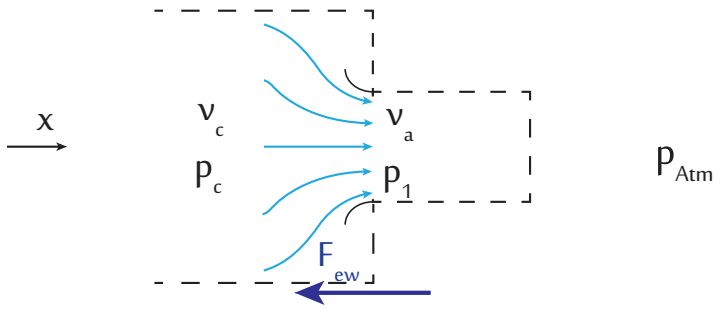

Figure 11: Qualitative description of the current lines in proximity of the ending wall and of the fan inlet (section 1) .

proximity of the fan inlet behaves as a converging field (Fig. 11), in which the air accelerates from the velocity within the chamber v_c up to the duct velocity in section 1 $v_1 = v_a$. While flowing through this converging field, the airflow is *squeezed*, with F_{ew} being the projection along the x axis of this squeezing force. Thus, according to the momentum conservation principle, F_{ew} is written as:

$$-F_{ew} + p_c \cdot A_c - p_1 \cdot A = \dot{m} \cdot (v_a - v_c) \tag{21}$$

Thus,

$$F_{ew} = p_c \cdot A_c - p_1 \cdot A - \dot{m} \cdot (v_a - v_c) \tag{22}$$

Substituting F_{ew} into Eq. 20 we obtain:

$$\begin{aligned} p_c \cdot A_c - p_c \cdot A_c + p_1 \cdot A + \dot{m} \cdot (v_a - v_c) + F_{fan} - p_{Atm} \cdot A \\ = \dot{m} \cdot (v_5 - v_c) \end{aligned} \tag{23}$$

and being $v_5 = v_a$ under the assumption of homogeneous flow at the fan exit the final form is obtained:

$$F_{fan} = (p_{Atm} - p_1) \cdot A \tag{24}$$

or

$$\Delta p_{fan} = \frac{F_{fan}}{A} = p_{Atm} - p_1 \tag{25}$$

which is the final result.

The magnitude of the Δp_{fan} term is expected to be close to the fan pressure p_f defined by the Standard. The reader shall not be deceived by the difference between p_f and p_3 curves of Fig. 10. In fact, at section 3 the airflow has been accelerated up to the annulus velocity c_a and the static pressure p_3 decreases accordingly.

It is then concluded that an Actuator Disk Model cannot describe the axial fan pressure Δp_{fan} in terms of the ISO 5801 standard parameter. By contrast, this result is achieved in the following paragraph, involving energies instead of forces.

2.3.2 Energy Equation applied to the Inlet-Chamber Axial fan case

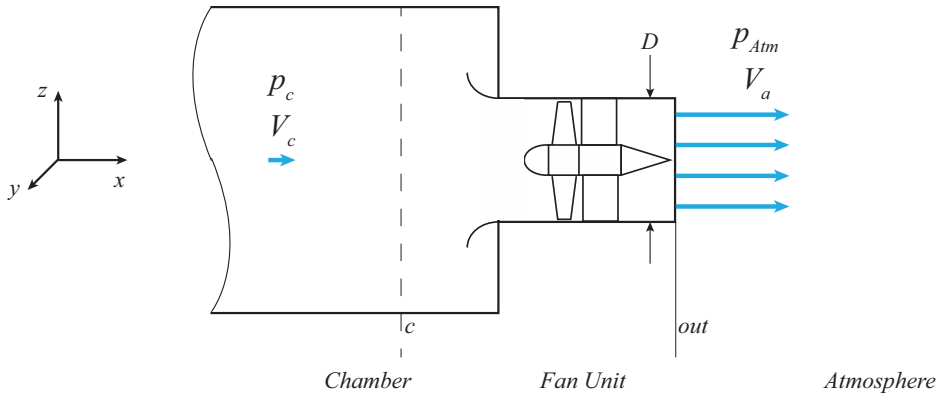

Figure 12: Ventilation system.

In this paragraph the Standard parameters are approached starting from the Energy equation. According to the hypothesis provided in the previous

paragraph, the Energy equation for the ventilation system of Fig. 12 can be written as:

$$\rho q_v \cdot \left(\frac{v_{out}^2 - v_c^2}{2} + \int_c^{out} \frac{1}{\rho} dp + L_{c-out} - q_{c-out} + L_\tau \right) = 0 \tag{26}$$

where

- $v = \frac{\Delta x}{\Delta t}$ is the generic fluid velocity at the reference section;
- $v_{out} = v_a$;
- q_v is the volumetric flow rate $[\frac{m^3}{s}]$;

$$\begin{aligned} q_v = A \cdot v = A \cdot \frac{\Delta x}{\Delta t} \\ = \frac{m}{\rho \Delta t} = \frac{\dot{m}}{\rho} \end{aligned} \tag{27}$$

  with m the mass of the system $[kg]$ and $A = \pi \frac{D^2}{4} [m^2]$ the fan duct area;

- dp is the variation of the static pressure $[Pa]$;
- L_{c-out} is the fan work for the mass unit $[\frac{J}{kg}]$;

$$\begin{aligned} L_{c-out} = \frac{W_{fan}}{m} \\ = \frac{F_{fan} \cdot (v \cdot \Delta t)}{\rho q_v \Delta t} \\ = \frac{F_{fan}}{\rho A} = \frac{\Delta p_{fan}}{\rho} \end{aligned} \tag{28}$$

- q_{c-out} is the heat transferred to the fluid per unit mass $[\frac{J}{kg}]$;
- L_τ is the shear work due to viscous stresses $[\frac{J}{kg}]$.

In the *ideal* case of frictionless fluid ($L_\tau = 0$) and absence of heat transfer ($q_{c-out} = 0$) the energy equation turns into the Bernoulli equation: *the variation of the kinetic energy of the (fluid) system within the time interval* Δt *is equal to the sum of the works performed by the internal and external forces acting on the system* [26]. Under these simplifications ($L_\tau = 0$ and $q_{c-out} = 0$) and writing the chamber section area as a multiple of the fan duct one A

$$A_{chamber} = A_1 = k \cdot A$$

(with k>5 according to the Standard [11, p. 115]), Eq. 26 can be written as:

$$\rho A \frac{\Delta x}{\Delta t} \left[\frac{(\frac{\Delta x}{\Delta t})^2 - \frac{1}{k^2} \cdot (\frac{\Delta x}{\Delta t})^2}{2} + \frac{p_{Atm} - p_c}{\rho} + \frac{\Delta p_{fan}}{\rho} \right] = 0 \tag{29}$$

Removing the mass term outside the parenthesis we obtain:

$$v^2 \frac{1 - \frac{1}{k^2}}{2} + \frac{p_{Atm} - p_c}{\rho} + \frac{\Delta p_{fan}}{\rho} = 0 \tag{30}$$

that finally gives:

$$\begin{aligned} \Delta p_{fan} &= \frac{1}{2} v^2 (1 - \frac{1}{k^2}) + (p_{Atm} - p_c) \\ &= (p_{Atm} + \frac{1}{2} v^2) - (p_c + \frac{1}{k^2} \cdot \frac{1}{2} v^2) \\ &= p_{t_{out}} - p_{t_c} \end{aligned} \tag{31}$$

that is equal to the fan pressure p_f as measured according to the Standard [11]. Equation 31 can be written also as:

$$\begin{aligned} \Delta p_{fan} &= (p_{Atm} - p_c - \frac{1}{k^2} \cdot \frac{1}{2} v^2) + \frac{1}{2} v^2 \\ &= p_{sf} + p_{df} \end{aligned} \tag{32}$$

showing that the Δp_{fan} is equal to the sum of the fan static pressure (total-to-static) and the fan dynamic pressure.

2.4 DIMENSIONLESS PARAMETERS

The need of comparing the performance of fans with different size and rotational speed requires the conversion of the fan parameters in a dimensionless form. Provided that the Reynolds number is above a critical value (e.g., $Re_c \gtrsim 2 \cdot 10^4$, see [27]), the dimensionless characteristic curves of a given fan are generally assumed as representative of the characteristics of any geometrically similar fan [28, p. 10]. Several dimensionless coefficients are used in the fan literature for the same parameter; this unpleasant situation seems to be embedded since many years [7, p. 200]. The dimensionless coefficients used in this work are defined as follows:

$$\begin{aligned} \Phi &= \frac{q_v}{(\pi \frac{D^2}{4})(\frac{\pi n \cdot D}{60})} = \frac{v_a}{\omega R} \\ \Psi_f &= \frac{p_f}{\frac{1}{2}\rho(\omega R)^2} \\ \Psi_{sf} &= \frac{p_{sf}}{\frac{1}{2}\rho(\omega R)^2} \end{aligned} \tag{33}$$

These dimensionless coefficients are coherent with the works [5, 15, 18, 29], but not with the ISO Standard [11]. They have been chosen for two reasons: *i)* their immediate physical sense (they represent ratios of intuitive velocities and velocity pressures), and *ii)* according to the specific performance, they generally span the range 0-1 (a fundamental property of normalized variables [30]). The flow coefficient Φ is related to the annulus mean flow coefficient Λ by the following:

$$\Lambda = \frac{\Phi}{1 - v^2} \tag{34}$$

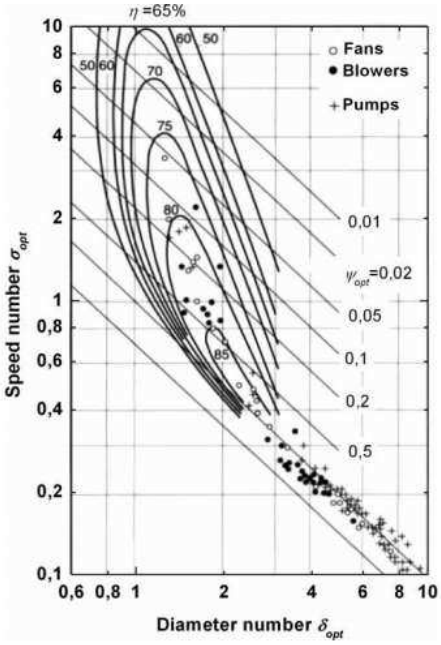

Figure 13: The Cordier Diagram from the original Publication [31].

While Φ represents the operational duty of the entire fan, Λ is useful for the design of the blading [15, p. 142]. In addition, specific speed and diameter are largely used in the turbomachinery field as well:

$$\sigma = (2\pi^2)^{0.25} \frac{\frac{n}{60} \cdot q_v^{0.5}}{(\frac{\Delta p}{\rho})^{0.75}} \qquad (35)$$

$$\delta = \frac{D \cdot (\frac{\Delta p}{\rho})^{0.25}}{(\frac{8}{\pi^2})^{0.25} \cdot q_v^{0.5}}$$

A physical interpretation of these last parameters is provided in [29]. In particular, the coefficients σ and δ are used in the well-known Cordier Diagram for turbomachines ([31] and see Fig. 13), that is the subject of the following Section. Specific speed and specific diameter can be linked to the flow and pressure coefficients, as follows:

$$\sigma = \frac{\Phi^{0.25}}{\psi^{0.75}}; \quad \delta = \frac{\psi^{0.25}}{\Phi^{0.5}} \qquad (36)$$

Notice that a generic pressure rise Δp has been used in Eq.s 35: the reasons are reported in the next Paragraph.

2.5 THE TYPICAL AXIAL FAN RANGE AND THE CORDIER DIAGRAM

The original diagram by Cordier [31], dated 1953 and based on experimental performance at "*optimum*" operation, is presented in Fig. 13. Its principal

meaning was providing turbomachine designers with a tool to select the suitable type of machine (centrifugal or axial) for the required application [32, p. 16]; in particular, axial fans and blowers are reported for specific speeds $\sigma > 0.4$ [5]. Nonetheless, some authors (e.g., [5, 33]) use directly the diagram in the design process as well, obtaining the machine rotational speed n for a given diameter D or vice-versa. However, both Wallis [12, p. 178] and Osborne [15, p. 38] report that this procedure is sparingly used for fans. The likely reason is that the rotor speed and the fan diameter are usually not freely available design variables (i.e., they are imposed). Major fan manufacturers are expected to have their own Cordier-type diagram [32], being part of the manufacturer's intellectual property.

The Cordier diagram represents a milestone in the history of turbomachine development and is still a reference for any low-speed fan and pump designer. Recalling the definitions of specific speed and diameter (Eq. 35), the explanation underneath the Cordier line (i.e., the line that best interpolates the data of Fig. 13) is that for a given couple of requirements (flow-rate and pressure rise) there is an optimum bijective relation between the machine diameter and the rotor speed. In other words, there is a (mean) velocity triangle that will achieve the required operation with higher efficiency with respect to all the others possible.

The main problem related to the original Cordier Diagram is that it is not specified whether the specific speed and diameter were calculated with the fan pressure p_f or with the static one p_{sf} [5, 34]. However, looking at the efficiency magnitudes presented along the range of axial machines ($\sigma > 0.4$) in Fig. 13, they are too high to have been obtained with fan static pressures, as will be discussed more in detail in Chapt. 4.
In this work specific speed σ and diameter δ are computed with the fan pressure p_f. Using Eq.s 36, Lewis [32, p. 18] replotted the Cordier-line (i.e., the mean line that best fits the scattered points within Fig. 13) in terms of the flow and pressure coefficients. In the same reference, recalling the information reported in [28], the range of the operational duties of the axial fans obtained from a statistical analysis was provided as well; both these indications are reported in Fig. 14.

Outside the Axial fan area (denoted with the solid line in Fig. 14), the right hand side should represent the range of propeller fans (axial fans with a short casing, called partition fans in [6]), while operational points on the top left corner of the plot should pertain to mixed and centrifugal machines [32] (even if centrifugal fans actually cover a much wider area, see [28]).

2.6 RADIAL EQUILIBRIUM AND AXIAL VELOCITY DISTRIBUTION

When radial equilibrium exists there is no motion along the radial direction and the flow develops along cylindrical surfaces. Such behavior can be easily observed using tufts at the exit flange of a rotor-only fan (Fig. 15) For

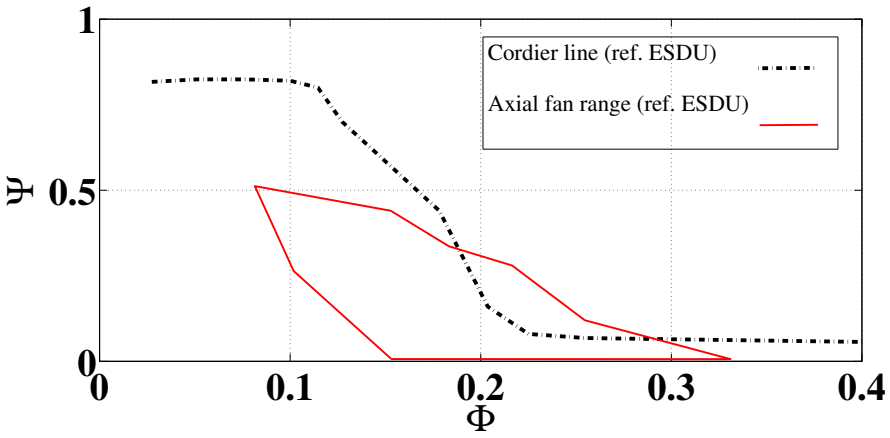

Figure 14: The Cordier line and the Axial fan range according to [28].

such equilibrium to exist, it is necessary that the following condition subsists for the generic fluid element:

$$\frac{dp}{dr} = \rho \frac{v_u^2}{r} \tag{37}$$

The most familiar vortex flow is the free-vortex one, in which the tangential velocity (swirl) develops according to $v_u(r) = \frac{K}{r}$, being K a suitable constant. Free-vortex flows can be generated providing an iso-energetic distribution along the radius and feature the peculiar characteristic of a constant axial velocity $v_a = const.$ Nonetheless, there are infinite possible vortex flows, according to the swirl distribution $c_u(r)$ generated by the blade (notice that velocities within ducts are identified with v, while velocities within the fan annulus with c). Radial equilibrium reestablishes at the blade exit, however the flow axial velocity is not constant along the radius (as is, on the contrary, in free-vortex cases).

The computation of the $c_a(r)$ distribution according to the vortex flow is a necessary step of an accurate fan design, to allow a proper computation of the velocity triangles along the blade. Such distribution can be obtained considering the total pressure difference between the upstream (sec. 1) and downstream (sec. 2) sides of the blade [35]. [7] For constant radial conditions at the blade inlet (e.g., with no upstream stator blades), the axial velocity distribution at the rotor exit (sec. 2) can be computed solving the integral of the following equation:

$$\rho c_{a2} \frac{dc_{a2}}{dr} = \rho\omega \frac{d(\eta_{tt} \cdot r \cdot c_{u2})}{dr} - \rho c_{u2} \frac{dc_{u2}}{dr} - \rho \frac{c_{u2}^2}{r} \tag{38}$$

The resulting velocity distribution shall also satisfy the continuity equation:

$$q_v = 2\pi \int_{r_h}^{R} c_{a2} r dr \tag{39}$$

7 This approach neglects the radial component of the velocity while considering the total pressure difference between the upstream and downstream side of the blade, see [35].

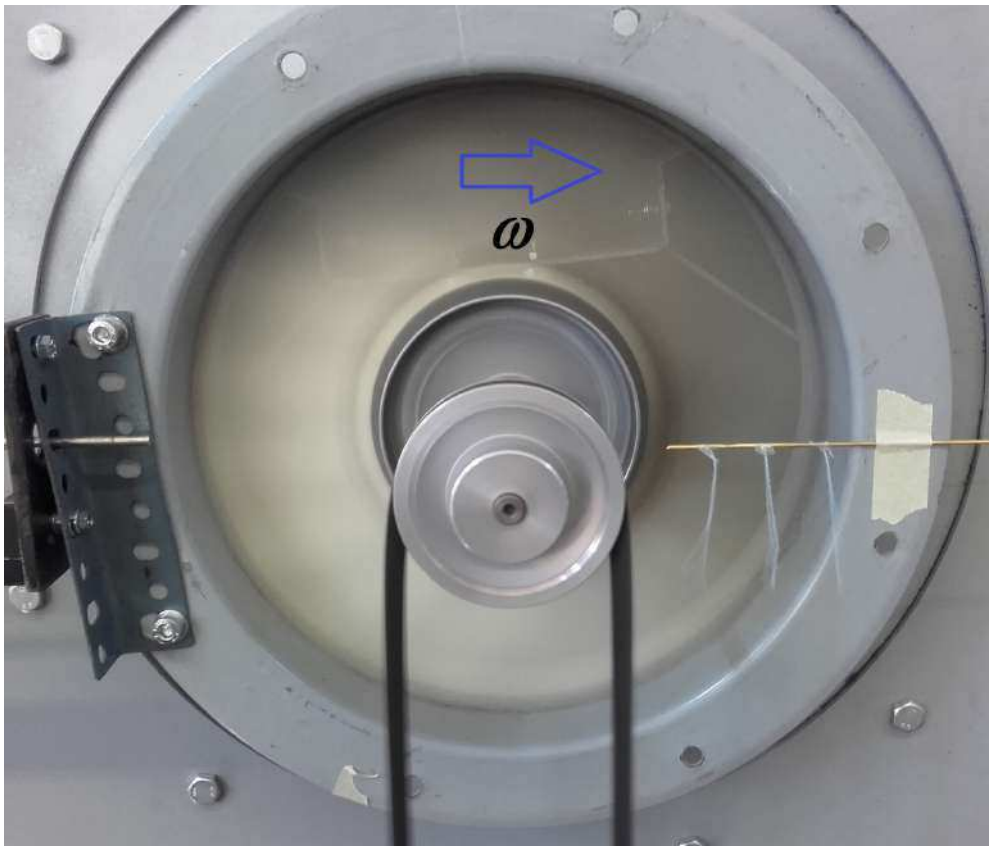

Figure 15: Radial Equilibrium at the exit of a Rotor-only axial fan. The tufts are almost parallel, indicating flow along cylindrical surfaces.

Equations 38 and 39 must be solved simultaneously to obtain the $c_{a2}(r)$ distribution.

2.7 LOADING FACTOR EQUATION

As reported previously, blading design for low-speed axial fans is based on the *Blade Element Momentum Theory*. The principal design formula derives from momentum considerations on an airfoil cascade and is referred as *Loading Factor* equation:

$$C_L = \frac{2}{\sigma \cos \beta_m} \frac{c_{a_m}}{} \frac{\Delta c_u}{w_m^2} - C_D \tan \beta_m \tag{40}$$

where

- c_{a_m} is the local mean axial velocity;
- Δc_u is the difference in terms of tangential velocity through the blade;
- w_m is the local mean velocity relative to the blade;

- C_L: is the blade element lift coefficient (with respect to the mean velocity w_m);
- $\sigma_{bl} = \frac{n r_{bl} \cdot ch}{2\pi r}$: is the local blade solidity;
- C_D: is the blade element drag coefficient (with respect to the mean velocity w_m);

Several formulations of Eq. 40 exist; this general form is presented as derived in [36, p. 19].

The Loading Factor equation is obtained neglecting the stress terms due to the blade element wake [12, p. 185]. However, it is extremely useful for blading design purpose, containing the basic ingredients of the blade design *inverse method*: the velocity angles $\beta_1, \beta_2, \beta_m$ obtained from the required velocity distribution (and thus, from the required pressure rise), the solidity distribution σ_{bl} (i.e., the chord length for a given number of blades) and the aerodynamic characteristics of the blade section C_L and C_D.

BIBLIOGRAPHY

[1] R. A. Wallis. "Definition and determination of fan duties". In: *Journal of the Institution of Heating & Ventilating Engineers* (May 1964), pp. 49–59.

[2] J Barrie Graham. "The importance of fan total pressure". In: *Heating, piping and air conditioning* 66.9 (1994), pp. 75–80.

[3] PEng John Cermak PhD. "Select fans using fan total pressure to save energy". In: *ASHRAE Journal* 53.7 (2011), p. 44.

[4] Brake DJ Rick. "Fan total pressure or fan static pressure: Which is correct when solving ventilation problems". In: *Mine Ventilation Society of South Africa* 55.1 (2002), pp. 6–11.

[5] Ph Epple, Franz Durst, and Antonio Delgado. "A theoretical derivation of the Cordier diagram for turbomachines". In: *Proceedings of the Institution of Mechanical Engineers, Part C: Journal of Mechanical Engineering Science* 225.2 (2011), pp. 354–368.

[6] International Standard Organization. *Fans - Vocabulary and definitions of categories (ISO 13349:2010)*. 2010.

[7] Hermann Glauert. *The elements of aerofoil and airscrew theory*. Cambridge University Press, 1926.

[8] R. A. Wallis. "Fan Unit Definitions and Related Problems". In: *Journal of the Institution of Heating & Ventilating Engineers* 37 (May 1969), pp. 45–48.

[9] Michael Brendel. "Selecting Fans for Minimum Energy Consumption". In: *ASHRAE Journal* 57.8 (2015), p. 52.

[10] PEng John Cermak PhD and Michael Ivanovich. "Fan efficiency requirements for Standard 90.1-2013". In: *ASHRAE Journal* 55.4 (2013), p. 24.

[11] International Standard Organization. *Industrial fans - Performance testing using standardized airways (ISO 5801:2009)*. 2009.

[12] R Allan Wallis. *Axial flow fans and ducts*. Krieger, 1993.

[13] Frank Bleier. *Fan Handbook: selection, application, and design*. McGraw-Hill Professional, 1998.

[14] Archibald Bathgate McKenzie. "Axial flow fans and compressors". In: *Aerodynamic Design and Performance* (1997).

[15] William C Osborne. *Fans*. Vol. 1. Pergamon Press Oxford, 1966.

[16] Bottin B. *Conventional Wind Tunnels.* Lecture series on Introduction to Ground Testing facilities-Von Karman Institute, BEL, November 2016.

[17] EC. "COMMISSION REGULATION (EU) No 327/2011 of 30 March 2011 implementing Directive 2009/125/EC of the European Parliament and of the Council with regard to ecodesign requirements for fans driven by motors with an electric input power between 125 W and 500 kW". In: *Official Journal of the European Union* (2011).

[18] Konrad Bamberger. "Aerodyamic Optimization of Low-Pressure Axial Fans". PhD Thesis. Siegen, Ger: University of Siegen, 2015.

[19] Massimo Masi, Federico Fontana, and Andrea Lazzaretto. "On the Choice of Suitable Parameters for the Assessment of Industrial Fans Performance and Efficiency". In: *ASME Turbo Expo 2017: Turbomachinery Technical Conference and Exposition*. American Society of Mechanical Engineers. 2017, V001T09A007–V001T09A007.

[20] A Lazzaretto et al. "Confronto tra metodi di prova normalizzati per ventilatori". In: *Termotecnica* 54.9 (2000).

[21] Bruno Eck. "Fans". In: *1st English ed., Pergamon Press, Oxford* (1973), pp. 139–153.

[22] International Standard Organization. *Industrial fans - Performance testing using standardized airways (ISO 5801:2017)*. 2017.

[23] Stefano Castegnaro, Massimo Masi, and Andrea Lazzaretto. "Preliminary experimental assessment of the performance of rotor-only axial fans designed with different vortex criteria". In: *Proceedings of the XII European Turbomachinery Conference ETC12, Stockholm, Sweden*. 2017.

[24] Konrad Bamberger, Thomas Carolus, and Markus Haas. "Optimization of Low Pressure Axial Fans and Effect of Subsequent Geometrical Modifications". In: *Proc. Fan 2015* (2015).

[25] E Barton Bell. "Test of Single-Stage Axial-Flow Fan". In: *NACA Rep.* 729 (1942).

[26] Alberto Cavallini and Lino Mattarolo. *Termodinamica applicata*. Cleup, 1992.

[27] Masi Massimo, Castegnaro Stefano, and Lazzaretto Andrea. "Experimental Investigation on the effect of Reynolds Number on the efficiency of Single-stage Axial-flow Fans". In: Under Evaluation for *ASME Turbo Expo 2018: Turbomachinery Technical Conference and Exposition*. American Society of Mechanical Engineers.

[28] ESDU. *A guide to fan selection and performance*. Data Item 79037. London, GB: Engineering Sciences Data Unit, Apr. 1980.

[29] Reinhard Willinger and Michael Köhler. "Influence of Blade Loading Criteria and Design Limits on the Cordier-Line for Axial Flow Fans". In: *ASME Turbo Expo 2014: Turbine Technical Conference and Exposition*. American Society of Mechanical Engineers. 2014, V01AT10A002–V01AT10A002.

[30] Jean-Marie Buchlin. *THEORY OF MODELS. Dimensional Analysis and Similarity*. Lecture series on Introduction to Ground Testing facilities-Von Karman Institute, Belgium, November 2016.

[31] Otto Cordier. "Ähnlichkeitsbedingungen für Strömungsmaschinen". In: *BWK Bd* 6 (1953).

[32] RI Lewis. *Turbomachinery performance analysis*. Butterworth-Heinemann, 1996.

[33] Thomas H Carolus and Ralf Starzmann. "An aerodynamic design methodology for low pressure axial fans with integrated airfoil polar prediction". In: *ASME 2011 Turbo Expo: Turbine Technical Conference and Exposition*. American Society of Mechanical Engineers. 2011, pp. 335–342.

[34] Maria Teodora Pascu. "Modern Layout and Design Strategy for Axial Fans". PhD thesis. Ph. D. Thesis at Erlangen University, 2009.

[35] A Kahane. "Investigation of axial-flow fan and compressor rotors designed for three-dimensional flow". In: *NACA TN* 1652 (1947).

[36] Seymour Lieblein, Francis C Schwenk, and Robert L Broderick. *Diffusion factor for estimating losses and limiting blade loadings in axial-flow-compressor blade elements*. Tech. rep. National Advisory Committee for Aeronautics, Cleveland Lewis flight propulsion lab, 1953.

3 METHODS

This Chapter presents the numerical and experimental verification methods that have been used during the research to evaluate fan blading behavior, performance and efficiency. The numerical CFD model has been used to evaluate the *local* (i.e., the velocity field) and *global* (i.e., performance and efficiency) behavior of the fans that have been designed, before the manufacturing of the prototypes. The Standard facilities have been used for the experimental validation of the design indications as well as to obtain data that have been used in the construction of the fan databases that are presented in Chapter 4.

All the fan global performance (i.e., p_f and p_{sf}) and related efficiencies are defined and evaluated according to the ISO 5801 Standard. The numerical CFD model is presented first, followed by a description of the experimental apparatus.

3.1 NUMERICAL CFD MODEL

Due to their relative cheapness and rapidity, CFD simulations are used as a first verification step to evaluate whether the fan blading performs as expected, both in terms of local velocities at the rotor exit and fan characteristic curves. CFD usually provides an easier way of performing local analysis [1] (e.g., to evaluate the blade-surface pressure distribution) with respect to experiments. Furthermore, the aerodynamic behavior of *ideal* geometries (i.e., impracticable for structural or manufacturing reasons) can be evaluated and used as reference (for instance, to evaluate an analytic model that cannot take into account geometry modifications for structural reasons). In general, this is a peculiar important advantage of the numerical simulations with respect to experiments. Nonetheless, numerical results shall always be validated against experimental data, whenever these lasts are available.

The *RANS* (Reynolds Average Navier-Stokes) CFD model herein used has been proposed in [2]. This simplified model has been chosen as an appropriate compromise between computational effort and accuracy of the results. The model underwent a rather extensive validation on ducted-axial fans experimental performance, providing reliable results within the stable part of the fan characteristic and especially in proximity of the best efficiency duty ([2–4]).

The description that follows is limited to the model used for this investigation. The reader is referred to specific references (e.g., [5]) for a comprehensive and deeper treatise on the CFD subject.

All the computations were performed using the commercial code CD-Adapco StarCCM+© ver. 10.04.011- 12.02.010 on an Intel™ i7-5500U. Simulation time was usually around twenty-thirty minutes with a parallel computation on three cores.

3.1.1 Geometrical Domain

The domain is represented in Fig. 16. It is composed by a straight cylinder, whose basis are identified by the fan annular surface divided by the number of blades. Such geometry takes advantage of the periodicity of the physical system within the fan blading. The effects related to upwind components such as electric motor and struts are considered of minor entity and neglected accordingly.

The domain is subdivided in three regions (see Fig. 16): the *rotor* one that contains the rotating blade, and the two regions *upstream* and *downstream*. The three regions are connected at the planes 1 and 2. The inlet and outlet sections of the domain are positioned at four and six chord lengths ch_r upwind and downwind of sections 1 and 2, respectively [2]. In case of simulations on a Vane-axial fan, the fixed bladings would be positioned upstream or downstream of the *rotor* region and the domain dimensions changed suitably.

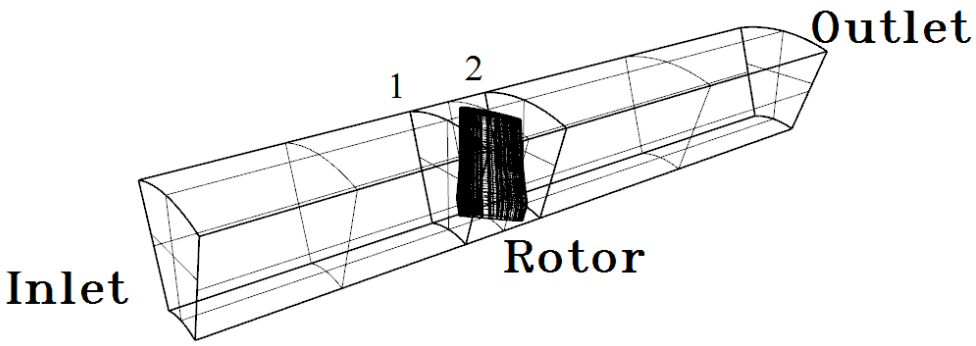

Figure 16: Geometrical Domain for CFD simulations. Notice the subdivision into three regions and the fan blade within the Rotor one.

All the dimensions of the domain are parametric with respect to the chord length at the blade root ch_r (see Tab.2). In particular, the rotor region depth is equal to the projection of the chord length at the blade root ch_r, extended of $10\%ch_r$ on both upwind and downwind sides. The tip clearance is omitted (i.e., the surface develops from the lower surface of the domain continuously to the upper one), to provide a comparison with the performance and estimation model presented in Chapt. 6 that cannot take directly into account tip-clearance effects. Simulations with the actual blade tip-clearance have been performed as well, showing the typical decrement of both fan performance and efficiency and a better estimation of the fan characteristic.

All the geometries are imported in STAR-CCM+ as *step* files.

Table 2: Dimensions of the geometrical domain

Upstream	$\simeq 4 \cdot ch_r$
Rotor	$ch_r \cdot \cos(\xi) + 0.2 \cdot ch_r$
Downstream	$\simeq 6 \cdot ch_r$

3.1.2 Grid

The entire domain has been meshed using an unstructured polyhedral grid. Such solution offers the benefits of: *i)* a quick automatic grid generation even on complex geometries, *ii)* a progressive refinement of the grid only in proximity of the blade, thus reducing the overall number of cells. Both the aspects represent an important advantage for the fan designer, who is allowed to spend rather little time on both the domain geometry construction and the grid generation. Furthermore, the reduced number of cells with respect to an hexahedral solution translates into a reduced simulation time. A specific grid refinement has been necessary according to the airfoils used, to ensure a proper local reconstruction of the blade profile, in particular at the blade leading edge and trailing edge.

Grid independence

For each simulation, tests with subsequent grid refinements have been performed to ensure that the results were not dependent of the grid. The number of cells to achieve the grid-independence varies according to the fan geometry, size and turbulence model. As an indication, 235000 cells were used with the $k-\omega$ model to successfully estimate the characteristics of a 10 blade 315 mm diameter rotor-only fan in [6]. The largest part ($\simeq$ 95%) of the cells were located within the *rotor* region.

3.1.3 Physical Model

The fluid domain is modeled as incompressible air at standard conditions.

BOUNDARY CONDITIONS A mass airflow equal to $\frac{\rho \cdot q_v}{n r_b}$ is imposed at the inlet surface of the domain (see Fig. 16). A gauge pressure of 0 Pa is imposed at the outlet side (i.e., $p_{out} = p_{atm}$). The *slip* condition is applied at the upper and lower surfaces, avoiding the generation of the boundary layer and allowing for wall velocities different than zero. Periodic conditions are imposed on the lateral surfaces, thus copying the fluid conditions from one side to the other. The *no-slip* condition is applied at the Solid surfaces (i.e., the blade, the hub, and the casing). Other parameters feature the default STAR-CCM+ value.

3.1.4 Numerical Model

The simulation is three-dimensional and stationary. The fan rotating motion is modeled with the *moving reference frame* option [7], that is applied uniquely at the *rotor* region except for the fan casing that is fixed. Accordingly, in the rotor region the fluid-motion equations are solved with respect to a reference frame that is rotating at the same speed of the rotor. The segregated solver was used with a second order upwind scheme and the simple-type algorithm.

3.1.5 Turbulence Model

The $k-\omega$ turbulence model was retained the approach that provided grid independence with the lowest number of cells [4]. This model was used for most of the simulations with a *low y+* approach [7], that avoids the use of *wall-functions* even in proximity of the walls. Such approach required a careful refinement of the prismatic grid layer, to ensure $y+ \simeq 1-3$ on the walls of the blade and of the hub.

Because of the relative low-speed conditions, regions with a laminar boundary layer might exist in the front part of the blade sections, close to the leading edge. In such regions, the simulations with turbulence models as the $k-\omega$ might fail the prediction of wall stresses τ as well as the detachment of the laminar sublayer. It is not ensured that such laminar conditions exist on actual operating fans, due to blade surface imperfections and to the relatively high turbulence intensity upstream of the rotor [8]. However, the use of a *turbulence suppression model* [7] has been evaluated in [6]. Such approximated approach nullifies the turbulence parameters within a given region of the domain. In terms of the fan characteristics, the CFD model with the turbulence suppression approach provided a better prediction of the fan behavior in proximity of the blade stall with respect to the fully-turbulent model.

3.1.6 Estimated parameters

Pressure and velocities are detected upstream and downstream of the rotor, at sections 1 and 2 respectively (see Fig. 17). According to the Standard [9] the *fan pressure* and the *fan static* (total-to-static) *pressure* are computed once again as

$$p_f = p_{t2} - p_{t1}$$
$$p_{sf} = p_2 - p_{t1}$$

In particular:

- the inlet total pressure p_{t1} is computed as a mass-flow average;
- at section 2, the static pressure p_2 is computed as average on the cross-sectional area.

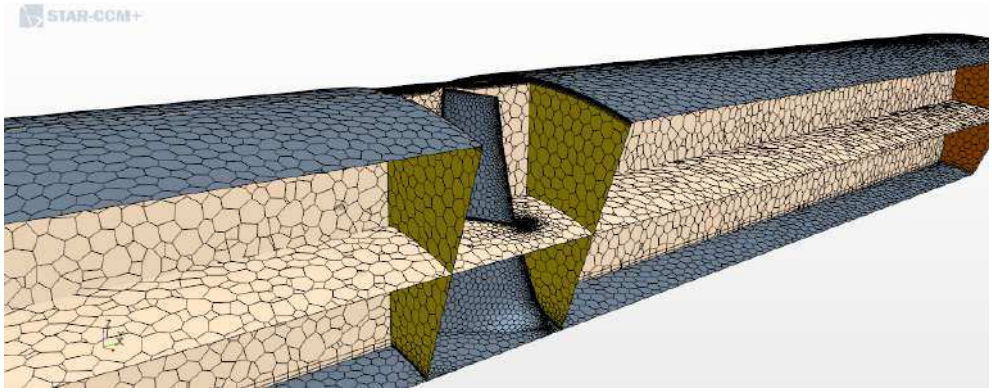

Figure 17: Particular of the sections 1 and 2 where pressure and velocities are computed.

- the fan dynamic pressure $p_{df} = \frac{4q_v}{\pi D^2}$ is summed to p_2 to compute the total pressure p_{t2}.

The first simulation is performed at the design flow-rate and is considered concluded when the residuals are lower than 10^4 and feature a constant trend. After that the mass flow-rate q_m is augmented or reduced and the simulation repeated, thus detecting several point on the stable part of the fan characteristic.

3.2 EXPERIMENTAL APPARATUS

The purpose of the experimental tests was obtaining the fan characteristic curves as well as performing local observations on the flow field in proximity of the fans. The experimental facilities and instrumentations that have been used within the research are presented in this section. Only the peculiar aspects of the experimental apparatuses are described; the reader is assumed to be familiar with the ISO 5801 Standard procedure.

The two test rigs installed in the *Laboratorio di Macchine Aerauliche e Termiche* of the University of Padova have been used. Both the rigs feature the inlet-chamber configuration and have been designed and built according to the ISO 5801 Standard [9]. Due to the relatively low-pressure rises generated by the axial fans tested, incompressible conditions can be assumed. Accordingly, the simplified method for $Ma_{2_{ref}} \leqslant 0.15$ and $p_f < 2000Pa$ has been used [9, pp. 50;129] to compute the fan characteristics from the measured parameters.

As most of the fans that have been tested are prototypes manufactured with the *3D printing Fused Deposition Modeling* technique, some insights on the dimensional accuracy of the manufacturing technique are provided at the end of the Chapter.

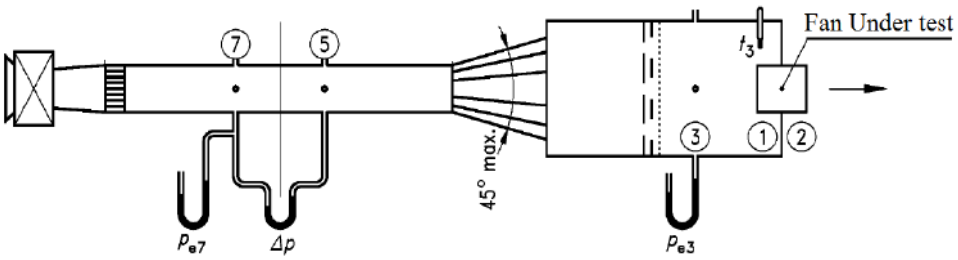

Figure 18: Scheme of the medium-size rig (adapted from [9]).

Twenty-two different fans have been tested since the beginning of the research, most of them featuring the tube-axial variable-pitch configuration. With the variation of the blade positioning angle and, for some rotors, of the tip clearance, the total number of experimental tests counts more than one hundred cases.

3.2.1 Medium Test Rig

The medium-size test rig for fan testing is shown in Fig. 8; the main components are visible in the scheme of Fig. 18. It is here referred as *medium* due to the presence in the Laboratory of a third smaller outlet-chamber test rig that is normally used to test cross-flow fans (e.g., [10]). The medium test bench features a *type* 2 inlet-chamber [9] with pressure tappings on the walls; the flow rate is measured with orifice plates in the upstream duct. Due to the chamber dimension, the maximum fan diameter under test is constrained to 480 mm. Moreover, the maximum flow-rate is limited at 0.325 $\frac{m^3}{s}$, due to the inlet duct dimensions. Obtaining the dimensionless characteristic curves at the higher flow coefficients was only achievable by reducing the fan rotor speed, as performed for instance in [11]. However, this occurrence reduces the Reynolds number with consequent detrimental effects on fan performance and efficiency, as will be show in Par. 5.2. For a 315 mm fan, the maximum Reynolds number allowed is $Re_u \simeq 450000$ (computed on the fan diameter D and the blade tip speed U). The Reynolds number computed on the blade chords is an order of magnitude lower.

3.2.2 Large Test Rig

The large test rig (see Fig. 19) has been specifically built to avoid the problems of fan size and flow-rate limitations encountered with the medium-size rig. A further minor requirement was allowing for a quick change of the fan under test. Thus, the large-rig allows the testing of fans up to D =

800 mm (according to the 2009 version of the Standard [9])[1] with flow-rates higher than 8 m^3/s.[2].

The main functional difference with respect to the medium-size rig is the use of a multi-nozzle system for the flow-rate measurements (instead of the orifice plates). Accordingly, a *type 3* inlet-chamber has been designed and the total pressure within the chamber is directly measured with a pitot tube (see [9, p. 125]). The entire design and commissioning of the rig is presented in [13].

Comparative tests have been computed testing the same 315 mm fan at the same rotational speed on both medium and large rig. The comparison showed good agreement on pressure and efficiency curves, demonstrating a satisfactory experimental repeatability.

3.2.3 Measurements and Instrumentation

The instrumentation is the same for the two test rigs (see Tab. 3). Most of the instruments are of the analogue type, providing the advantage of an easier and direct calibration with respect to digital instruments. In turn, the tests cannot be automatized and need the presence of one or two experimenters.

The fan characteristic is built as a curve of point-wise measurements, with each observation lasting at least for a minute. For each point of the characteristic the following measurements are taken:

- fan shaft rotational speed n, [rpm]
- fan shaft torque T_a, [Nm]
- gauge pressure upstream of the differential flow-meter (p_{e7} according to the Standard, see Fig.s 18 and 19), [Pa]
- differential pressure between the flow-meter sides (Δp according to the Standard), [Pa]
- gauge pressure in the chamber (p_{e3} according to the Standard).[3]

The impeller torque T_r (i.e., the aerodynamic torque) is obtained from the measurement after subtracting the ball-bearing frictional contribution [9]. The environmental conditions in the laboratory are measured as well:

- barometric pressure p_{atm}, [Pa]
- dry bulb temperature T_d [K]

1 The latest version of the Standard [12] reduced the testable inlet diameter to 700 mm; see also [13]

2 The ISO 5801 Standard considers the 800 mm size as the first diameter for *large* fans. The maximum flow rate tested so far is $q_v \simeq 3.7 \frac{m^3}{s}$

3 This is a static pressure for the medium-rig *type 2* chamber (that uses the wall pressure tappings), and a total pressure for the *type 3* chamber of the large rig (that uses the pitot-tube).

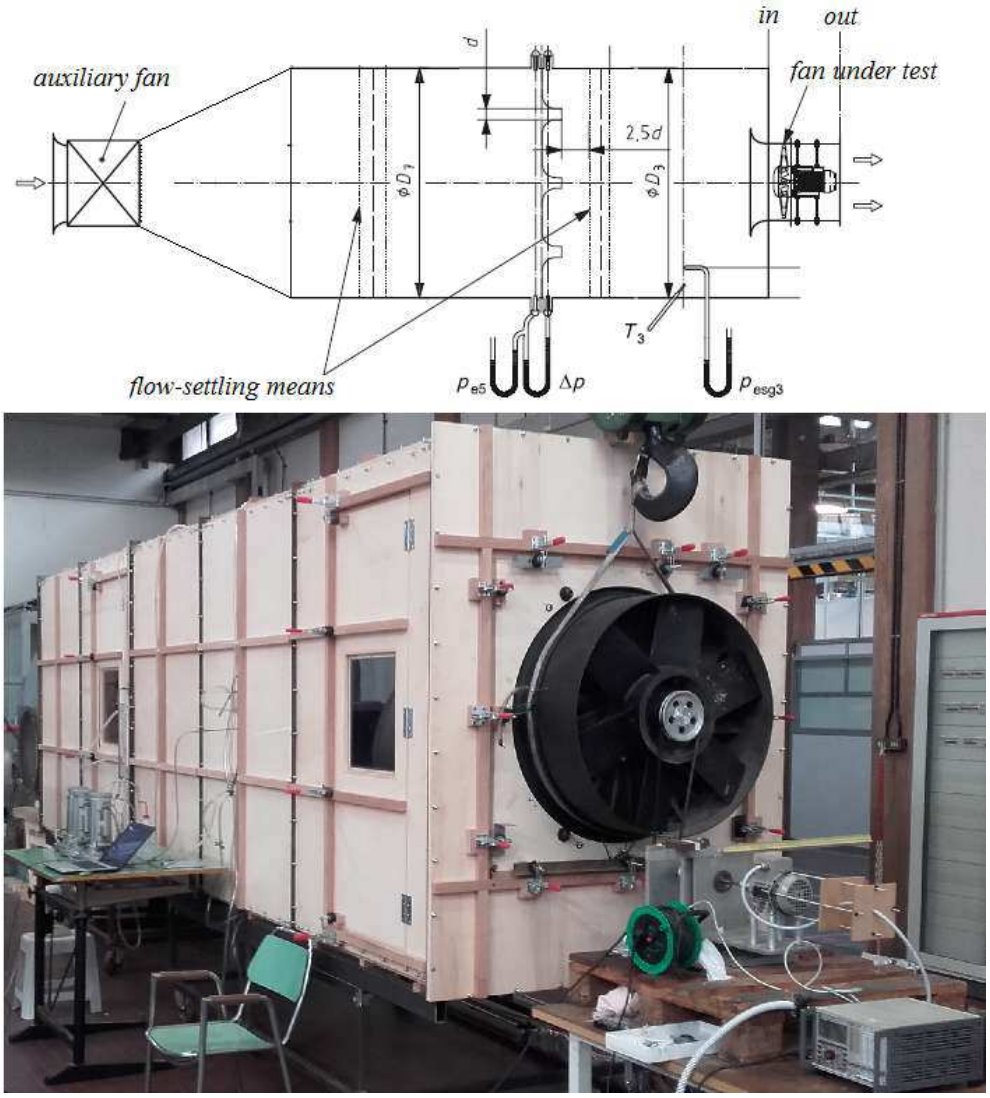

Figure 19: The large test rig (end-wall chamber side) and related scheme (adapted from [9]). The picture shows a 800 mm *PR* fan under test.

Figure 20: The torque crane used to measure the shaft torque T_a, installed on the medium-size rig.

- wet bulb temperature T_w [K]

at the beginning, during, and at the end of the test and averaged. Due to the relatively large size of the laboratory, the air parameters are mostly stable.

Table 3: Instruments with estimated accuracy at 90% confidence level.

Revolutions counter	Hasler Bern®	± 2	[rpm]
Water micro-manometers	Regulator Spa®	± 0.5	[Pa]
Thermometers	–	± 0.2	[K]
Digital Barometer	Texas Instrument®	± 100	[Pa]
Digital bubble level	–	± 0.3	[°]
Torque-crane weight distance	–	± 5	[mm]
Digital mass scale	Acculab®	± 0.5	[g]

TORQUE MEASUREMENTS The shaft rotor torque T_a is measured with the custom-built torque-crane (see Fig 20) on which the electric motor is mounted. The arm of the crane is leveled shifting the weights during the measurements. A digital bubble level is installed over the arm. The weights are measured at the beginning of each test. The rotor torque is transferred to the fan shaft through a pulley-belt system. According to the standard [9], the impeller torque T_r (i.e., the aerodynamic torque) is obtained subtracting from the measured shaft torque T_a the *parasite* torque T_{par} generated from the shafts' ball-bearings, the pulley-belt system and the motor cooling fan. The contribution T_{par} is measured at the end of each test removing the fan and running the system at the same speed alone. This procedure could not be used for the 800 mm rotor (due to its excessive weight), whose efficiency refers to the shaft torque T_a, therefore.

FLOW VISUALIZATION During the tests, the evolution of the flow field at the rotor exit is observed by using tufts positioned at different radial heights (see Fig. 15).

Table 4: Minimum Relative Experimental Uncertainty [9].

Atmospheric Pressure	± 0.2%
Ambient Temperature	± 0.2%
Humidity	± 0.2%
Gauge/differential pressure	± 1.4%
impeller rotational speed	± 0.5%
nozzle/diaphragm throat diameter	± 0.1%

Table 5: Uncertainty estimation for the results of a *demanding*-case test at the large test rig (D = 315 mm, 1000 rpm.)

u_n	± 0.20%
u_{p_f}	± 3.03%
u_{q_m}	± 1.97%
u_{T_r}	± 1.86%
u_η	± 4.07%

3.2.4 Experimental Uncertainty

All the instruments of Tab. 3 comply with the requirements of absolute accuracy of the ISO 5801 standard.[4] The uncertainty estimation is performed for each test according to the indications of [9, pp. 64-65] and [15, p. 18]. The *absolute* experimental uncertainties u in Tab.3 are related to the measurements in proximity of the fan peak efficiency to compute the *relative* uncertainty [9]. Thus, the estimation of the uncertainty varies according to the machine under test (with higher uncertainties on smaller fans running at low speeds). During each test, effort has been put into respecting the values of tab. 2 ([9, p. 64]). In some *demanding* cases (small fans running at speeds $\leqslant$ 1000rpm) the experimental tests have been repeated up to four times to enable a statistical post-processing of the results, thus decreasing the result uncertainty. As reference, the uncertainty estimation for the results (at peak efficiency [9]) of a single test performed at the large test rig on a 315 mm 10 blade rotor-only fan running at 1000 rpm are reported in Tab. 5

3.2.5 Fan Prototypes

Several of the tested fan rotors have been manufactured with a *3D* Fused Deposition Modeling technique. The blades and the rotor are manufactured separately and subsequently assembled (see Fig. 21) due to the production dimensional limits. This rapid prototyping technique builds the CAD drawing through the deposition of a fused polymer wire (ABS) along succeeding planar paths. The fused adjacent wires join together originating the final

4 This is another reason that favored the analog instrumentation with respect to the digital one. In particular, the micro-manometers feature a resolution that is 50-100 times higher than most of the pressure sensors available on the market. As a matter of fact, micro-manometer are generally used to calibrate other instruments rather than for direct measurements [14].

Figure 21: A 315 mm arbitrary-vortex 3D printed rotor with $\nu = 0.32$.

shape. The dimensional uncertainty declared by the manufacturer is 0.1 mm on the chord length and 0.25 mm on the blade height; the minimum feasible dimension is 0.2 mm. No dimensional differences have been measured with respect to the nominal dimensions. The surface roughness has been measured along the radial direction and along the chords for three different blades. Measurements provided constant values of $Ra_{rad} = 18.6\,\mu m$ and $Ra_c = 11.4\,\mu m$.

The anisotropic structure that results from the manufacturing technique does not permit an immediate verification of the mechanical stiffness of the 3D-printed blades. Preliminary computations under the assumption of isotropic mechanical behavior ensured that for the 315 mm fans the blade shape is maintained under the typical loading conditions experienced during a test.

BIBLIOGRAPHY

[1] JH Horlock and JD Denton. "A review of some early design practice using computational fluid dynamics and a current perspective". In: *Transactions of the ASME-T-Journal of Turbomachinery* 127.1 (2005), pp. 5–13.

[2] M Masi and A Lazzaretto. "CFD models for the analysis of rotor-only industrial axial-flow fans". In: *Proceedings of FAN 2012 Conference. France*. 2012.

[3] S Castegnaro. "Effects of NACA 65-blade's Trailing Edge Modifications on the Performance of a Low-speed Tube-axial Fan". In: *Energy Procedia* 82 (2015), pp. 965–970.

[4] Massimo Masi, Manuel Piva, and Andrea Lazzaretto. "Design guidelines to increase the performance of a rotor-only axial fan with constant-swirl blading". In: *ASME paper GT2014-27176* (2014).

[5] Jiyuan Tu, Guan Heng Yeoh, and Chaoqun Liu. *Computational fluid dynamics: a practical approach*. Butterworth-Heinemann, 2012.

[6] Stefano Castegnaro. "Incremento delle prestazioni di pale a vortice arbitrario per ventilatori assiali a sola girante: verifica sperimentale e numerica". In: *MS Thesis-University of Padova* (2014).

[7] STAR-CCM User Guide. *version 8.02. 011*. 2013.

[8] RA Wallis. "The F-series aerofoils for fan blade sections. The Institute of Engineers Australia". In: *Mechanical Engineering Transactions* (1977), pp. 12–20.

[9] International Standard Organization. *Industrial fans - Performance testing using standardized airways (ISO 5801:2009)*. 2009.

[10] M Spinola et al. "Effect of Reduced Suction Side Volume on Cross-Flow Fan Performance". In: *Proceedings of FAN 2015 Conference. France*. 2015.

[11] RJ Downie, MC Thompson, and RA Wallis. "An engineering approach to blade designs for low to medium pressure rise rotor-only axial fans". In: *Experimental thermal and fluid science* 6.4 (1993), pp. 376–401.

[12] International Standard Organization. *Industrial fans - Performance testing using standardized airways (ISO 5801:2017)*. 2017.

[13] S Castegnaro, M Masi, and A Lazzaretto. "Design and Testing of an ISO 5801 Inlet Chamber Test Rig and Related Issues with the Standard". In: Under Evaluation for *Proceedings of FAN 2018 Conference. Germany*. 2018.

[14] Schram C. *Unsteady Pressure Measurements*. Introduction to Measurement Techniques, Lecture Series -Von Karman Institute. 2016.

[15] British Standard and BSEN ISO. “Measurement of fluid flow by means of pressure differential devices-BS EN ISO 5167-1”. In: (2003).

4 PERFORMANCE CHARTS FOR DESIGN PURPOSE

This chapter treats two aspects that are at the basis of any fan design: the selection of the fan configuration and the swirl distribution.

One of the first tasks in a new design is the selection of the fan configuration among rotor-only, rotor-straightener, preswirler-rotor, etc. Ideally, the configuration that achieves the requirements with the highest efficiency should be selected. Fan designers generally perform this task on the basis of their experience, while the literature provide only partial information on the subject. The information presented in this Chapter provide the reader with theoretical and empirical guidelines to select the axial fan configuration.

Sometimes limitations on the fan length or purchase costs oblige for the adoption of the rotor-only fan layout. Whether the rotor speed is also limited (e.g., for acoustic purposes), the achievement of the pressure requirement might necessitate blade design according to *non-free-vortex NFV* distributions. Thus, the selection of the suitable design vortex distribution for Rotor-only fans is treated in the second part of the Chapter. A brief discussion on the application of *NFV* distributions on stator-vane machines is included as well.

4.1 SELECTION OF THE AXIAL FAN CONFIGURATION THROUGH A NEW CORDIER DIAGRAM

A new Cordier diagram is proposed to guide the selection of the Fan configuration. At first, the motivations that originated this investigation are presented, along with some issues related to the original Cordier diagram. The performance of each fan configuration as well as the experimental diagrams are reported next and explained.

A rigorous treatise of the argument is extremely difficult. According to the need of simplification, the discussion that follows assumes good fan conditions (i.e., low tip clearances and Reynolds number above the critical value).

4.1.1 Issues on the subject of Fan Configuration Selection

In the technical literature, the selection of fan configuration on the basis of the required duty is still an unclear argument. For instance, there are no general indications that state when leaving the Tube-axial configuration (i.e., rotor-only ducted fans) for the Vane-axial one (i.e., with stator vanes), or which is the most suitable configuration between the Preswirler-rotor and

the Rotor-straightener one. After an extensive study of the main international fan design references [1–6], it was concluded that the only available criterion to distinguish among the different configurations is the one based on the annulus flow coefficient Λ proposed by Wallis [1, p. 302]:

- $\Lambda < 0.2$ Rotor-only machines (i.e., without stator vanes).
- $0.2 \lesssim \Lambda \lesssim 0.4$ Fans with stator vanes (IGV or OGV), generally known as *Vane-Axial* fans.
- $\Lambda \gtrsim 0.4$ Contra-rotating Fans; Multistage units.

It is author's opinion that this criterion lacks somehow of completeness, as general indications on the selection of the fan layout should be based on both the main requirements of flow-rate and pressure rise (in terms of their dimensionless coefficients Φ and Ψ), instead of referring to Λ only, and target the highest possible efficiency. According to this need, an investigation has been performed to seek indications that could be summarized in the form:

$$\texttt{Fan Configuration} = f(\Phi, \Psi)$$

that means evaluating whether, in the operational range $(\Phi; \Psi)$ typical of axial fans, one configuration is more appropriate with respect to the others (in terms of efficiency and of eventual additional constraints).

The work also addressed a second vexed aspect related to the layout of Vane-Axial fans: the dichotomy between preswirler-rotor and rotor-stator machines (i.e., with IGV and OGV, respectively). Nowadays, the literature does not exhaustively clarify when the pre-swirler (IGV) should be employed instead of the straightener (OGV) when designing a new fan. All the referenced fan authors dedicate a section to this problem in their books [1–6]; however, the indications provided in favor of one layout or the other are mainly qualitative rather than quantitative. Furthermore, these indications are sometimes in contradiction: for instance, Wallis [1, p. 211] and McKenzie [3, p. 24] refer that preswirler-rotor fans are used when high-pressure rises are required, while Marcinowsky (in Eck, [4, p. 272]) states that this layout is preferred to the rotor-straightener one only in presence of low hub-to-tip ratios (i.e., low pressure rises) and low blade efficiencies.

4.1.2 Issues with the original Cordier Diagram

The Cordier diagram has been introduced in Par. 2.5 in relation to the typical operational range of axial fans.

In spite of the time-wise technical importance of this diagram, it is fair to highlight some issues related with it:

a) In the original Cordier diagram it is not specified whether the specific speed and diameter have been calculated with the fan pressure p_f or with the static one p_{sf} [7, p. 105] and related efficiencies [8]. The difference between p_f and p_{sf} increases with the flow-rate elaborated q_v and can be substantial for axial-flow fans.

b) The diagram presents 120 cases of centrifugal machines [8]. However, the number of fans and blowers in the range of axial machines (i.e., $\sigma_{opt} > 0.4$ [8]) is limited to 21.

c) The use of logarithmic axes graphically reduces the distinction between data (i.e., fans with substantially different performance graphically appear relatively close). This is particularly tedious in those areas of the graph where data-scatter is present (e.g., for $0.8 \leqslant \sigma_{opt} \leqslant 1.3$; see Fig. 13).

d) As anticipated, no indications of the fan configuration are reported, although Marcinowsky (in [4]) accomplished with including trends for the optimum hub-to-tip ratios within the diagram.

The most vexed aspect is the one reported in point *a)*. As reported previously however, focusing on the axial fan range (i.e., $\sigma_{opt} < 0.4$), the efficiency values reported in Fig. 13 are too high to refer to static ones. This evidence might suggest that the data within the diagram have been obtained referring to the fan pressure p_f, rather than p_{sf}. However, it is also possible that specific speeds and diameters have been computed with static (total-to-static) performance, while efficiency values refer to total ones (as this is the way some authors (e.g., [2, 9]) and manufacturers present fan characteristics).

4.1.3 Simple Analytical-Empirical approach to Fan Configuration Selection

The velocity triangles for each single-stage axial fan configuration are presented in Fig. 22. After studying all the indications on axial fan configuration selection, it was felt that a general method of configuration selection shall:

i) be related to the required duty Φ, Ψ and take into account fan efficiency considerations, as well;

ii) rely on theoretical basis;

iii) provide a numerous database of existing fans' performance related to the different layouts.

THEORETICAL CONSIDERATIONS According to the first two requirements, a simple mean-line analytical model that compares the performance of the three major single-stage fan configurations (i.e., Rotor-only, Rotor-straightener, and Preswirler-rotor) has been developed. On the basis of the Euler (inviscid) equation, the total pressure rise at the generic radius r for each machine configuration is given by the following Equations (see also [5]):

$$\begin{aligned} \text{Rotor} - \text{Only} \qquad & p_{t_{RO}} = \rho u c_{u2} - \frac{1}{2}\rho c_{u2}^2 \\ \text{Rotor} - \text{Straightener} \qquad & p_{t_{RS}} = \rho u c_{u2} \\ \text{Preswirler} - \text{Rotor} \qquad & p_{t_{PR}} = \rho u c_{u1} \end{aligned} \tag{41}$$

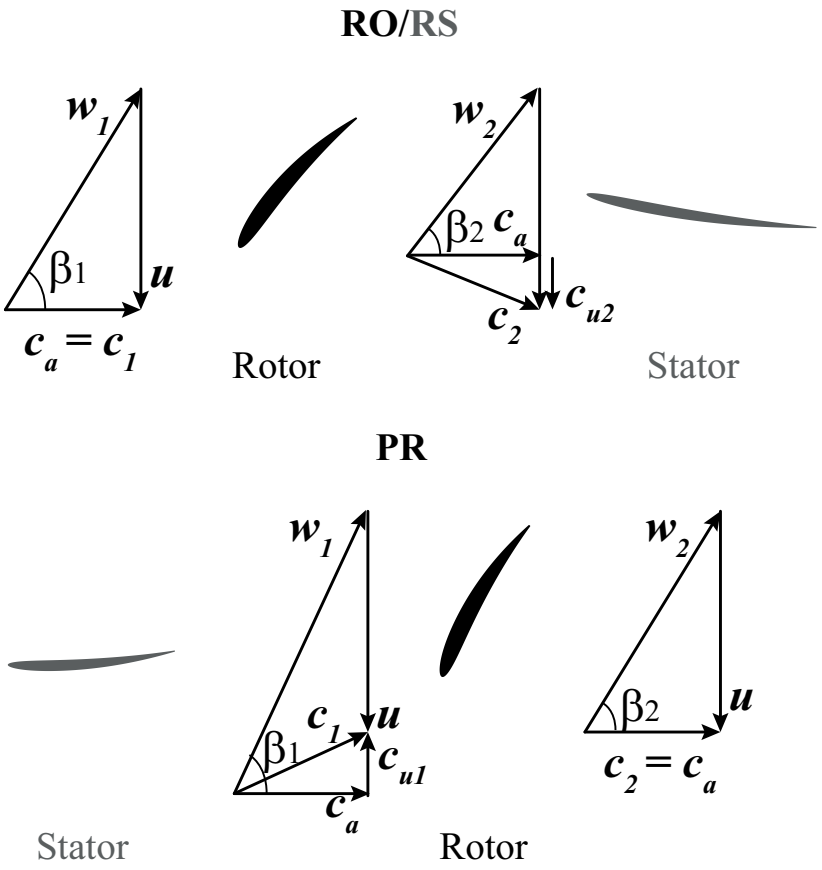

Figure 22: Velocity triangles at design condition according to the fan blading configuration.

Equations 41 have been obtained under the assumption that the second blade row (stator or rotor, according to the case), if present, is able to convert all the swirl component into static pressure, thus providing a purely axial flow at the annulus exit (Fig. 22). At the same time, Eq. 41 for the *RO* configuration assumes that there is no natural diffusion of the swirl component. Equations 41 have been applied at the mean radius r_{MS}, assuming the pressure rise at midspan *MS* to be representative of the performance of the entire fan and that the axial velocity c_a is constant along the radius (the algebraic developments are reported in Appendix A). Then, the pressure coefficient $\Psi = \frac{p_t}{0.5 \cdot \rho U^2}$ of each configuration has been expressed in terms of the flow coefficient Φ and of the fan geometry (ν and β angles) as follows:

$$\begin{aligned} \Psi_{RO} &= (1+\nu) \cdot \left[\frac{1+\nu}{4} - \left(\frac{\Phi}{1-\nu^2} \right)^2 \cdot \frac{(tan\beta_2)^2}{1+\nu} \right] \\ \Psi_{RS} &= (1+\nu) \cdot \left(\frac{1+\nu}{2} - \frac{\Phi}{1-\nu^2} \cdot tan\beta_2 \right) \\ \Psi_{PR} &= (1+\nu) \cdot \left(\frac{\Phi}{1-\nu^2} \cdot tan\beta_1 - \frac{1+\nu}{2} \right) \end{aligned} \tag{42}$$

Equations 42 can be applied within the Axial fan operational range $0.08 \lesssim \Phi \lesssim 0.4$ for *representative* geometries ν and β (i.e., that span the range of values commonly used in actual machines).[1] Accordingly, Eq.s 42 have been plotted in Fig. 23 for three ν values $(0.3, 0.5, 0.7)$, with three values for β_1 ($70°$,$75°$,$80°$) and for β_2 ($60°$,$70°$,$80°$). Observations on Fig. 23 are reported in the following:

- Each point of the curves of Fig. 23 represents the potential design point of a specific fan configuration.
- The curves pertaining to the Rotor-only and Rotor-stator configurations might represent also the theoretical characteristics of fans, under the assumption of the constancy of the exit flow angle β_2 with the flow coefficient Φ [3, p. 9] (on the basis of the Kutta-Joukowsky condition [1, p. 154]). At the same time, the points of the same curves might represent the performance of different fans (with same ν) that achieve the same β_2 angle at different Φ (for instance, changing the blade camber).
- *PR* Curves of Fig. 23 have been obtained at constant β_1 angles: each point of those curves represents the design performance of different PR bladings with equal hub-to-tip ratio ν.
- Three sectors can be identified within the Φ range of each graph of Fig. 23: one exclusive of the RO/RS fans (top-left zone), a central area ($0.1 \lesssim \Phi \lesssim 0.25$) where all the configurations are able to operate, and a third area exclusive of the PR fans, at relatively high flow and pressure coefficients (top-right zone). Such trends, thus, suggest that

1 Equations 42 and Fig. 23 do not take into account the eventual blade stall for excessive flow deflections $\theta = \beta_1 - \beta_2$ for some duty points.

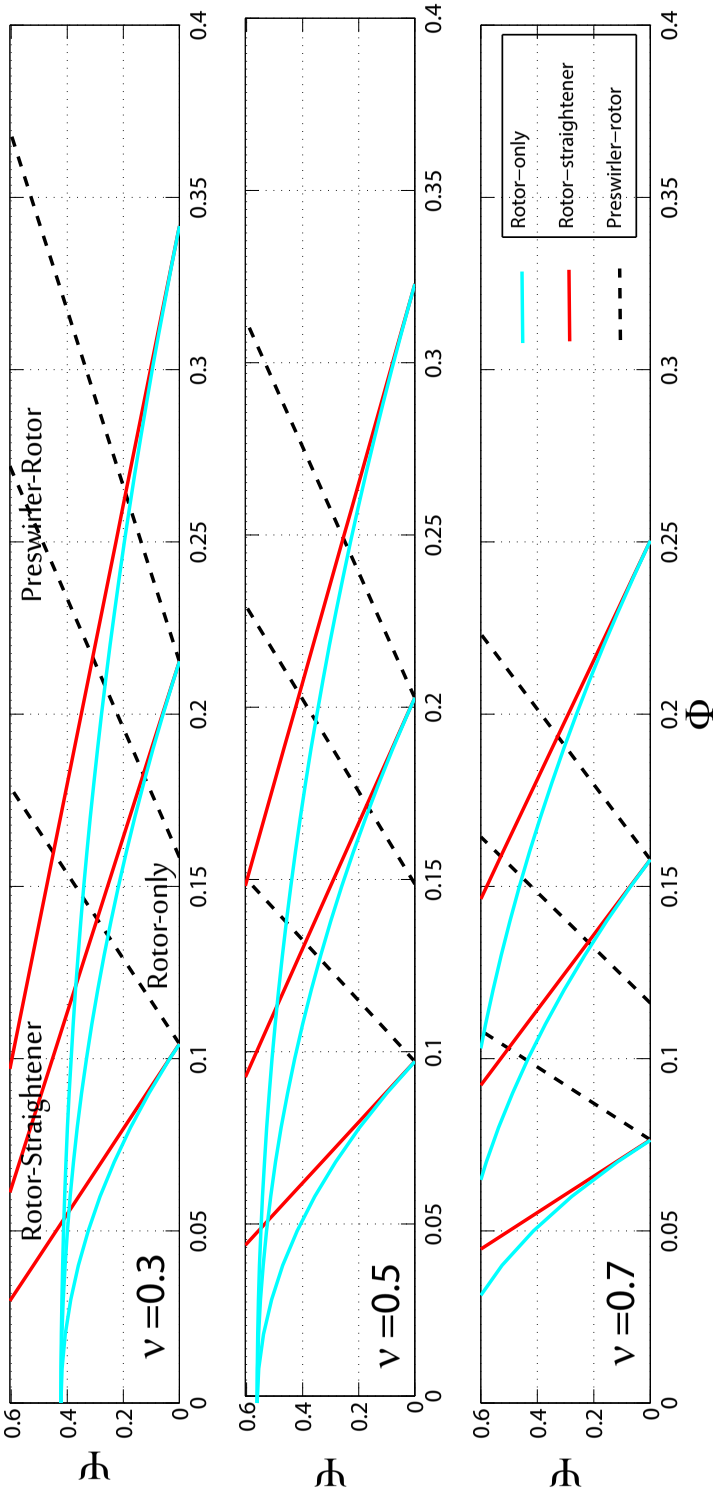

Figure 23: Theoretical Performance according to the Single-stage fan configuration.

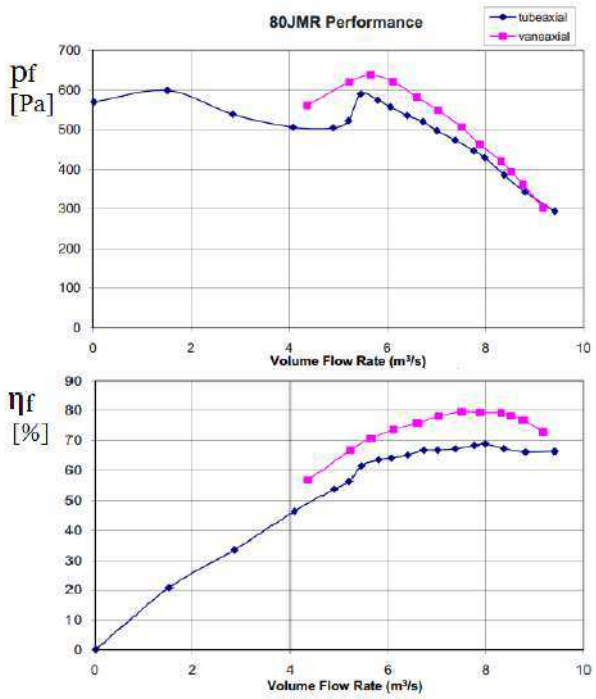

Figure 24: Tube axial vs Vane Axial fan performance using the same rotor; adapted from [10, p. 81].

the Preswirler-rotor configuration is the only layout that can deal with requirements of high pressure coefficients $\Psi \gtrsim 0.2$ and high flow-rates $\Phi \gtrsim 0.22 - 0.3$ at the same time. This is particularly evident for $\nu \leqslant 0.5$.

- As expected, Rotor-only units achieve lower pressure coefficients with respect to the Rotor-straightener configuration within the whole Φ range, due to the lack of recover of the swirl dynamic pressure. It is nonetheless interesting to notice that the difference in *ideal* performance (i.e., inviscid) between RO and RS fans appears negligible at low pressure coefficients ($\Psi \lesssim 0.2$). At higher pressure rises the difference becomes relevant due to the decrease of the slope of the $\Psi_{RO} = f(\Phi)$ curves (at given ν and β_2). This slope variation with decreasing Φ is due to the quadratic term inside the parenthesis of the first of Eq.s 42 and can be experimentally observed in the performance comparison between a tube-axial fan and the *correspondent* (i.e., using the same rotor) vane-axial geometry of Fig. 24.

- The operational difference between *PR* and *RS* configurations is reduced with the increase of the hub-to-tip ratio (Compare the upper and the lower graphs of Fig. 23).

Summarizing, on the basis of the inviscid Euler equation for turbomachines the potential operational sectors of each axial fan configuration have been crudely identified. Although simplified, this theoretical treatment provides the basis for the analysis of the experimental performance database that is

presented in the following paragraph. Fan configuration performance have been treated regardless of efficiency configurations; considerations on the subject are reported in the next Section.

EMPIRICAL GRAPHS According to the *iii)* point itemized previously, the performance (at design or best efficiency duty) of 47 axial fans (12 Rotor-only, 10 Preswirler-rotor, 19 Rotor-straightener and 6 Contra-rotating fans) have been collected and summarized in $\Phi - \Psi_f$ (Fig. 25) and $\sigma - \delta$ (Fig. 26) graphs. The fan data are tabulated in Appendix B.1. It is here remarked that these graphs were built considering *fan pressure* data (performance p_f and efficiency η_f) and with linear axes. Contra-rotating machines have been included as well for completeness, although being rigorously *multistage* machines.

The criteria for considering fan data into the data-base of B.1 and thus, into Fig.s 25 and 26, are: *i)* high-efficiency or *ii)* unique performance. According to the first criterion, the 11 Rotor-only fans that were presenting $\eta_f \geqslant 69\%$ have been extrapolated from [13]. The unique rotor-only exception is the DP1 fan [14], that was considered according to the unique performance criterion.

Referring at Fig.s 25 and 26, the following observations are reported:

- The axial fan operational range $\Phi - \Psi_f$ (Fig. 25) is approximately centered around the Cordier-line.

- The range of axial fans is markedly wider than what indicated in [11] (the red circled area of Fig. 25). In particular, the area identified in [11] misses most of medium and high-pressure machines that operate at flow coefficients $\Phi \geqslant 0.2$. Thus, it is likely that such area has been traced considering mostly Rotor-only machines, due to the statistical industrial predominance of this fan configuration.

- **Rotor-only** *RO* fans with $\eta_f \geqslant 70\%$ operate at pressure coefficients $\Psi_f \lesssim 0.2$. This is in accordance with the results obtained from the inviscid mean-line model (Fig. 23): at $\Psi_f < 0.2$ the absence of the straightener is negligible in terms of pressure-rise. However, it is still appreciable in terms of efficiency: *RO* fans maximum efficiencies are limited to $\eta_f \sim 75 - 78\%$. Such magnitudes are in accordance with most of the authors (e.g., [2, 5]).

  RO fans operate also at pressure coefficients $\Psi_f > 0.2$, as will be shown in Sec. 4.2; however, such machines suffer an excessive efficiency penalization with respect to the Rotor-Straightener fans. This penalization is mainly caused by the dissipation of the swirl component at the fan exit, see Fig. 23).

  With reference to Fig. 26, high-efficiency Rotor-only fans operate at $\sigma \gtrsim 1.4$. Moreover, most of the data pertaining to this configuration rely at higher specific diameters with respect to fans with stator vanes and contra-rotating machines. This means that a *RO* fan needs a larger

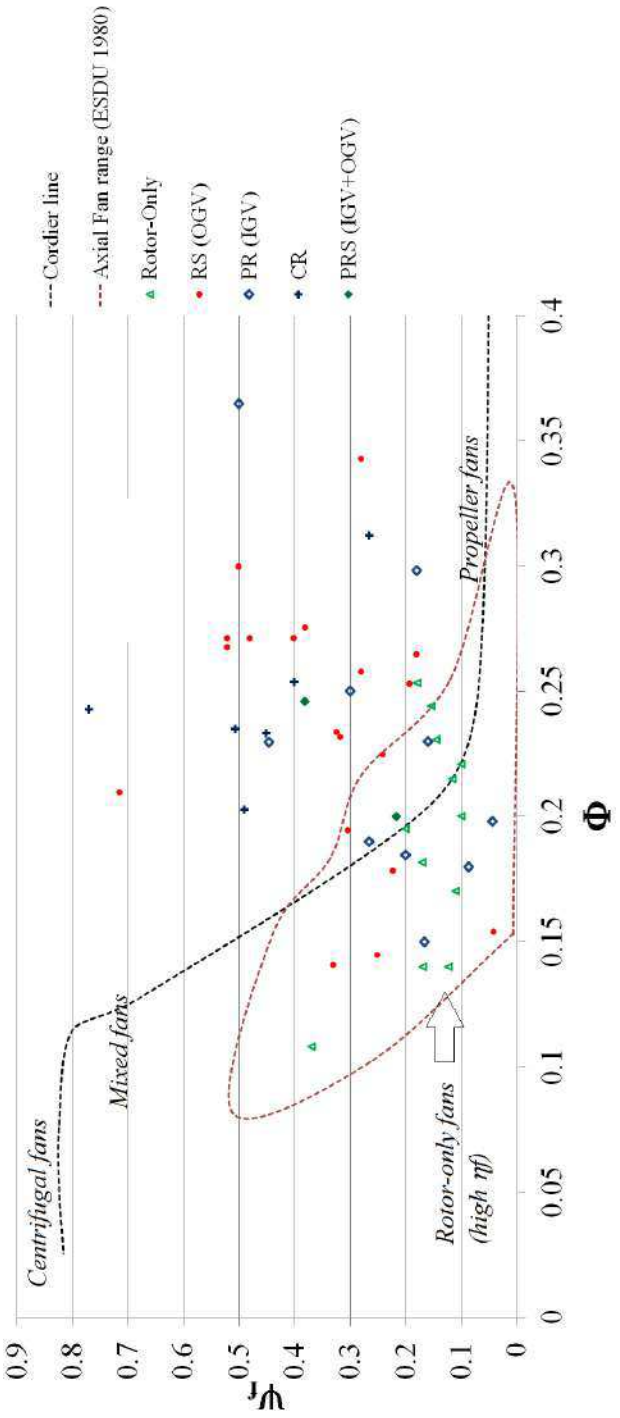

Figure 25: Performance of Axial Fans with different configurations with respect to the Cordier line and the Axial fan range identified in [11] (**a coloured print of the graph is recommended**). Mixed and Centrifugal fan ranges as indicated in [12].

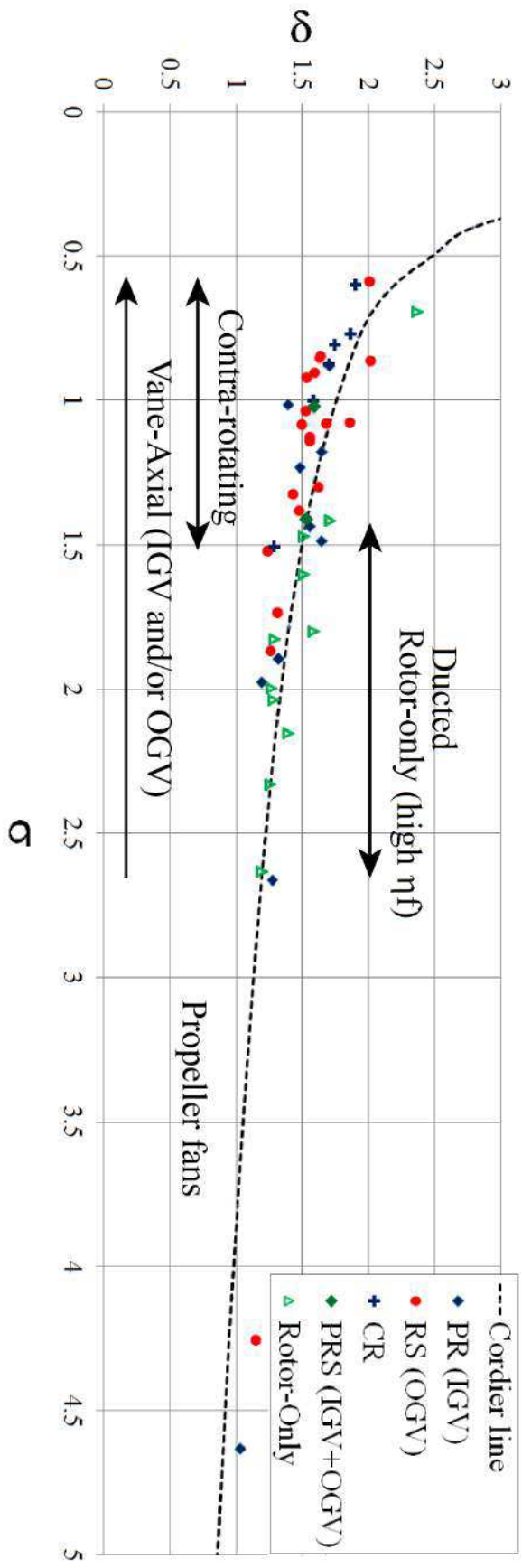

Figure 26: Specific speed and diameter for axial fans of different configurations (**a coloured print of the graph is recommended**).

diameter to achieve the same requirements ($q_\nu - p_f$) with respect to a vane-axial fan running at the same rotational speed n. This evidence suggests that a Cordier-curve specific for the *RO* fan configuration would be shifted towards higher specific diameters with respect to the original one. This argument will be treated in Sec. 4.3. Intuitively, Rotor-only fans can be considered as Rotor-Straightener machines with completely inefficient stator vanes (thus, the necessity of using this configuration at low pressure rises).

- **Rotor-Straightener** Among the three fan categories with stator vanes (*PR, RS, PRS*), the Rotor-Straightener one is the most numerous, as claimed by most of the authors. Referring at Fig. 25, all the *RS* machines operate at $\Psi_f \gtrsim 0.18$ (except one particular case, discussed in the following). Highest fan efficiencies are around 90-93%, in accordance with what suggested in the literature (e.g., [2, p. 4.39]). Most of the authors identify the *RS* as the most efficient fan configuration (e.g., [1, p.265]), thanks to the swirl recover and the lower air velocities with respect to the blades.

  From Fig. 26 it is evident that most of *RS* fans operate at $\sigma \lesssim 1.5$. However, the possibility of using this stator-vane fan layout also at low Φ and Ψ_f, such as for the cooling tower fan presented in [1, p. 312], allows the achievement of relevant specific speeds ($\sigma > 4$).

- **Preswirler-Rotor and Preswirler-Rotor-Straightener** The *PR* and *PRS* configurations are treated together. The *PRS* can be conceptually seen as a *PR* that, at design duty, provides a flow deflection in excess with respect to the axial direction.

  Differently from the *RO* and *RS* configurations, no unique operational areas are identifiable in Fig. 25 for this fan layout: *PR* fans operate at low $\Phi - \Psi_f$ magnitudes (left hand side corner in Fig. 25) as well as at higher pressure and flow coefficients. This last evidence eventually agrees with what suggested by the inviscid Euler approach in the previous paragraph. The maximum efficiencies achieved (up to $\eta_f = 88\%$) are lower with respect to Rotor-straighteners. Although a dedicated systematic investigation would be needed, the data tabulated in Appendix B.1 suggest that the Preswirler layout is always less efficient with respect to the Straightener one, when conditions allow the operation of both the configurations (i.e., regardless of constraints on dimensions or speed). This is in accordance with the higher air velocities (and thus, higher losses) that occur within the blades of the *PR* layouts.

  In absence of further available data, some reasonings are here reported. The *PR* configuration is likely to be always less efficient with respect to the *RS* one, whether this last is feasible. As a matter of fact, several *PR* fans are actually efficient *trade-off* solutions that are used when space limitations are imposed on the axial length of the blading [1, p. 306].

However, the preswirler layout *PR* (or the *PRS*, for what reported before) may represent the mandatory (i.e., most efficient) solution under the contemporary presence of: *i)* demanding pressure rises at relatively high flow-rates, and *ii)* limited fan diameter D and rotational speed n. This statement can be explained considering again the Euler integral equation for the fan unit:

$$\frac{\overline{\Delta p_{tt}}}{\rho} = \eta_f \cdot (\omega \bar{r} \cdot \overline{\Delta c_u}) \tag{43}$$

Whether the rotational speed ω is limited (e.g., for direct coupling with the motor or for acoustical reasons) and the fan radius $R = \frac{D}{2}$ is imposed as well (e.g., for space constraints), a higher hub-to-tip ratio ν might be selected to increase the mean radius $\bar{r}$ (and thus $\overline{\Delta p_{tt}}$). However, there is a natural limit to the increase of ν (especially at the high flow-rates, see the ν_{opt} trends reported in 5.1), because of the unavoidable increase of the losses within the fan annulus (due to the higher velocity) and in the necessarily-longer tail-cone diffuser. Thus, under such conditions, the most effective way of obtaining the demanding pressure rise $\overline{\Delta p_{tt}}$ is increasing the average flow deflection $\overline{\Delta c_u}$ with the preswirler. For what previously reported, the resulting fan efficiency is expected to be lower than the corresponding *RS* fan that achieves the requirements at the same rotational speed ω but with a larger diameter D (regardless of any Reynolds number contribution). Indications in support of these conclusions are reported in the description of the *PRS* case presented in [1, pp. 307,336].

Further indications on the dichotomy between stator-vane configurations are also obtained considering Fig. 25. In particular the entire set of *PR* fans is shifted at higher specific speeds with respect to the *RS* one. However, the limited number of data does not permit further considerations about.

- **Contra-rotating fans** *CR* fans are compact multi-stage machines [1, p. 309] and are used when demanding pressure rises are required. This is evident from Fig. 25, where all *CR* fans feature $\Psi_f > 0.26$. According to these relevant pressure rises, most of contra-rotating data rely at low specific speeds $\sigma < 0.1$ (Fig. 26). Also in this case, the data are shifted towards lower specific diameters with respect to the Cordier line.

  The exceptional efficiency $\eta_f = 94\%$ (from tests on a scaled model) measured for the best *CR* seems proportionate in light of the relevant design effort required for the drive system of the Modane Wind Tunnel [15].

- **Cordier line for Vane-axial** Referring at Fig. 26, it appears that generally most of Vane-axial fans (i.e., all the configurations with stator vanes) for $\sigma \leqslant 1.3$ operate at lower specific diameters with respect to the Cordier-line. This is further enhanced if Contra-rotating fans are included as well. Such indication is an accordance with the fact

that machines with a second blade row are able to achieve the same pressure rise with a smaller diameter with respect to a Rotor-only fan running at the same speed. Accordingly, a specific Cordier-diagram for Vane-axial fans is expected to rely at lower δ with respect to the original Cordier-line; the argument will be recalled in Par. 4.3.

4.2 SELECTION OF THE SUITABLE SWIRL DISTRIBUTION FOR ROTOR-ONLY FANS

In spite of all the possible configurations available for axial fans, the typical industrial machine is the rotor-only one. By contrast with the simplicity of these machines, the higher degrees of freedom permitted by the absence of stator vanes (and of the tail-cone, eventually) makes a comprehensive treatment of this fan configuration more complex. As a matter of fact, most of the books on fans treat the design of vane-axial machines while neglect the rotor-only one. For the Rotor-only configuration, the most important design aspect is the selection of the aerodynamic loading distribution along the span (i.e., the design vortex criterion) and how this affects fan performance and efficiency. These aspects are treated in this section.

4.2.1 On Rotor-Only Fans

Rotor-only machines are not the fans that feature the highest efficiency. Nonetheless, they are the most diffused configuration, representing the best trade-off between performance, efficiency and purchasing costs for several applications. Moreover, for numerous industrial applications where the axial length of the fan is limited, the rotor-only configuration represents the mandatory solution.

A peculiar aspect of Rotor-only machines that distinguishes their performance from those of the other axial fan configurations is that the total-to-total pressure rise Δp_{tt} delivered to the fluid by the impeller differs from the fan pressure p_f, regardless of any dissipation effect. This is because the ISO standard [16] computes p_f with the mean axial velocity only, considering completely dissipated the dynamic pressure associated to the tangential velocity at the rotor outlet (refer to Par. 2.2). Accordingly, most of the authors are used to present fan characteristics in terms of fan static pressure p_{sf} (i.e., total-to-static) and efficiency η_{sf}. Such total-to-static parameters are proper to compute the fan-system matching for machines installed in the *exhaust* configuration (i.e., at the system exit, with no useful work downstream of the fan) [1, p. 346]. Nonetheless, rotor-only fans are commonly installed in *in-line* configurations as well (i.e., ducted-ducted path, upstream and downstream); in that case the fan pressure shall be used [1, p. 346].

Among design aspects for rotor-only fans, two hold major importance than the others: the hub-to-tip ratio and the swirl distribution. These two

aspects are strongly correlated when the fan operation at highest efficiency is targeted.

NON-FREE-VORTEX BLADES Regarding the aerodynamic loading distribution along the blade span, it is a fact that most of industrial *RO* fans feature *Non-Free-Vortex* (*NFV*) blades [1, 2, 6, 17]. In addition to manufacturing advantages (such as reduced blade-root chord lengths that avoids blade overlapping and excessively long rotor hubs), *NFV* loading distributions have aerodynamic advantages in particular conditions. Although several authors proposed design methods to obtain fan blades with span-wise variation of circulation (e.g., [17, 18]), quantitative indications on the best operational conditions for a particular swirl distribution and on the related advantages/-drawbacks in terms of fan performance and efficiency are quite rare and mostly qualitative. In particular, Vad [19] suggests that *NFV* criteria allow to achieve relatively high flow-rates and pressure rises with relatively small fan diameters and low rotor speeds. Bamberger [14, pp. 56-57] indicates that shifting the aerodynamic load towards the blade tip is suitable for fans whose specific speed and diameter feature lower magnitudes with respect to the Cordier-line.

SIMPLIFIED CLASSIFICATION Typical *NFV* distributions are the Constant Swirl (*CS*, $c_u = const$) and the Rigid-Body (*RB*, $c_u = const \cdot r$) one. In the *RB* case, the tangential velocity linearly increases towards the blade tip from a zero value at the fan axis. However, the possible distributions of swirl velocity c_u along the span are infinite and the free-vortex distribution $c_u = \frac{const}{r}$, the constant swirl and the rigid-body ones are particular cases in which the radial development of the tangential velocity is easily described by a simple math equation. To account for all the vortex possibilities, a simplified classification is presented in Fig. 27 according to the blade shapes, that groups together different $c_u(r)$ distributions with similar macro-behavior. This simplified classification is described in the following:

- **Free-Vortex** *FV*: $c_u = \frac{const}{r}$, $\frac{d\Gamma}{dr} = 0$. This class represents a set with a single element (the free-vortex swirl distribution).
- **Arbitrary-Vortex** *AV*: distributions featuring c_u decreasing linearly along the radius up to $c_u = const$ included; $\frac{d\Gamma}{dr} > 0$. This swirl design is extremely common for industrial application [1, p. 409]. The constant-swirl distribution (*CS*, $c_u = const$) is a particular case.
- **Forced-Vortex** *ForV*: all swirl distributions that increase along the blade height. The rigid-body *RB* distribution $c_u = const \cdot r$ represents a particular case. Typical applications are air-conditioner external-unit fans (small-to-medium size units, see e.g., Fig. 1) that feature limitations on both the axial and transversal dimensions, as well as on the rotor-speeds (for acoustical reasons).

***Free-vortex**:* tapered blade, highly twisted

***Arbitrary-vortex**:* approximately constant chord, low twist

Forced-vortex: chord length span-wise increasing, low twist

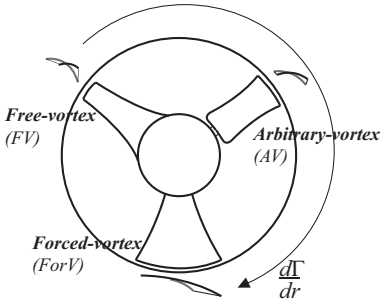

Figure 27: Schematic representation of the blade shapes deriving from the application of different spanwise gradients of circulation; inspired from [6].

4.2.2 Rotor-only Performance charts

The performance of several Rotor-only fans have been tabulated in Appendix B.2 [13]. Experimental data at design-point were considered; when DP was not declared, the fan performance at BEP were considered. The methods of data-collection and classification are reported in the Appendix B.2.

The performance of the rotor-only fans in Appendix B.2 have been organized in the graphs of Figure 28: data are presented in terms of both fan pressure p_f and fan static pressure p_{sf} coefficients (Ψ_f and Ψ_{sf}, respectively) to help readers that are accustomed only to the second one. From Fig. 28 appears that:

- Free-vortex fans are not numerous in the rotor-only ducted configuration (i.e., Tube-axial fans);
- Arbitrary-vortex rotors are by far the largest group for ducted industrial applications. Although slightly shifted towards the left side of the graph, this swirl class basically spans flow-coefficients $0.1 \leqslant \Phi \leqslant 0.27$;
- Forced-vortex fans operate at higher pressure rises and flow-rates with respect to the classical Cordier-line. This configuration is largely used for exhaust installations. [2]

In Fig. 29 the same fan performance are plotted in terms of $\sigma - \delta$. Among the three classes:

- the free-vortex class fits the Cordier-line, in particular towards the propeller fan range (for $\sigma > 2$).
- Arbitrary vortex fans operate at $\sigma \leqslant 2$, on both upper and lower sides of the Cordier curve.

2 In spite of the wide diffusion of Forced-vortex rotor-only fan applications, the small number of *ForV* cases here reported is due to the limited availability in the literature of experimental data regarding this swirl class.

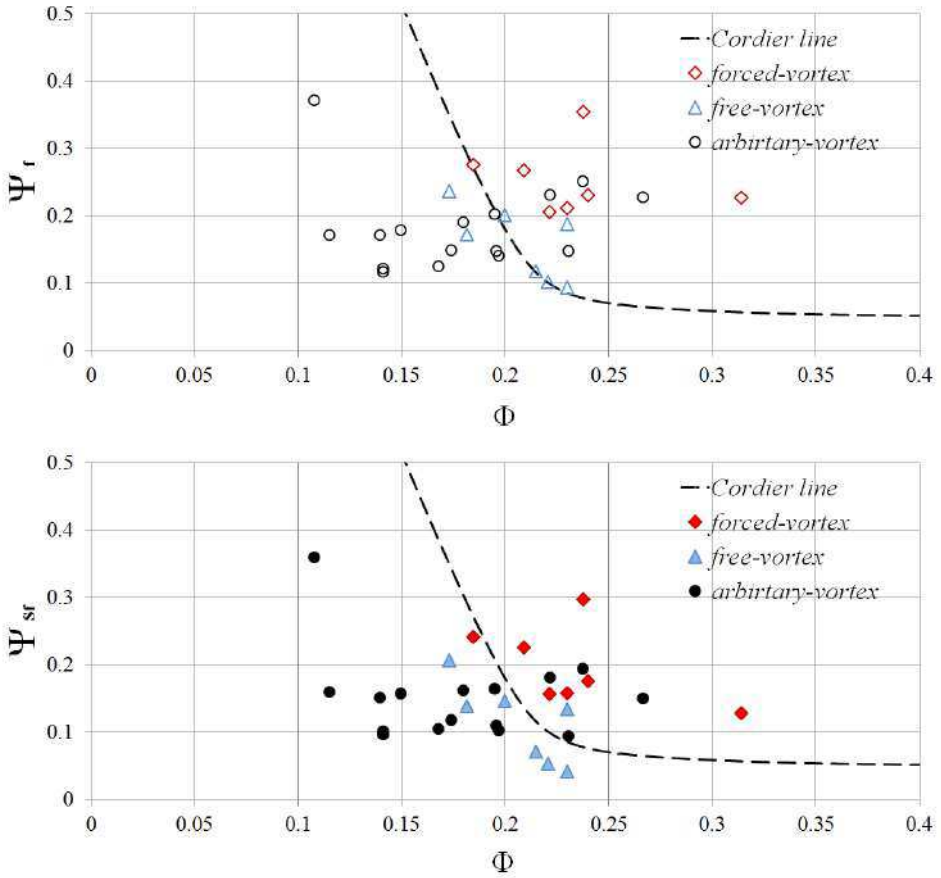

Figure 28: Performance of rotor-only fans at DP or BEP for different vortex criteria: FV (triangle markers), AV (circles), ForV (diamonds). Empty markers indicate *fan pressure* amounts, full markers total-to-static ones.

- Forced-vortex fans operate at $\sigma \leqslant 1.8$ at lower $\sigma - \delta$ conditions, confirming what indicated in [20]. This evidence suggests that Forced-vortex criteria are suitable to obtain the required fan operation $p_f - q_v$ with smaller fan diameters.

When the data are plotted in terms of flow and pressure-rise coefficients against efficiencies (Fig.s 30) further trends can be observed. Fan static efficiencies η_{sf} show a decreasing trend with the increase of the flow-coefficient, as natural (upper graph of Fig. 30). Regardless of the vortex-criteria instead, fan efficiencies η_f are quite unaffected by the flow-coefficient (at least in the larger part of the Φ range), as was suggested in [21]: most efficient fans feature η_f between 60% and 77% (see the cloud of empty markers reported in the upper diagram of Fig. 30). On the contrary, a decrease of η_f with the fan pressure-coefficient is observed in the middle graph of Fig. 30. This trend was expected, as at larger pressure rises the flow deflection is higher and so is the dissipation of the dynamic pressure associated to the tangential component that cannot be recovered because of the absence of straightener, as referred in Par. 4.1.3. At last, fan static efficiencies η_{sf} are plotted against

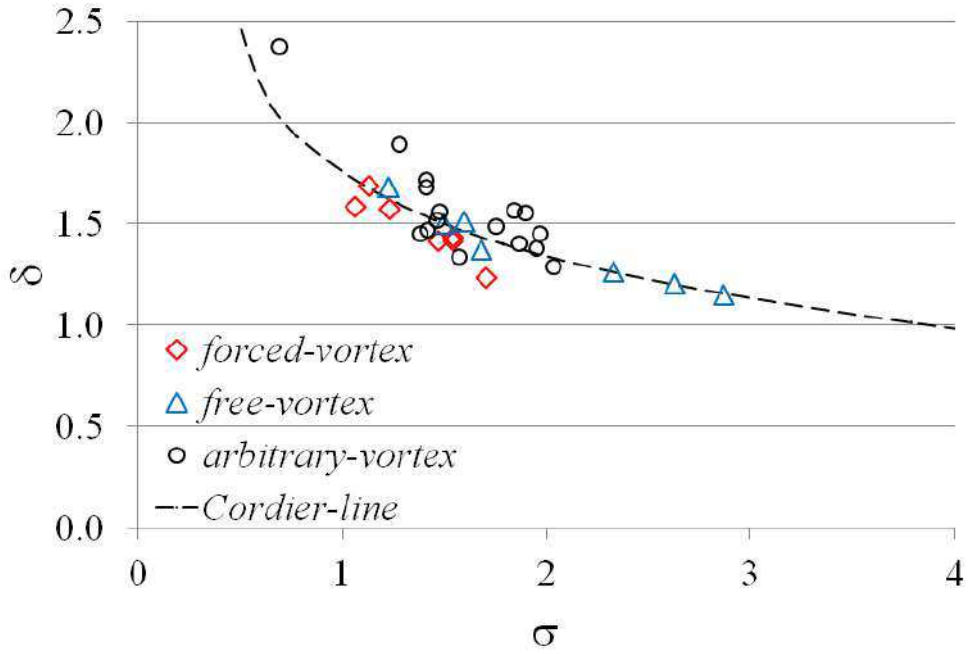

Figure 29: Specific speed and diameter of rotor-only fans featuring different design vortex criteria: FV (triangle markers), AV (circles), ForV (diamonds).

Ψ_{sf} in the last graph of Fig. 30; in this case however, major trends are not noticeable.

According to the minor relevance of the flow-coefficient on η_f, Fig. 31 reports the performance of fans in the range $0.18 < \Phi < 0.24$. Hub-to-tip ratios are reported as well, to relate the fan geometry with the vortex-distribution and the operating condition. Focusing on Fig. 31 the following observations are reported:

- Highest fan efficiencies are achieved by *FV* rotor-only fans of low pressure rise coefficients ($\Psi_f \sim 0.1$) and low hub-to-tip ratio ($\nu \sim 0.2 - 0.3$).

- On the opposite side, forced-vortex fans achieve relevant pressure-rises at lower efficiencies. It is remarked that rotor-straightener fans may achieve equal pressure coefficients with higher efficiency (compare the rotor-only data with rotor-straightener ones in Appendix B.1). Accordingly, the application of forced-vortex criteria is appropriate for constrained designs (i.e., limitations on both fan dimensions and rotor speed).

- Arbitrary-vortex fans of decreasing swirl distribution (rotors with $\nu = 0.4$ and 0.45) reach peak efficiencies similar to the highest η_f of the free-vortex rotors.

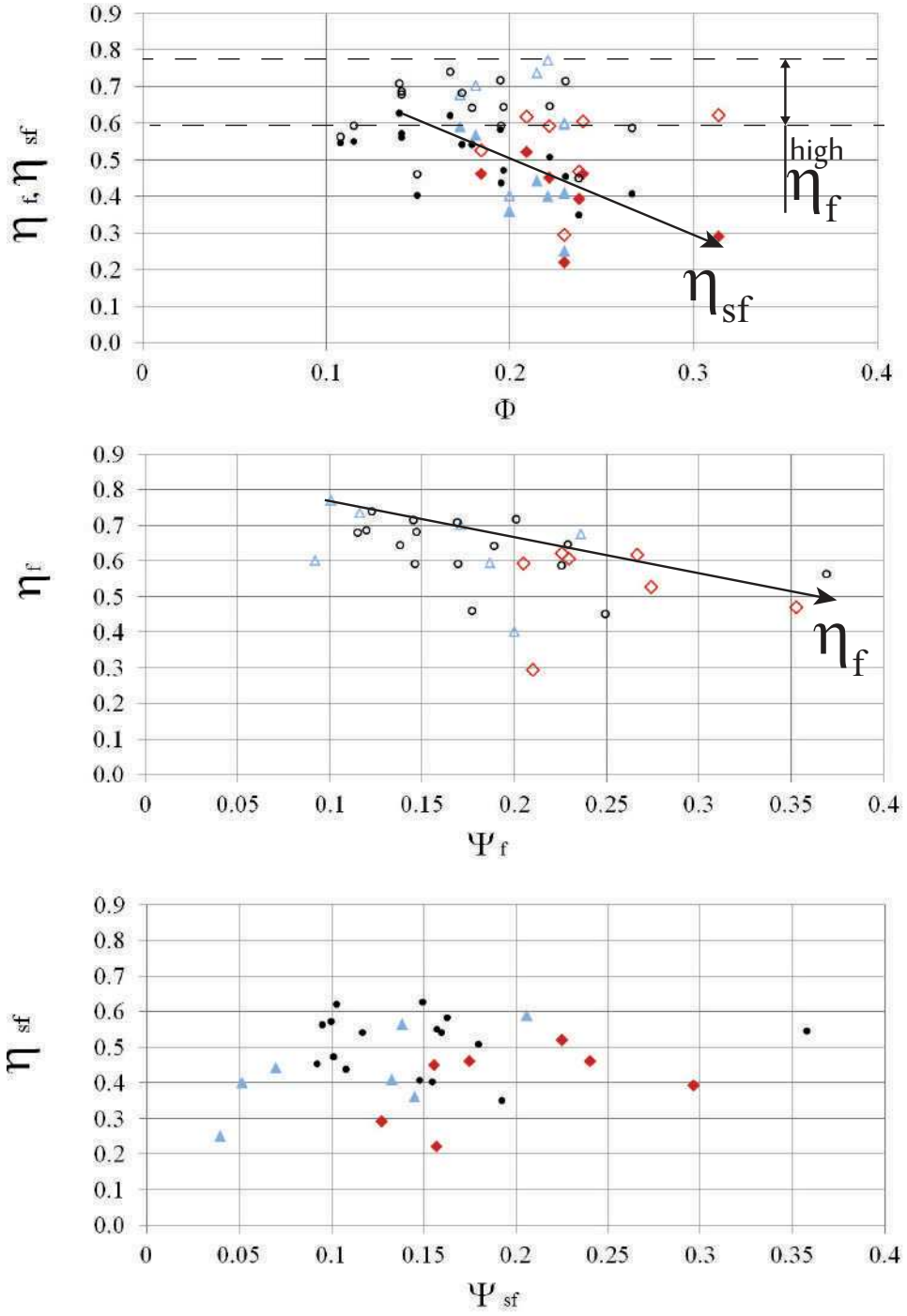

Figure 30: Trends of fan efficiency (empty markers) and fan static efficiency (full markers) against the flow coefficient Φ and the pressure coefficients Ψ_f and Ψ_{sf}.

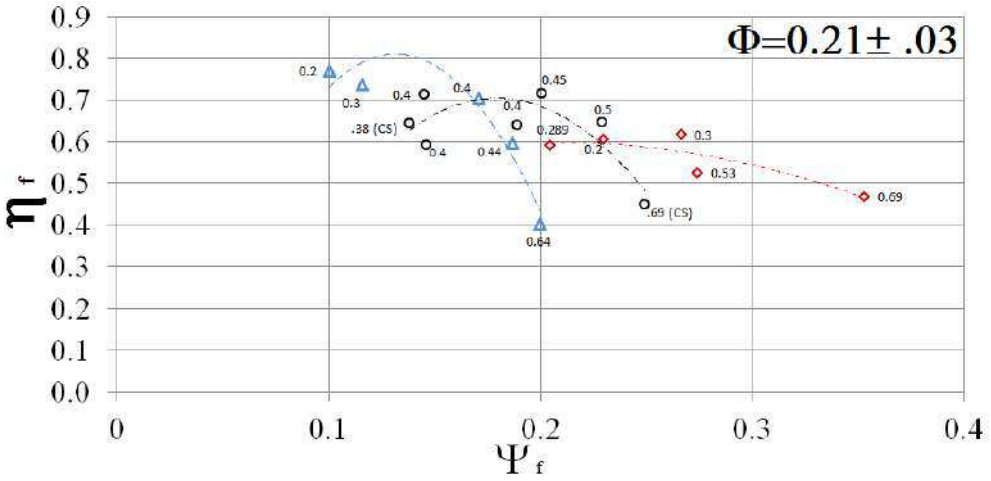

Figure 31: Relations between rotor geometries (ν), vortex-criteria and pressure-rise coefficients for fans with similar flow-rate coefficients ($0.18 < \Phi < 0.24$)

4.2.3 Discussion on Results

The comprehensive treatment presented in 4.2.2 neglects relevant effects such as those related to the Reynolds number and the tip-clearance (see in 4.2.4). Furthermore, it is not ensured that the fans herein considered as pertaining to the three classes are all of the highest aerodynamic quality. A sound systematic experiment would compare rotor-only fans of different vortex criteria with similar Re_c and equally small tip clearances ($\frac{tc}{D} \simeq 0.1 - 0.2\%$). However, such an experiment is not available at present. According to these issues, the trends presented in Fig 30 cannot be considered rigorous from a quantitative point of view: the intersections' coordinates might slightly change, for instance. Nonetheless, these trends represents an $\eta_f - \Psi_f$ pareto front and graphically explain the suitable operational range pertaining to the blade shapes of Fig. 27.

4.2.4 Tip clearance performance and efficiency drops in relation to the vortex criteria

The losses of fan performance due to the increase of the tip clearance have been investigated as well. Kahane [18] states that these losses are relatively small for fans of the *RB* type, while both Wallis [1] and Vad [22] report opposite trends on *NFV* rotors. As industrial fans are likely to operate at relevant magnitudes of $\frac{tc}{D}$ ratios, this aspect will be taken into consideration in Par. 5.5.1.

4.2.5 Non-free vortex bladings on Machines with stator vanes

A brief insight is reported on Vane-axial fans with *NFV* blades as well. The use of vortex distributions different than the free-vortex one is quite

common in vane-axial fans (e.g., [4, p. 272]) and multi-stage axial compressor as well (e.g., [3]). Radial motions are likely to be of reduced entity with respect to the rotor-only case, due to the rotor-stator interaction. Nonetheless, the design issue between free-vortex and non-free-vortex still remains as a major discussion since a long time [23, p. 56]. Figure 29 showed that designing blades with c_u distributions that increase towards the tip is suitable for operations at lower specific speeds and diameters; it is unknown if similar conditions might be the case of non-free-vortex vane-axial machines as well.

4.3 COMPARISON OF PERFORMANCE FOR ROTOR-ONLY AND VANE-AXIAL FANS

As suggested in [21], it is of design interest presenting a Cordier-type diagram pertaining to each kind of axial fan. This is done considering in a single graph the specific speeds and diameters of the three macro-categories: Rotor-only, Vane-Axial and Contra-rotating fans tabulated in Appendix B.1. This diagram is presented in Fig. 32, in which power regression lines have been plotted across the data. As reported previously, different curves appear pertaining to each fan category. In particular, the Rotor-only line lies at higher specific diameters with respect to the Vane-axial one and the Contra-rotating one within the range of ducted machines ($\sigma \leqslant 3$), and especially for $0.7 \leqslant \sigma \leqslant 2$. Although based on a limited number of data, the line for Contra-rotating machines lies considerably below the original Cordier line ($\Delta\delta \simeq 0.4$).

4.4 SUMMARY ON AXIAL FAN CONFIGURATION SELECTION

On the basis of the performance and efficiency data collected in Appendix B and in Fig.s 25, 26, 32 the following summary Table is presented:

Table 6: Operational range of axial fan configuration according to data.*Propeller fans maximum efficiency according to [2].

Category	Configuration	High η_f Range	max. η_f	Usable range
Rotor-only	Propeller	$\sigma \gtrsim 2.5$	70%*	–
	Ducted	$1.5 \lesssim \sigma \lesssim 2.6$	$\simeq 75-78\%$	$0.7 \lesssim \sigma \lesssim 2.8$
Vane-Axial	*RS*	$0.6 \lesssim \sigma \lesssim 1.8$	90%	$0.6 \lesssim \sigma \lesssim 4.3$
	PR/PRS	$1 \lesssim \sigma \lesssim 2.7$	88%	$1 \lesssim \sigma \lesssim 4.7$
Multi-stage	*CR*	$0.6 \lesssim \sigma \lesssim 1.5$	94%	–

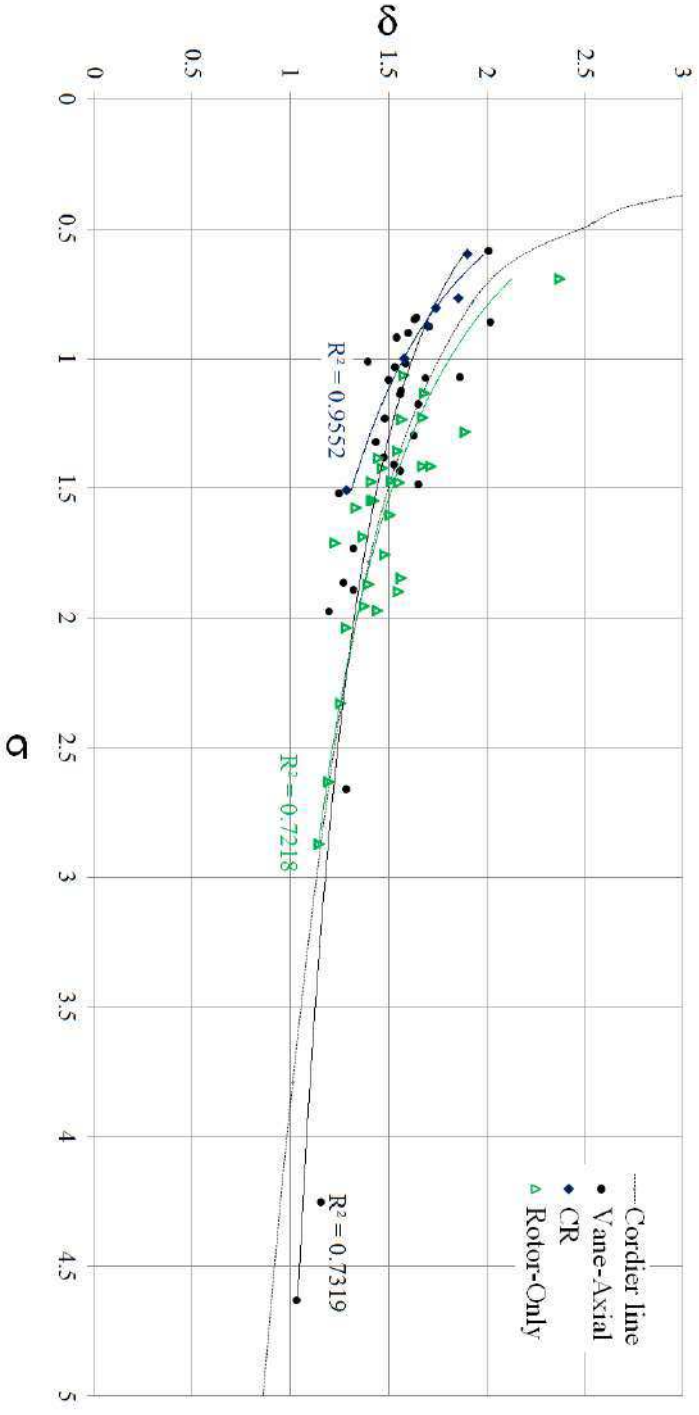

Figure 32: Specific speed and diameter for axial fans of different configurations.

BIBLIOGRAPHY

[1] R Allan Wallis. *Axial flow fans and ducts*. Krieger, 1993.

[2] Frank Bleier. *Fan Handbook: selection, application, and design*. McGraw-Hill Professional, 1998.

[3] Archibald Bathgate McKenzie. "Axial flow fans and compressors". In: *Aerodynamic Design and Performance* (1997).

[4] Bruno Eck. "Fans". In: *1st English ed., Pergamon Press, Oxford* (1973), pp. 139–153.

[5] William C Osborne. *Fans*. Vol. 1. Pergamon Press Oxford, 1966.

[6] William Cory. *Fans and ventilation: a practical guide*. Elsevier, 2010.

[7] Maria Teodora Pascu. "Modern Layout and Design Strategy for Axial Fans". PhD thesis. Ph. D. Thesis at Erlangen University, 2009.

[8] Ph Epple, Franz Durst, and Antonio Delgado. "A theoretical derivation of the Cordier diagram for turbomachines". In: *Proceedings of the Institution of Mechanical Engineers, Part C: Journal of Mechanical Engineering Science* 225.2 (2011), pp. 354–368.

[9] LS Marks and JR Weske. "The Design and Performance of Axial-Flow Fan". In: *ASME Trans., AER-56-13* 56.11 (1934), pp. 807–813.

[10] Eleftherios Andreadis. *Design of a low speed vaneaxial fan*. MS Thesis,Cranfield, UK University of Higher Education. 2011.

[11] ESDU. *A guide to fan selection and performance*. Data Item 79037. London, GB: Engineering Sciences Data Unit, Apr. 1980.

[12] RI Lewis. *Turbomachinery performance analysis*. Butterworth-Heinemann, 1996.

[13] Stefano Castegnaro, Massimo Masi, and Andrea Lazzaretto. "Preliminary experimental assessment of the performance of rotor-only axial fans designed with different vortex criteria". In: *Proceedings of the XII European Turbomachinery Conference ETC12, Stockholm, Sweden*. 2017.

[14] Konrad Bamberger. "Aerodyamic Optimization of Low-Pressure Axial Fans". PhD Thesis. Siegen, Ger: University of Siegen, 2015.

[15] Alain Godichon. *FAN DESIGN: Past, Present and Future*. Keynote at FAN 2015 Conference. 2015.

[16] International Standard Organization. *Industrial fans - Performance testing using standardized airways (ISO 5801:2009)*. 2009.

[17] RJ Downie, MC Thompson, and RA Wallis. "An engineering approach to blade designs for low to medium pressure rise rotor-only axial fans". In: *Experimental thermal and fluid science* 6.4 (1993), pp. 376–401.

[18] A Kahane. "Investigation of axial-flow fan and compressor rotors designed for three-dimensional flow". In: *NACA TN* 1652 (1947).

[19] J Vad. "Correlation of flow path length to total pressure loss in diffuser flows". In: *Proceedings of the Institution of Mechanical Engineers, Part A: Journal of Power and Energy* 225.4 (2011), pp. 481–496.

[20] Konrad Bamberger, Thomas Carolus, and Markus Haas. "Optimization of Low Pressure Axial Fans and Effect of Subsequent Geometrical Modifications". In: *Proc. Fan 2015* (2015).

[21] Massimo Masi, Stefano Castegnaro, and Andrea Lazzaretto. "A Criterion for the Preliminary Design of High-Efficiency Tube-Axial Fans". In: *ASME Turbo Expo 2016: Turbomachinery Technical Conference and Exposition*. American Society of Mechanical Engineers. 2016, V001T09A006–V001T09A006.

[22] János Vad et al. "Comparative investigation on axial flow pump rotors of free vortex and non-free vortex design". In: *Periodica Polytechnica. Engineering. Mechanical Engineering* 46.2 (2002), p. 107.

[23] Alexey Joakim Stepanoff. *Turboblowers: theory, design, and application of centrifugal and axial flow compressors and fans*. Wiley, 1955.

5 DESIGN VARIABLES AND CORRELATIONS. ROTOR-ONLY FANS

After performing the selection of the fan configuration and of the swirl distribution, the geometrical design of the machine shall be initiated. All the fan components that interact with the fluid contribute to the proper operation of the machine. However, some affect the machine characteristic more than others.

All the components and features of axial fans of the rotor-only type are presented in this Chapter, together with related effects on the machine operation and design indications. Whenever possible, these design indications have been collected into graphs and/or correlations. The informations presented in this Chapter form the basis of the Design Method presented in Chapter 6.

All the design variables reported in Tab. 1 in Chapt. 1 are treated, except for the Blading Configuration and the Span-wise aerodynamic loading that have been analyzed in Chapt. 4. In particular, the chapter is subdivided into the following paragraphs:

- Hub-to-tip Ratio;
- Reynolds Effects;
- Hub, Casing and Centre-Bodies;
- Blades;
- Rotor Blade Clearances;

For the design aspects that have not been directly investigated, a brief discussion is reported together with indications from the literature, whether available.

5.1 HUB-TO-TIP RATIO

The hub-to-tip ratio ν is one of the most important and distinctive parameters of axial fan design. Among axial machines, the Fan Vocabulary [1] distinguishes between *low-*, *medium-*, and *high-pressure* fans according to the ν ratio:

- Low-Pressure $\nu \lesssim 0.4$
- Medium-Pressure $0.4 \lesssim \nu \lesssim 0.71$
- High-Pressure $\nu \gtrsim 0.71$

The physical explanation underneath this categorization is easily obtained from the integral form (i.e., representative of the entire blade, *overline* sign) of the Euler equation for turbomachines:

$$\frac{\overline{\Delta p_{tt}}}{\rho} = \overline{\eta_{tt}} \cdot (\omega \bar{r} \cdot \overline{\Delta c_u}) \tag{44}$$

Equation 44 states that the overall increase of total pressure delivered to the fluid by the rotor $\overline{\Delta p_{tt}}$ is proportional to the representative mean radius $\bar{r}$. Thus, increasing the mean radius $\bar{r}$ of the machine with a higher ν ratio allows to increase the $\overline{\Delta p_{tt}}$ for a given mean flow deflection $\overline{\Delta c_u}$ (and total-to-total rotor efficiency $\overline{\eta_{tt}}$).

On the other hand, the search for high efficiencies usually involves low hub-to-tip ratios, with the aim of keeping the meridional airflow velocity (and thus, the losses) as low as possible [2, p. 15]. Wallis [3, p. 3], for instance, states that well-designed machines usually feature ν ratios between 0.4 and 0.7. The previous indications finds support in the database presented by Osborne [4, p. 151], where most efficient fans feature $\nu \leqslant 0.55$.

An optimum ν exists for each fan operational requirement. In spite of the fundamental importance of this parameter however, several authors do not present any criterion to select the proper hub-to-tip ratio. A method to compute the lowest feasible ν ratio as function of the fan requirements (Φ, Ψ) is based on the *Strscheletzky* criterion, that requires a minimum meridional velocity with respect to the tangential velocity to avoid a dead-wake recirculation zone downstream of the impeller larger than the impeller hub [2, p. 15]. This criterion is applied to the hub design imposing a minimum hub diameter d_h that is equal to the diameter of the dead-wake core [5, p. 266], as verified for fan design purposes by Marcinowsky [2, pp. 15-16] under the assumption of free-vortex flow. However, the dead-wake core diameter can be increased by straightening the flow [5, p. 267]. Accordingly, the criterion presents two different forms depending on the presence (or not) of the straightener blading. In the axially Constrained (subscript *C*) case (e.g., for the Rotor-Straightener configuration) the criterion takes the form

$$\frac{\Phi}{\Psi_{tt_{th}}} = \frac{1 - \nu_C^2}{2\nu_C} \tag{45}$$

where $\Psi_{tt_{th}}$ is the theoretic inviscid pressure coefficient [5, p. 58]. Conversely, for the axially Unconstrained (UC) case the ν relation is

$$\frac{\Phi}{\Psi_{tt_{th}}} = \frac{1}{2}\sqrt{\frac{1}{2\nu_{UC}^2}(1-\nu_{UC}^2)^2 - (1-\nu_{UC}^2)^2 \ln(\nu_{UC})^{-1}} \tag{46}$$

In Fig.s 34 and 33 the Eq.s 45 and 46 are applied and the optimum hub-to-tip ratios are compared within the ranges $0.08 \leqslant \Phi \leqslant 0.3$ and $0 \leqslant \Psi_{tt_{th}} \leqslant 1$: Rotor-straightener machines need larger hub diameters with respect to the Rotor-only ones; the difference $\Delta\nu$ between the two cases is presented in Fig. 35. Equation 46 for Rotor-Only fans is applied at three dimensionless duties $(\Phi = 0.1, 0.15, 0.2)$ in Fig. 36.

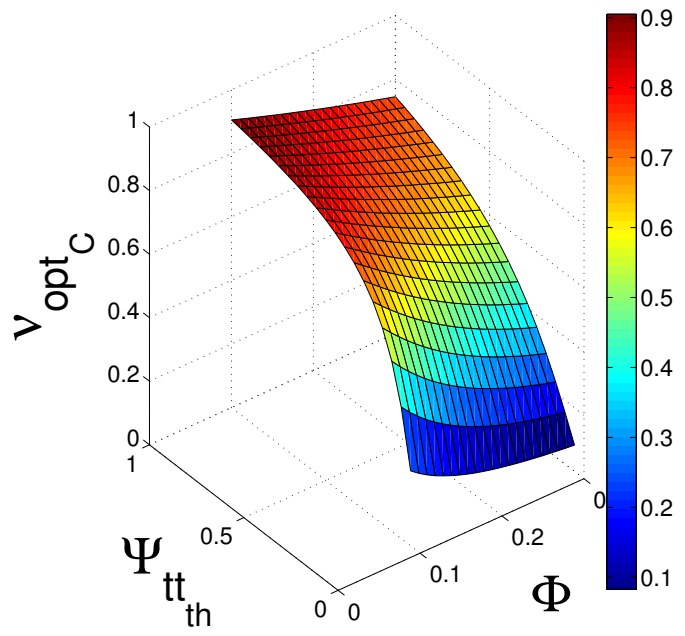

Figure 33: Minimal Hub-to-Tip ratio for the Axially Constrained case (e.g., Rotor-Straightener Fans).

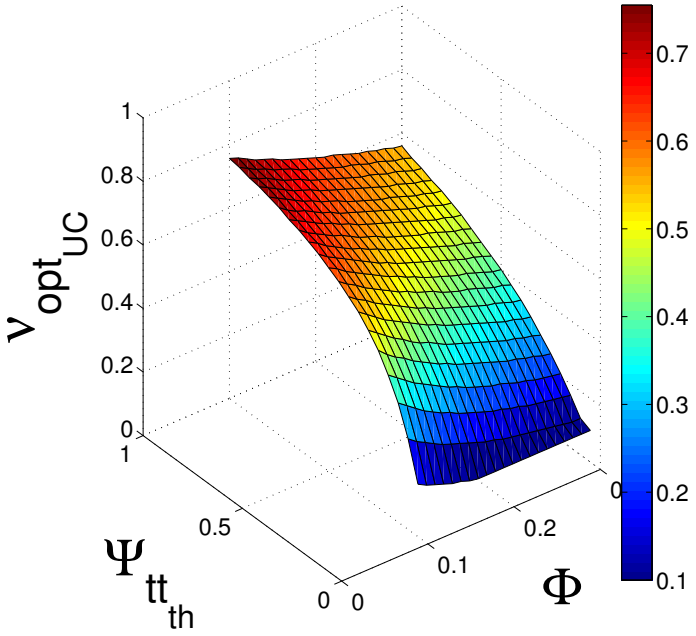

Figure 34: Minimal Hub-to-Tip ratio for the Axially Unconstrained case (Rotor-Only Fans).

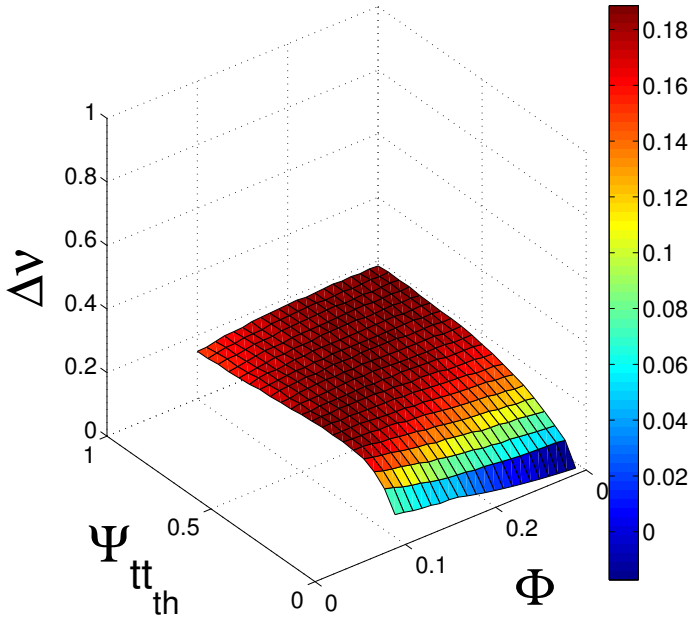

Figure 35: Differences $\Delta\nu = \nu_{opt_C} - \nu_{opt_{UC}}$.

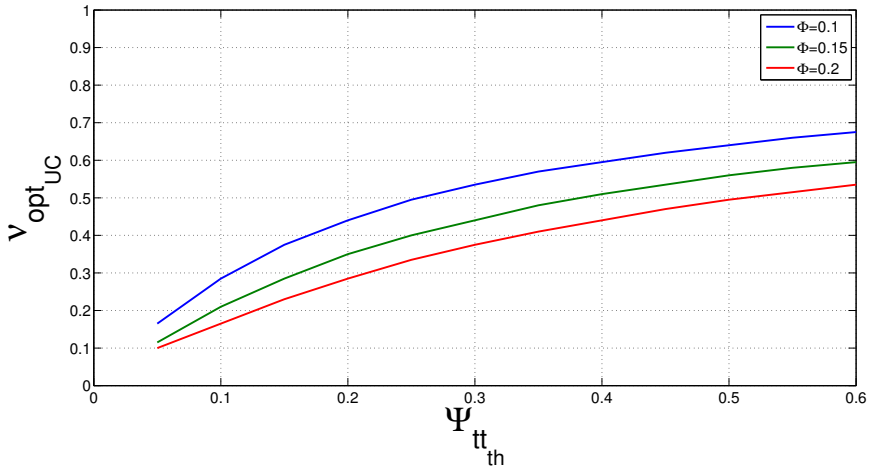

Figure 36: Equation 46 for Rotor-only fans applied at three different flow-coefficients.

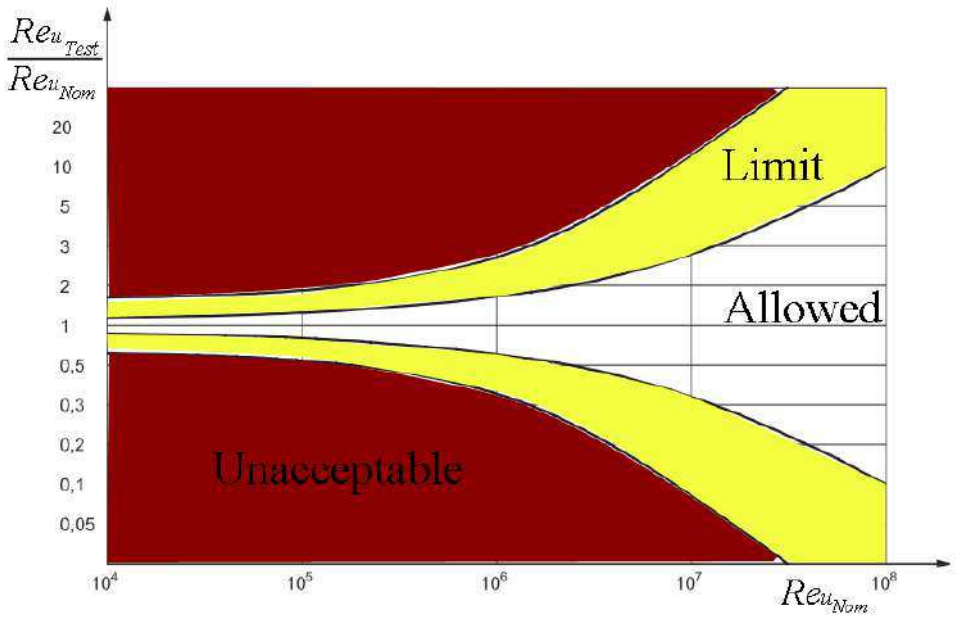

Figure 37: Allowed Reynolds ratios between Test and Nominal Conditions (adapted from [10]).

5.2 REYNOLDS EFFECTS

The Reynolds number $Re = \frac{\rho v l}{\mu}$, with v and l characteristic velocity and length of the flow, represents the ratio between inertia and viscous forces. It is a global flow parameter [6] and is used to identify the flow regime [7]. It is clearly not a design variable; nonetheless, designers shall be aware of the effects on the fan characteristics related to this parameter.

As stated by Carter [8]: *"[..] the very marked* scale *effect must not be forgotten [in turbomachinery applications]"*, although what is generally quoted as *scale* effect should be more correctly referenced as *Reynolds* effect [9].

Testing a single fan and then converting the measured performance to other geometrically similar fans of different size is quite common in the fan industry [4, 10, 11]. This procedure assume fan performance and efficiency to be Reynolds independent. However, this is allowed by the Standard [10] only for a limited range of Reynolds ratios (see Fig. 37).

Both fan performance and efficiency vary with the Reynolds number. This behavior is related to the continuous variation of the airfoils' polars with Reynolds (e.g., [12, 13]) and acknowledged by the Standard, that allows for an increase of both Ψ and η with an increase of Re [10, p. 52]. Eckert (in [14]) provided curves of $\Psi = f(\Lambda \cdot Re)$ and $\eta = f(\Lambda \cdot Re)$: both parameters increase monotonically with the Reynolds number. Variations on fan performance and efficiency characteristics with Re have been observed on tests of different fans and fan configurations tested at the large test rig of the Laboratory [15].

5.2.1 Which Reynolds number?

There is no agreement in the turbomachine literature on a unique definition of the Reynolds number: different Re can be computed depending on the choice of the characteristic velocity v and length l [3, p. 18].

MACHINE REYNOLDS NUMBER The ISO Standard uses the rotor diameter D_r and the blade tip speed $U = \omega R$, to compute what is generally known as *Machine Reynolds number*:

$$Re_u = \frac{\rho U D_r}{\mu}$$

The standard accounts for the possibility that Re testing conditions may differ from the *nominal* actual operating conditions of the fan. To consider the test results as representative of the nominal conditions, the ratio between the Reynolds number at tests and the nominal one $\frac{Re_{u_{Test}}}{Re_{u_{Nom}}}$ cannot exceed the ranges allowed in Fig. 37. Unless $Re_{u_{Nom}} > 10^7$ however, this ratio is not far from unity.

CHORD REYNOLDS NUMBER Fan designers normally relate the blade section performance with isolated airfoils or cascade parameters obtained at the wind tunnel. Accordingly, the blade chord *ch* is used as characteristic length to assess the flow regime on the blades [3, p. 18] and the related characteristic velocity should be the mean one relative to the blade w_m. However, the use of the blade tangential speed at the reference radius $u = \omega r$ is generally accepted as well for engineering purpose, resulting only in a slight underestimation. The related parameter is called the *Chord Reynolds Number*:

$$Re_c = \frac{\rho \cdot w_m \cdot ch}{\mu} \gtrsim \frac{\rho(\omega \cdot r)ch}{\mu}$$

Notice that, on axial turbomachinery, the chord Reynolds number Re_c and the machine one Re_u normally differ of an order of magnitude, because of the dimensional difference between the rotor diameter D_r and the blade chord ch. This might induce into considering the flow within the fan to be completely turbulent. On the contrary, most of the blade sections of small to medium axial fans ($D < 0.8$) are likely to experience transition conditions between the laminar and turbulent range, with a laminar extension depending on the surface roughness and on the inlet turbulence intensity as well. It is remarkable that Jacobs and Sherman [12] suggest the use of a multiplying factor k to compute an *Effective Reynolds number* $Re_{c_{eff}}$, to account for inlet turbulence intensity effects: according to the magnitude of k, $Re_{c_{eff}}$ can be two (or more) times larger than the Re_c [12].

REFERENCE RADIUS Differently from most of axial compressors, the major part of axial fans feature hub-to-tip ratios $\nu < 0.5$. Thus, the difference between the blade velocity at the hub and the tip is relevant. The chord length may vary along the radius as well, allowing ratios $\frac{ch_t}{ch_r}$ between 0.6

Table 7: Main parameters of the two geometrically similar medium-to-large fans tested at equal tip speed [16].

D [m]	n [rpm]	Re_u
0.6858	1160	$2.87 \cdot 10^6$
1.0287	1750	$4.28 \cdot 10^6$

and 2 according to [3, 4]. This characteristic feature of axial fans complicate the identification of a reference radius at which the chord Reynolds number Re_c is considered as representative of the overall flow development on the blades.

As a preliminary indication for design purpose (e.g., to choose the airfoil), the computation of the Reynolds number with the chord length and the blade tangential velocity at the mean radius is here suggested:

$$Re_{c_{MS}} = \frac{\rho(\omega \cdot r_{MS})c_{MS}}{\mu}$$

.

5.2.2 Critical Reynolds Number

The ESDU Report [11, p. 10] states: "*The function $\Psi(\Phi)$ representing the characteristic of a given fan may be used to represent the characteristic of any geometrically similar fan*". As anticipated, this sentence assumes fan performance to be Reynolds independent. Two emblematic cases are reported: in particular, the second case shows that when the Reynolds number falls under a particular value, called *Critical Reynolds Number*, the $\Psi(\Phi)$ function cannot be considered representative *at all* of the characteristic of any geometrically similar fan.

FIRST CASE Bleier [16, p.5.9] provides the characteristics of two similar medium-to-large size fans running at the same blade tip speed.[1] When the dimensional characteristics (see [16, p.5.9]) are made dimensionless, the curves coincide (Fig. 38). It is remarkable that the ratio between the Machine Reynolds numbers Re_u for the two fans is $\simeq 1.5$; such value allows the characteristic of the smaller fan to be representative of the larger (and vice-versa), in accordance with the ISO Standard [10] (see Fig. 37).

SECOND CASE The dimensionless characteristics of a 315 mm rotor-only fan running at 1000, 1750 and 2500 rpm are presented in Fig. 39. The curves at 1750 and 2500 rpm are similar. In contrast with the previous case however, the fan performance at 1000 rpm shows a marked decrease in the stable part of the curve with respect to the curves at higher speeds. The marked deterioration featured by the curve at 1000 rpm is caused by operating conditions below the critical Reynolds number $Re_{c_{crit}}$, with related problems of laminar separation [5, p. 237].

1 The ISO Standard [10] considers fans to be large when $D \geqslant 0.8$ m.

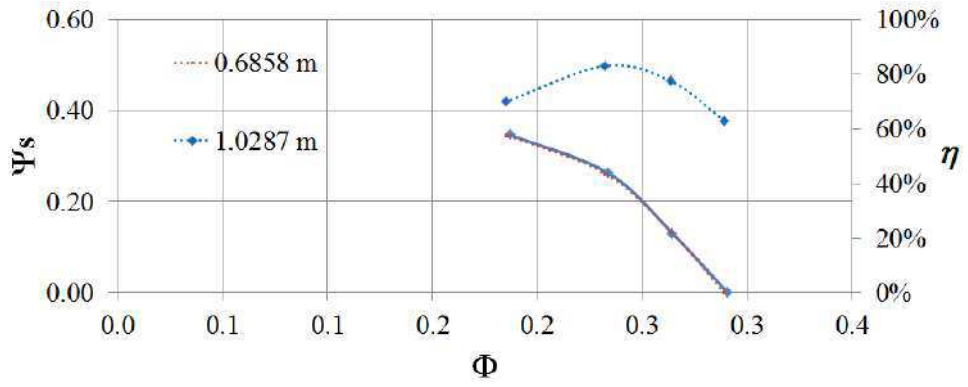

Figure 38: Dimensionless Characteristics of the two geometrically similar medium-to-large fans [16]. In this case the performance and efficiency curves perfectly coincide.

Table 8: Main parameters of the 315 mm fan tested at the Large-size Rig at several rotational speed.

D [m]	n [rpm]	Re_u	Re_{cMS}
0.315	1000	$3.36 \cdot 10^5$	$3.17 \cdot 10^4$
0.315	1750	$6.06 \cdot 10^5$	$5.54 \cdot 10^4$
0.315	2500	$8.59 \cdot 10^5$	$7.85 \cdot 10^4$

There is not agreement on the $Re_{c_{crit}}$ value (compare for instance [3, 5]). According to the laboratory tests presented in [15], the magnitude of the critical Reynolds number suggested by Eck (20000-40000) is reliable.

5.2.3 Reynolds Effects on Fan Operation

The ISO standard [10, p. 53] suggests that a difference $\simeq 4\%$ can be obtained for a Machine Reynolds number ratio equal to 20. Such difference appears rather conservative, also referring at Eckert (in [5, p. 269]) who suggests the following division of the fan operational range, based on the flow coefficient Λ and the Reynolds number *Re*:

$$\begin{aligned} \Lambda \cdot Re < 80 \cdot 10^3 \qquad & \eta \text{ decreses almost linearly down to } 10\% \\ \Lambda \cdot Re > 80 \cdot 10^3 \qquad & \eta \text{ increases up to } 90\% \end{aligned} \tag{47}$$

Eckert reports a similar trend for the rotor performance as well [14].

Fan efficiency curves are affected in terms of peak magnitudes and on the overall shape, as well: for Rotor-Only and Rotor-Straightener fans, with the increase of Re, the peak of the curve moves towards higher flow coefficients and the high-efficiency range widens (see e.g., [15]). On the contrary, the peak efficiency duty shifts towards lower flow-rates for Preswirler-Rotor fans (see [15]).

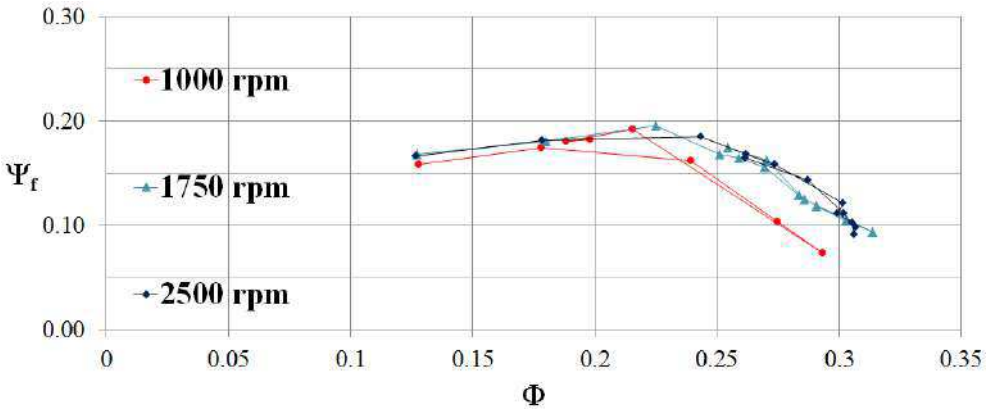

Figure 39: Dimensionless Performance Characteristics of the same 315 mm Rotor-Only fan running at three different speeds. The characteristic at 1000 rpm is markedly lower with respect to the other two curves.

5.3 HUB, CASING AND CENTRE-BODIES

Suitably shaped fairings upstream and downstream of the rotor boss are essential parts of a good design [3, p. 3].

5.3.1 Nose fairing

The nose fairing is important to ensure even inlet flow conditions to the blading, to avoid eventual edge-caused recirculations that would negatively affect the operation of the blade elements in proximity of the root. A smooth converging passage accelerates smoothly the flow from the duct velocity v_m to the annulus one c_a, before entering the blade passage. This is particularly important when the rotor is the first blading row.

DESIGN INDICATIONS According to aeronautical indications, the ideal nose-fairing is a streamlined body of revolution [3]. When the fairing is attached to the rotor is called *spinner*. Hemisphere ([3, 17]) or paraboloid (see [18] and Fig. 40) are the most common solutions for fan applications. Other shapes exist as well (see for instance [5, p. 279]).

The spinner length is usually sacrificed due to dimensional limitations. This might cause significant performance penalizations (e.g., [17]), with a more pronounced effect expected for designs featuring relevant hub-to-tip ratios ($\nu \gtrsim 0.55$) and relatively large flow-rates. In Tab. 9 the results of three experimental investigations dealing with different nose-fairings are tabulated. The effects of reducing the nose-fairing length appear relevant at the high flow-rate coefficient ($\Phi = 0.375$) and $\nu = 0.5$ case. In this case, the references [3, 14] do not include experimental details that give confirmation to the data reported in Tab. 9; in particular, the losses due to absence of the spinner appear overestimated. However, such detriments could be justified if parts of the blades of the high-flow-coefficient fan experience bad-

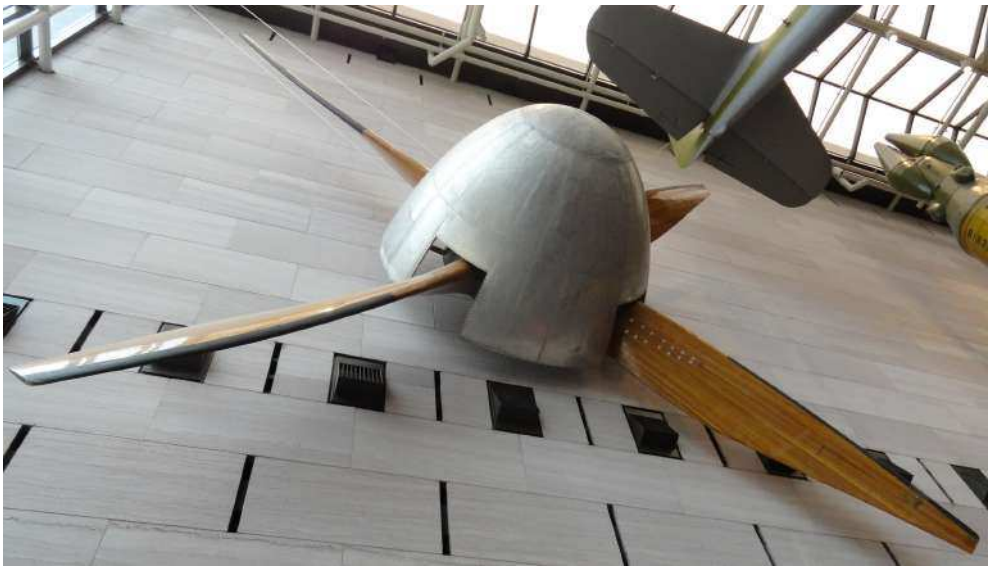

Figure 40: NASA 10.6 m Fan with a parabolic spinner. The fan was installed in the Full Scale Wind Tunnel (Hampton, Virgina) and is now visible at the Smithsonian Museum, Washington DC.

condition flows (i.e., recirculations and uneven flow distributions) caused by the absence of the spinner. On the contrary, the two fans designed for $\Phi = 0.14$ do not experience measurable performance or efficiency drop with the substitution of the hemispherical fairing. Wallis, as well, reports that no differences in fan performance were observed on a $\nu = 0.4$ Rotor-only fan without spinner [3, p. 416]. In [19], however, an increase of the absorbed power was observed at a different blade stagger angle ($\xi_h = 62°$).

The pressure losses (e.g., due to friction) related to well-designed nose-fairings or spinner are usually neglected [3, p. 249].

Table 9: Effect of different fairing geometries on fan performance and efficiency.* Assumed referring to fan pressure.

Ref.	Φ	ν	Fairing	Ψ_f^*	η_f*	$\Delta\Psi_f$	$\Delta\eta_f$
[3, 14]	0.375	0.5	hemisphere	$\simeq 0.53$	$\simeq 74\%$	-	-
			30%d long	$\simeq 0.48$	$\simeq 64\%$	$\simeq 9\%$	$\simeq 14\%$
			absent	$\simeq 0.24$	$\simeq 38\%$	$\simeq 54\%$	$\simeq 49\%$
Ref.	Φ_{Des}	ν	Fairing	Ψ_{sf}	η_{sf}	$\Delta\Psi_{sf}$	$\Delta\eta_{sf}$
[17]	0.14	0.45	hemisphere	$\simeq 0.13$	$\simeq 56\%$	-	-
			Flat disk with rounded edge (3.7%d)	$\simeq 0.13$	$\simeq 56\%$	$\simeq 0\%$	$\simeq 0\%$
[19] $\xi_h = 59°$	0.14	0.4	hemisphere	$\simeq 0.12$	$\simeq 59\%$	-	-
			Flat plate	$\simeq 0.12$	$\simeq 59\%$	$\simeq 0\%$	$\simeq 0\%$

5.3.2 Tail cone

Downstream of the blading the air axial velocity shall decrease from the annulus value c_a back to the duct one v_m. Differently from the case of the nose-fairing, generally the flow quality downstream of the fan is not essential to ensure that the machine operates properly [10].[2] As a matter of fact, many industrial fans are actually manufactured without tail-cone. The addition of a well-designed tail-cone creates a smooth diverging passage, allowing the partial conversion of the axial velocity pressure within the annulus ($\frac{1}{2}\rho c_a^2$) into static pressure at the fan exit. Another way of looking at the action of the tail-cone is that it reduces the recirculation downstream of the fan hub, thus limiting the total pressure losses within the fan unit. In any case, the dead-air zone downstream of the hub naturally creates a diverging passage for the bulk annulus flow. However, this action is not free of losses and decreases fan pressure-rise. The losses related to the tail-cone absence increase with the flow-rate and with the hub-to-tip ratio, making the tail-cone inclusion more important for high-pressure fans.

A $\nu = 0.4$ Preswirler-Rotor fan (D=800 mm) featuring a paraboloid tail-cone with $\frac{l}{D} = 0.375$ was tested at the large test rig of the University of Padova, with and without tail-cone. The performance characteristics are compared in Fig. 42. The difference is appreciable (i.e., larger than the measurement uncertainty) only at free-delivery operation ($\Delta\Phi \simeq +14\%$). This is in accordance with the use of spinning tail-cone in marine propulsion (see Fig. 41a)). Higher differences are expected at larger flow-coefficients.

DESIGN INDICATIONS Downstream fairings usually feature streamlined shapes (see Fig.s 41) or conical ones, eventually truncated at 10-20% cone length in proximity of the apex (e.g., [3, 20]). Both fixed and spinning solutions exist. The minimum tail-cone length ratios $\frac{l}{D}$ suggested in [3] for fans with $0.4 \leqslant \nu \leqslant 0.75$ are presented in Fig. 43. The tail-cone length can be truncated at a distance of $10-20\%l$, thus further reducing the overall length [3, p. 255].

Wallis [21] reports that no difference were observed using a streamlined or a conical tail-cone (of similar length) on the performance of a $\nu = 0.5$ Rotor-Straightener fan. Furthermore, he adds that the pressure losses related to the two geometries are virtually equal [3, p. 96].

TAIL-CONE EFFICIENCY The tail-cone is an unavoidable feature of any installation seeking for the highest efficiency. Tube-axial fans (of any hub-to-tip ratio), by contrast, are generally manufactured without tail cone. Being a diffusing passage, tail-cone's performance are strongly affected by the flow conditions at the annulus exit as well as by the Reynolds number [21].

2 An exception is represented by bulky obstacles that might obstruct the fan duct exit, see the ISO Standard[10].

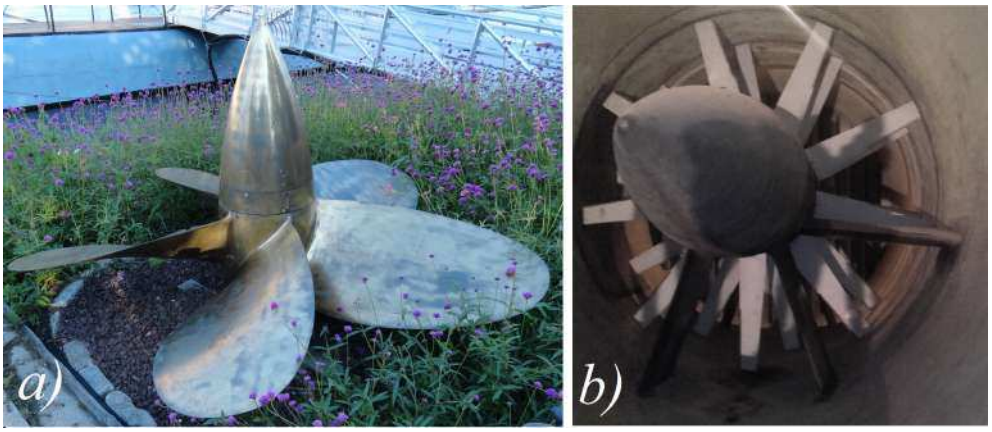

Figure 41: Streamlined tail-cones for different applications. *a)* Submarine's propulsive propeller; *b)* 4.2 m Contra-rotating Axial fan of the Von Karman Institute *Low-Speed* Wind Tunnel (Belgium)

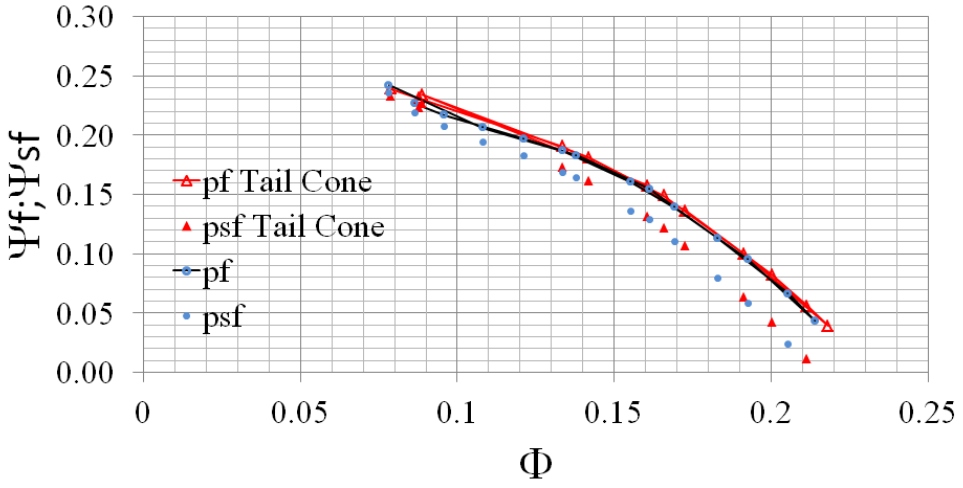

Figure 42: Performance characteristics of a $\nu = 0.4$ Preswirler-Rotor fan with and without spinning tail-cone.

The diffuser efficiency is defined in [3] as

$$\begin{aligned}\eta_{Tc} &= \frac{p_{out} - p_{An}}{\frac{1}{2}\rho(\overline{c_a}^2 - \nu_m^2)} \\ &= \frac{p_{out} - p_{An}}{\frac{1}{2}\rho\overline{c_a}^2[\nu^2(2-\nu^2)]}\end{aligned} \tag{48}$$

where p_{An} is the static pressure at the annulus exit and p_{out} is the static pressure at the fan outlet flange.

Depending on the Reynolds number and the inlet flow quality, the efficiency achievable for a well-designed tail-cone is $\eta_{Tc} = 80 - 90\%$, being 94% the theoretical maximum limited by the skin friction [3, pp. 91-92-254]. Wallis [3, p. 254] indicates that a small residual swirl can be beneficial to the tail-cone performance.

The efficiency of the diverging passage that the dead-air zone creates naturally in absence of the tail-cone is a function of the hub-to-tip ratio; a linear variation extrapolated from [3, p. 95] is reported:

$$\eta_{nTc} = 0.8 - 0.2 * \nu \tag{49}$$

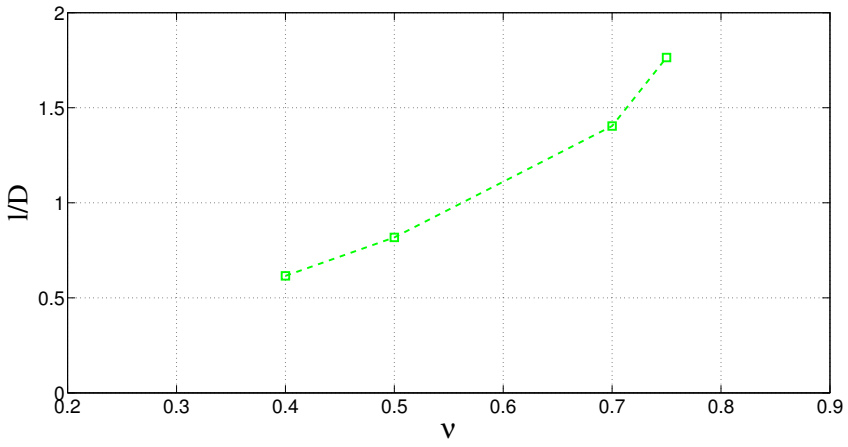

Figure 43: Minimum Tail-cone length ratios l/D for fans discharging into a cylindrical duct according to Wallis [3, p. 254].

5.3.3 Hub shape and length

Fan hubs usually feature a cylindrical shape. However, conical hubs have been used (see e.g., [18]), with the likely aim of reducing the static pressure rise through the rotor [3, p. 6]. Cases are reported [5, p. 301] of fans that feature a streamlined shape connecting together the spinner, the hub and the tail-cone. In some *adjustable pitch* rotor-only machine the hub is rounded along the axial direction to keep the root-clearance *rc* uniformly small at different blade positioning angles. However, this solution locally creates a convergent-divergent wall and is likely to favor the airflow detachment from the hub at fan operations at lower flow-rates [3, p. 226], although no quantitative indications are reported on the argument. Tests on conical hubs have been performed on compressor rotors [22] and on an approximately constant-swirl Rotor-only fan ($\nu = 0.4, \Phi \simeq 0.2$) [3, 23]. In this last case, a slight increase of the pressure rise was observed only at free-delivery operation. It was then concluded that the use of conical bosses is not justified for Rotor-only fans [3, p. 416].

Conical hubs are expected to be more detrimental for rotor-only fans operating at higher flow coefficients. The author is unaware of other design indications on hub shapes.

Hub Axial length

The fan hub shall be long enough to ensure the correct development of the flow along the blading. Friction losses in an annular passage can be computed according to Idel'chick [24, pp. 53-54,57]:

$$\Delta p_{loss} = \lambda_{ann} \frac{l_{ann}}{D(1-\nu)} \cdot \frac{1}{2} \rho c_a^2 \tag{50}$$

where l_{ann} is the longitudinal hub length (blading passages excluded, see in the following) and λ_{ann} is an empirical annulus friction coefficient [24] that is function of the wall roughness, the Reynolds number and the hub-to-tip ratio.

Because of the magnitude of the friction coefficient $\lambda_{ann} << 1$, the aerodynamic penalty related to friction is relatively small compared to other loss sources within the machine. However, the hub is a cost-effective component, in particular for Rotor-only machine. Some fan manufacturers substitute the cylindrical hub with a simple flat disk (for instance, see the large diameter fans of Fig. 1). According to the results presented in [17], this solution might cause a 7% drop of the fan static efficiency at *BEP* and an overall reduction of the curve.

DESIGN INDICATIONS A design practice can be extending the hub 10% ch_r upstream and downstream of the blade leading and trailing edges. However, this solution might involve excessive hub lengths, especially in case of free-vortex blades (that may feature long chords in proximity of the hub). In some cases the blade elements in proximity of the blade root are designed according to an arbitrary vortex criterion.

5.3.4 Motor Position

The motor presence might affect the fan aerodynamics due to its relatively important volume. Some installations feature a motor outside of the duct, with a belt-pulley system that brings the motion to the rotor. This solution has important advantages in terms of engine cooling and maintenance but involves transmission losses. There is a current industrial trend towards the direct-drive solution.

For direct-drive systems, the motor is usually embedded inside the fan hub fairing for Vane-axial configurations [3, p. 304]. In the Tube-axial one conversely, the fluted motors are positioned upstream or downstream of the rotor (A and B configurations, respectively [1]). In this case, the motor diameter is always slightly smaller than the fan hub diameter. However, struts and electric boxes interact in some manner with the airflow (e.g., [3, p. 253]). This occurrence is expected to affect somehow the fan performance, particularly for the upstream-motor solution that might induce some detrimental *inlet* effect [16, 25] on the aerodynamics. To the best of author's knowledge, there are no quantitative informations in the literature on the subject.

5.3.5 Casing Shape and Length

In most of fan applications, the casing shape that includes the fan blading is cylindrical, sometimes allowing for an upstream contraction and a downstream expansion (see e.g., [5]) or vice-versa. Converging ducts have been used to reduce the aerodynamic loading on the rotor blades [3, p. 6], then using a suitable diffuser to convert the subsequent velocity into static pressure. The obvious consequence is an non-uniform inlet velocity distribution, involving the necessity of a specific design with an increased complexity.

Casing length

The suggested minimum length of the cylindrical fan casing is the one related to the definition of *fan unit* (Sec.2.2). Accordingly, the casing shall include all the fan apparatus, comprehensive of the centre bodies such as nose and tail. This occurrence is expected to ensure uniform inlet flow conditions to the blading. According to Bleier [16, pp. 4.5-4.6] tube-axial and vane-axial casing length is at least one fan diameter. The pressure losses within the annular passage can be computed with Eq. 50.

Inlet Conditions

It is here remarked the fundamental importance of ensuring good-quality flow conditions at the blading entrance; it is a fundamental requirement particularly for rotor blades. Most of the fan rotors are designed under the assumption of uniform flows at the rotor entrance. Consequently, distorted flows can cause consistent variations of the fan performance. When unwanted, these distortions are generally referred as *system inlet effects* [25].

The problem of inlet distortion is obtaining a discrete research interest, especially in relation to innovative solutions for aeronautical propulsion systems [26].

Qualitative indications for a correct fan installation exist (e.g., [5, p. 301]). No quantitative indications have been found on the minimum distance required from the fan blading to upstream duct variations for ensuring homogeneous flow conditions.

5.4 BLADES

5.4.1 Loading Factor Design

The general form of the *Loading Factor* equation has been introduced in Par. 2.7. A different form of Eq. 40 is obtained under the assumption of constant axial velocity through the blade ($c_{a1} = c_{a2}$), and reported in Fig. 44 to highlight two different approaches to blade design. For a required velocity distribution, the designer can face with two different options: *a)* selecting a suitable lift coefficient C_L and then computing the required solidity accord-

$$C_L = \frac{2\cos\beta_m}{\sigma}(\tan\beta_1 - \tan\beta_2) - C_D\tan\beta_m \quad (A)$$

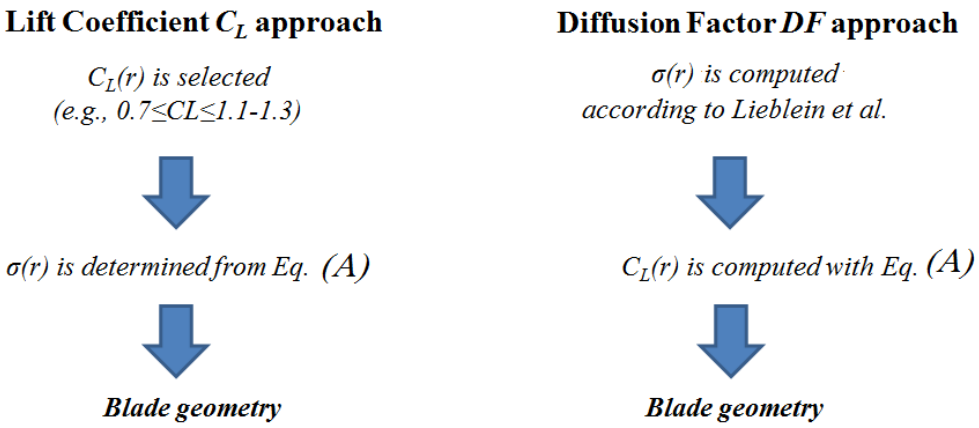

Figure 44: Opposite approaches to Blade design.

ingly, or *b)* selecting a suitable solidity distribution $\sigma(r)$, identifying in turn the required C_L and C_D (Fig. 44).

For a required operational duty the question if a particular lift coefficient distribution $C_L(r)$ provides a higher blading efficiency (once inserted into Eq. A in Fig. 44) with respect to others is legitimate. Wallis [27] reports:

> *"One of the vital phases of fan design is in fixing the design distribution of non-dimensional lift C_L along the span. "*

Being the question of the optimum $C_L(r)$ related to the optimum solidity distribution, the question must be faced jointly.

Lift Coefficient Approach

In the fan community blades are usually designed by using Eq. 40 and assuming a distribution of the lift coefficient along the blade span (e.g., [28, 29]). The selection of the lift coefficient C_L is related to the selection of the airfoil: for a given section family, there is a specific camber that will perform the required C_L with the highest lift-to-drag ratio $\frac{C_L}{C_D}$. To achieve this condition the angle of attack α at the highest $\frac{C_L}{C_D}$ shall be selected.

Being $C_D << C_L$, the second term of the right hand side of Eq. A in Fig. 44 is usually neglected (e.g., [19, 30])), leading to an overestimation of the blade-element lift coefficient.

Once a C_L value is assumed, Eq. A in Fig. 44 can be solved to obtain the corresponding local solidity σ. The efficiency of this approach relies on the arbitrary selection of the lift coefficient, however. Some C_L values are suggested in the literature for fan blade design: Turner [31] reports C_L equal to 0.6-0.7 at the blade tip and $\leqslant 1$ at the root, while Downie et al. [23] suggest to not exceed 0.7 and 1.3 at the blade tip and root, respectively. Examples of blade design with $C_L = 1.3$ all along the blade exist [28] as well, however.

Solidity Distribution Approach

Differently from the lift coefficient approach, some authors compute directly the solidity distribution (from the required velocity distribution) using empirical correlations, obtaining then the required lift coefficient from Eq. A in Fig. 44. In this manner, all the parameters of Eq. A in Fig. 44 are identified and the blade design is completed.

Two empirical methods of selecting the optimum σ distribution have been here considered. The physical principle underneath these approaches is selecting the lowest solidity that achieves the required flow deflection thus, reducing the aerodynamic skin friction but, contemporary, avoiding excessive losses caused by flow separation.

The first method is the well-known Lieblein's *Diffusion Factor DF* approach [32], where *DF* is given (for $c_a = const$) as:

$$DF = (1 - \frac{\cos\beta_1}{\cos\beta_2}) + \frac{\cos\beta_1}{2\sigma}(\tan\beta_1 - \tan\beta_2) \tag{51}$$

On the basis of NACA-65 cascade data analysis, Lieblein [32] suggests to keep $DF < 0.6$ to avoid excessive flow losses. Instead, analyzing actual rotor compressor data, he noted that lower DF values shall be selected ($DF < 0.45$) at the blade tip. The necessity of reducing the diffusion factor was noted only for the rotors and not for the fixed bladings [32].

A second empirical method has been proposed by McKenzie [33]: the simple Eq. 52 can be solved computing the distribution of the ideal (i.e., inviscid) pressure coefficient Cp_{th}, that is known from the required velocity triangles (see Eq. 53). According to McKenzie, the distribution $\sigma(r)$ computed with Eq.52 should enable local blade-section efficiencies $\eta_{tt} > 90\%$.

$$\frac{1}{\sigma} = 9 \cdot (0.567 - Cp_{th}) \tag{52}$$

where Cp_{th} is computed as

$$Cp_{th} = 1 - (\frac{W_2}{W_1})^2 \tag{53}$$

However, Eq. 52 can be used only for velocity ratios $\frac{W_2}{W_1} > 0.658$, while lower values, down to 0.55, can be used for single-stage fans [17, p. 15]. This restriction limits the applicability of Eq. 52 to hub-to-tip ratios magnitudes higher than the lowest usable value.

Other methods of optimum solidity selection have been tempted as well (see e.g., [3, pp. 203-211]). However, such indications generally provide excessively short chord lengths, that in turn substantially decrease the chord Reynolds number Re_c and cause a detriment on fan performance and efficiency (see Par. 5.2).

Summary: Optimum $C_L - \sigma$ Distribution

In spite of the importance of the argument of optimum C_L and σ distributions, to best of author's knowledge there are not systematic studies

available on the argument. Conversely, some ambiguities persist: Wallis, for instance, [3, pp. 315-322] uses alternatively the lift coefficient approach or the solidity distribution one according to the case.

The question of the selection of the optimum combination $C_L - \sigma$ for blading design has been treated in [34]. Even if a definitive answer to the problem has not been achieved so far, experimental and numerical comparisons performed by the author on blades featuring comparable chord lengths suggests that the *Diffusion Factor* approach ($DF_r = 0.55, DF_t = 0.4$) allows the achievement of the required pressure with a higher efficiency with respect to blades designed with the arbitrary imposition of the lift coefficient.

Nonetheless, it is here suggested (see Par. 6.3) to approach the blade design applying in parallel the two criteria (C_L and *DF* one) and comparing the results (also with the indications about suitable lift coefficients reported in Par. 5.4.1).

5.4.2 Isolated airfoil *vs* Cascade design method

The majority of axial fans is of the *low-* and *medium-* pressure type (i.e., ν <0.71). For these type of machines the solidity is usually lower than 1.2 at the blade root and decreases along the span. It is therefore justified the usual habit among fan designers of designing blade elements under the isolated airfoil assumption (i.e., with negligible effects of the adjacent blades). By contrast, cascade data are suggested for high-pressure fans that feature relevant solidities [3]. The two design methods are operationally different, being the first based on lift coefficient considerations, while the second on the required flow deflection $\theta = \beta_1 - \beta_2$. A case with $\sigma_{MS} = 0.6$ has been investigated in [35] to assess the most accurate design method for medium solidity conditions: results showed that the isolated airfoil approach, including an interference factor correction, is the most accurate solution even at medium solidity conditions. Unpublished results provided further confirmation and it was concluded that the isolated airfoil assumption is sufficiently accurate for engineering design purposes for blades with maximum solidity equal to $\sigma_h = 1.2$ and decreasing along the span. The inclusion of the interference factor, with its related complexity, turned out to be unnecessary.

5.4.3 Stagger Angle computation

In axial fan design the stagger angle ξ (i.e., the angle between the BE chord and the rotor axis, see Fig. 45) is usually computed subtracting the airfoil angle of attack α from the direction of a reference velocity [3]. In the literature there is not a general agreement on which velocity to refer to: if the inlet velocity W_1 or the mean one W_m, although this selection is fundamental for the *BE* to achieve the required flow deflection. In Fig. 45 the different geometries that result staggering the *BE* with respect to W_1 or W_m are sketched:

3 Another approach, used with the cascade design approach, compute the stagger angle as $\xi = \beta_1 - i - \frac{\theta_{cam}}{2}$ [3, p. 213]

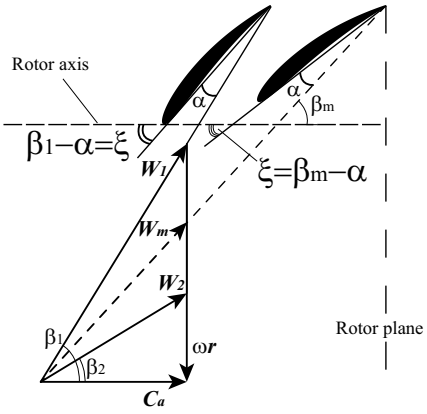

Figure 45: Different Approaches to Stagger the Blade elements, from [34].

the resulting ξ is higher in the first case and lower in the second. This angular difference depends on the magnitude of the flow deflection $\theta = \beta_1 - \beta_2$ and is larger at the blade root and smaller at the tip in the free-vortex case.

Vavra [36] demonstrated that the blade element *sees* the mean velocity W_m as the aeronautical one at the infinite, because of the induced flow deflection. The numerical results reported in [34] give support to this indication. Accordingly, the staggering of the elements with respect to W_m, according to

$$\xi = \beta_m - \alpha \tag{54}$$

is suggested for blading design featuring $\sigma_{bl_h} \leqslant 1.2$.

5.4.4 Number of blades nr_{bl}

Most of the authors agree that a minimum nr_{bl} shall be selected (at required solidity) to achieve high fan efficiencies, by decreasing the turbulence losses generated by the blade edges [16]. In particular, Bleier [16] reports that a single draped blade would be the most aerodynamically efficient configuration, but that practical solutions usually feature 5 to 12 blades. Schmidt [37] experimentally measured an increase of the fan efficiency with the reduction of the blades (at equal solidity).

The simple correlation proposed by Madison (in [38]) to compute nr_{bl} according to the fan hub-to-tip ratio is:

$$nr_{bl} = \frac{6\nu}{1-\nu} \tag{55}$$

that provides values between 3 and 14 for hub-to-tip ratios between $0.3 < \nu < 0.7$, respectively.

Fan applications with constrained axial dimensions may require higher nr_{bl} to limit the chord lengths. In addition to the turbulence losses, reducing the chord length can be detrimental for fan performance (see sec. 5.2).

Extended chords, with the increase of the Reynolds number, can be beneficial for blade aerodynamics [17, p. 17].

5.4.5 Stacking-line

The blade stacking-line *SL* is the line that connects the blade-section centroids along the span, from the root to the blade tip. A *SL* that lies on the geometrical radius of the fan conference is called a *radial* stacking-line. Conversely, when the airfoils are moved along the flow direction the *SL* is said to be *swept* (forward swept when the airfoils are moved toward the flow direction, backswept when airfoils are moved to the rear). If the airfoils are also moved perpendicularly to the flow (i.e., with the inclusion of a dihedral angle) the blade is said to be *skewed*. Further indications on the blade *SL* parameters the can be found in [39].

A radial stacking-line represents the simplest solution and allows the performance achievement with high efficiency for most of the fan applications. However, a radial *SL* is usually unpleasant in terms of noise production. Accordingly, several axial fans operating in a human environment feature non-radial stacking lines.

Sweep angles superior than 40° are required to achieve acoustic benefits according to Carolus and Starzmann [28]. The complexity of the blading design is increased to account for the loading decrease of the blade sections (with the aeronautical $\cos(\lambda)$ rule, e.g., [39]).

There are also evidences that forward swept blades can be beneficial to extend the stall margin [40] and to increase the efficiency of blades that feature positive gradients of circulation along the span $\frac{d\gamma}{dr}$ (e.g., [41, 42]).

DESIGN INDICATIONS A criterion to identify the sweep angle γ for blades designed for a Constant-swirl distribution has been proposed in [43] and experimentally verified in [44]. In the same work, the inclusion of additional sweep angle in the upper portion of the blade showed further relevant gains both in performance and efficiency extension; the reader is referred to the references [43, 44] for a deeper description of the subject.

5.4.6 Blade Roughness

Blade roughness can be a variable affecting the fan performance. For instance, Eckeret [5, p. 237] measured a 10% decrease of the fan efficiency comparing a rough blade and a polished one.

Design indications on the suitable blade surface roughness are reported in [45], where the effects of increasing the blade surface roughness on a $\nu = 0.8$ low-speed compressor (with $220000 < Re_c < 450000$) were investigated. Results show a relevant decrease of the adiabatic efficiency for the rough blade with respect to the polished ones. The efficiency drop is $\simeq 3\%$ in proximity of the peak pressure and increases constantly with the flow rate up to $\sim 33\%$; the pressure ratio characteristics show a decrease as well. It is

Table 10: Surface Roughness of the Blades tested at the Large and Medium Test rigs.

Production Process	Ra_rad [μm]	Ra_c [μm]
Metal Casting	2.2	3.0
3D Printing FDM	18.6	11.4

concluded that no performance and efficiency variation should be expected for aerodynamically smooth surfaces (i.e., for surfaces where the laminar sublayer of the boundary layer is sufficiently thick to cover the protuberances of the surface in question). The limit value indicated is

$$\frac{\rho \cdot v \cdot (k_s)}{\mu} < 100 \tag{56}$$

where v is the local flow velocity and k_s is the equivalent sand grain height [46].

Leading Edge Additional Roughness

The performance of the blade elements are also related to the turbulence intensity upstream of the blading. In some cases a decrease of the drag coefficient has been obtained in wind-tunnel cascade tests introducing an additional leading-edge roughness [47]. This occurrence forced the transition from laminar to turbulent of the boundary layer, thus avoiding a laminar separation that was the cause of an excessively thick downstream boundary layer.

Nonetheless, in contrast with the results obtained on cascade tests, the indications on blade roughness are quite univocal: the smoother the better.

5.4.7 Blade Attachment system

Axial fans usually feature elongated blades, with blade-section thicknesses that increase towards the hub for structural reasons. Blade roots, then, in general feature an enlarged structure to ensure a proper structural behavior (see Fig. 46).

This feature is generally neglected during the design process of the blading. The unique indications known to the author on the subject are reported in [48] where the effect of the attachment system has been investigated locally through CFD simulations. The numerical results showed a local increase of the axial velocity caused by the blockage due to the connection system.

5.4.8 Airfoil

Turbomachine designers generally do not design the airfoils, rather they select those suitable for their application. However, a good knowledge of the airfoil parameters and of the possible options for axial fans is required.

Figure 46: Particular of the blade attachment system of the 4.2 m Von Karman Institute wind tunnel CR fan.

Table 11: Suggested blade-sections for axial fan applications [3, 29].

Nation	Profile
Great Britain	C4
USA	NACA 65
Germany	Göttingen
-	Cambered plates

Important gains can be achieved selecting the appropriate blade profile for a given operation [8]. Fan designers however, usually choose blade profiles on the basis of their personal experience, sometimes with a limited awareness of other solutions' potential.

Surveys of airfoil families considered suitable for axial fan applications are presented in [3, 29] and reported in Tab. 11. According to Wallis [3, 49] the *F* blade sections (C4 airfoils with a composite camber line to eventually include a leading edge droop) are the favorite choice for axial fan purposes. No experimental confirmation was found in the literature, however. The reason for limiting the choice to the families of Tab. 11 is likely the low Re_c of the experimental data ($200000 \leqslant Re_c \leqslant 400000$), that is an important aspect for turbomachines [8]. The relevant characteristics of a proper airfoil selection are described in [8] and are summarized briefly in the following.

Keeping in mind that the options are limited, it is fair to know which are the effects related to each airfoil parameter. The following treatise concern mainly with the behavior of an airfoil section in isolated conditions (i.e., the interference effect of adjacent blade is negligible). This is the common assumption for most of axial fans. A brief discussion on interference effects is reported as well.

Camber-line type

Airfoil's performance largely depends on its camber-line characteristics [3, Cap. 6]. Camber-line shapes are determined by several parameters, with the camber θ and the maximum-camber position along the chord $\frac{b}{c}_{max}$ representing the most characterizing ones for turbomachinery applications.

Maximum camber

The airfoil camber is principally related to the required flow deflection θ through the following formula:

$$\theta_{cam} = \beta_1 - \beta_2 + (i - \delta) \tag{57}$$

where $\beta_1 - \beta_2$ is the flow deflection angle, i is the local incidence (i.e., the angle between the flow direction and the tangent to the camber-line at the leading edge) and δ is the deviation (i.e., the angular distance between the blade metal angle and the flow direction at the trailing edge). Indications on how to estimate i and δ are reported in [3].

From another view, if a lift coefficient magnitude is required, there is a specific camber that will achieve such C_L with higher lift to drag ratio than the others [34].

Maximum camber position

Neglecting composite camber-lines (i.e., camber-lines that are defined by different relations according to the chord-wise coordinate), the position of the maximum camber defines the camber-line shape. This parameter $\frac{b}{c}|_{max}$ has a strong influence on the velocity distribution on the suction side of the airfoil. In particular, convex velocity distributions with a high velocity-peak are associated with front $\frac{b}{c}|_{max}$ position along the chord, that translate into a wide low-drag operational range, high $C_{L_{max}}$ and an abrupt stall. All these characteristics make camber-lines with front $\frac{b}{c}|_{max}$ ($\simeq 30 \div 40\%$ of the chord *ch*) the best choice for low-speed axial turbomachines [8]. By contrast, it is worth of noticing that Bamberger [2, p. 72] suggests optimum values of $\frac{b}{c}|_{max}$ that range between 40 and 60%*ch* depending on the design operation of the fan. The design contrast between the previous author somehow provides support to the usual axial-fan habit of employing circular arc camber-lines (with a 50% maximum camber position) [5, p. 237].

Leading Edge Droop

According to author's best knowledge, the use of composite camber-lines on axial fan is limited to the eventual inclusion of the leading edge droop proposed in [49, 50] to extend the operational duty range. The leading-edge-droop modification substitute the usual circular arc camber-line with a cubic-law in the front part (up to $\simeq 0.2 \cdot ch$) of the airfoil. Wallis claims that this *LE* droop should be beneficial for blades operating at the typical

chord Reynolds number of axial fans [3, 49] and that 1% droop has been successfully employed on several industrial fans [50].

Although the author had a positive experience with tests performed on general-purpose axial fans that were incorporating some LE droop, currently no definitive confirmation on the beneficial contribution of this modification is known.

Maximum Thickness

The ideal solution to generate as less drag as possible should be an infinitesimally thin airfoil [8]. Clearly, this is impracticable from a structural point of view and profile-blades for axial fans normally feature thicknesses between 6 and 12% of the chord. However, Carter [8] claims also that the additional drag related to an increase of the thickness would not be excessively detrimental on the airfoil lift-to-drag ratio if $th|_{max} < 12.5\%$. This is in accordance with Wallis' indications as well [3]. For a given camber-line, in general increasing the maximum airfoil thickness will increase the minimum drag coefficient, lower the maximum lift coefficient (although making the stall less abrupt), and wide the low-drag range [51].

Stepanoff [52, p. 256] claims that no differences have been observed in terms of performance and efficiency when comparing identical fans that differ only for the blade thickness; experimental data (from Eckert) in support of this affirmation are reported. It is believed unlikely however that the characteristics of the two fans might actually coincide, in particular at the peak pressure point where the detrimental effect of a sharp leading edge would cause an earlier stall.

Position of Maximum Thickness

The position of the maximum thickness plays a role similar to the one of the maximum camber position [8]. Accordingly, a front position for th_{max} is suggested to achieve highest lift-to-drag ratios, $30 \div 40\%$ of the chord length being typical values. Carter's indications find support in Bamberger's design charts [2, p. 73], that suggests $\frac{th_{max}}{ch}$ relying approximately between 14-33% of the chord. The thickness distribution of laminar airfoils, with their rearward position of th_{max} (see [53]), is considered detrimental at low-speeds, accordingly. An indirect indication in this sense comes from the NASA Ames Wind Tunnel design presented in [54]. In that case the addition of thickness in the front part of the airfoil with respect to the conventional NACA 65 shape turned out into gains of the stall margin and a less abrupt stall behavior.

Leading Edge Radius

There are very limited informations on the matter of the leading edge size [8]. The effects on the airfoil performance are limited to some variation on the $C_{L_{max}}$ and the minimum drag coefficient $C_{D_{min}}$. In general, for a given thickness distribution, at subsonic speeds a larger LE radius allows a

wider operational range for the airfoil. Conversely, airfoil with smaller LE are expected to feature a reduced range of angle of attack and experience an abrupt stall[50]. At low-speeds typical of axial fans an appreciable drag reduction with smaller LE radii is not ensured [8, fig. 17].

Trailing Edge Radius

Trailing edge size is much more effective on airfoil performance than *LE*. The reason is mainly related to the importance of the Kutta-Joukowsky condition [55].

In general, thinner trailing edges are ideal to keep blade-wakes as thin as possible. However, manufacturing, vibrational and structural aspects must be taken into account in the actual fan operation.

Larger TE radii increase both the minimum drag and, more importantly, decreases the flow deflection performed by the airfoil cascade [51]. This has been confirmed by experimental tests on an actual fan, as well [56].

Design Angle of Attack (or Incidence)

As anticipated, the angle of attack (or incidence angle) α that ensures the maximum lift-to-drag ratio is the best option for axial fan blading design [18, 28, 29].

Using the angle centered in the minimum drag range can be suitable for high-speed operations, but not for low-speed applications[47].

C4 against NACA-65

It is of practical interest a brief digression to compare the two profiles that are claimed to be the best solutions for axial fans: the British C4 and the American NACA-65. The two airfoil series are compared in Tab. 12 for a 10% maximum thickness: for the reasons reported in the previous paragraphs on the position of th_{max} and LE radius, the C4 sections should be favorite for fan blades. It merits to be reported that Wallis repeatedly claims that laminar airfoils (e.g., NACA 65 sections) are not suitable for fans applications, as it is very unlikely that the low-drag bucket can exist in presence of *a)* surface imperfections; *b)* high turbulent intensity. Both these conditions are typical for general-purpose axial fans. Nonetheless,there are some particular fan applications where environmental conditions suitable for laminar airfoils are likely to exist (some kind of air-cooled heat exchangers, for example).

C4 and NACA-65 blades have been investigated at preliminary level (i.e., without a definitive experimental confirmation) in [34]. Results confirms what reported in [29] and the better low-speed behavior for blade profiles that feature a maximum thickness closer to the LE reported in [8] provide an explanation to these results. Nonetheless, although no systematic investigation are known, during the design of the fan system of the NASA wind tunnel they changed from C4 to NACA-65. The explanation, unfortunately, is not reported.

Table 12: Comparison between the parameters of C4 and NACA 65 airfoils (10% thick); percentage with respect to the chord length Data from [3, 47, 57]

	C4	NACA 65 (a=1)
camber-line	circular-arc	Symmetric cubic-law (similar to a circular-arc)
$\frac{b}{c}\|_{max}$	50%	50%
$\frac{th}{c}\|_{max}$	30%	40%
LE radius	1.20%	0.67%
TE radius	0.6%	0.15%
Airfoil C_L	Angle of Attack [°]	
0.6	2.5	2.3
0.7	3.0	2.6
0.8	3.5	2.9
0.9	3.6	3.2
1.0	4.0	3.5
1.1	4.4	3.8
1.2	4.6	4.1

5.5 ROTOR BLADE CLEARANCES

Due to the substantial impact on fan performance and efficiency a dedicated paragraph is reserved to the matters of tip and root clearances (although geometrically pertaining to the blade's sphere; see Sec. 5.4).

The rotor blade clearances are a characteristic aspect of turbomachinery. The effects on fan performance and efficiency are mainly related to:

- bleed flow through the gaps;
- secondary flows (e.g., the tip vortex).

Tip-clearance *tc* effects have been widely studied in the past (in particular for aero-engine blading) and are still one of the most investigated subject nowadays. Aero-engine blading, however, do not feature root-clearances *rc*, which is, on the contrary, a peculiar characteristic of general-purpose industrial fans that received very little research attention [3, p. 226].

WHICH DIMENSIONLESS PARAMETER? Generally, in the fan literature blade-clearances are presented as a dimensionless ratio between the gap and a suitable dimension. According to the specific author, the denominator within this ratio is the fan diameter D (e.g., [5]) or the blade span bs (e.g., [3])[4]. Both the approaches have advantages and drawbacks: $\frac{tc}{D}$, for instance, provides a figure of the aerodynamic quality of the machine (smaller gaps are used for highly efficient fans), while the ratio with respect to the blade-span

4 In the literature on Axial compressors the tip clearance is eventually divided with the chord length; see for instance: Horlock, J. H. (1967). Some recent research in turbo-machinery. Proceedings of the Institution of Mechanical Engineers, 182(1), 571-594.

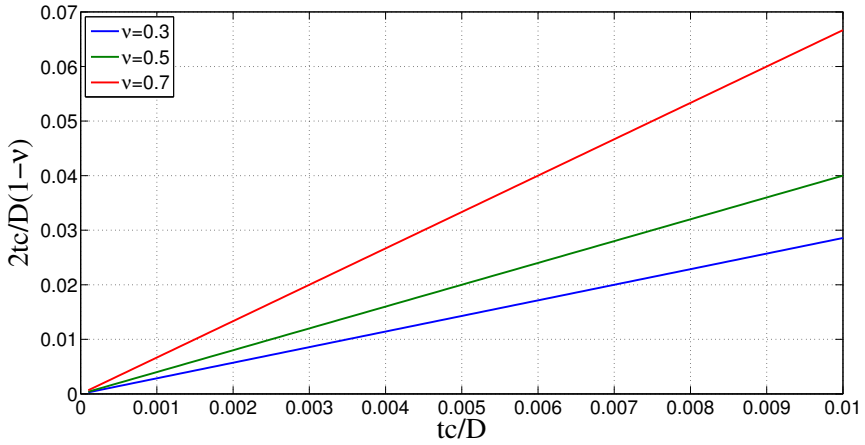

Figure 47: Relation between tip clearance ratios.

(e.g., $\frac{tc}{b_s}$) gives an information about the length of the "*useless*" part with respect to the effective one (i.e., the blade span).

It is author's opinion that a comprehensive treatment of the clearance aspect should resemble both the informations. Accordingly, the following dimensionless figures are suggested:

$$\begin{aligned} tc^* &= \frac{tc}{D} \cdot \frac{2}{(1-\nu)} \\ rc^* &= \frac{rc}{D} \cdot \frac{2}{(1-\nu)} \end{aligned} \tag{58}$$

These ratios represent the gap magnitude with respect to the maximum ideal blade height (i.e., the radial casing-hub distance $\frac{D}{2}(1-\nu)$). Although formally similar to the $\frac{tc}{b_s}$ ratio used in [3], the symbols of Eq.s 58 provide two additional informations: *i)* the pressure duty of the fan through the hub-to-tip ratio (*low- medium- high*-pressure, see Sec. 5.1), and *ii)* the manufacturing quality of the machine. The relation between the ratio $\frac{tc}{D}$ and tc^* is presented in Fig. 47 for three ν magnitudes.

As a rule of thumb, blade clearances shall be kept as low as possible to achieve the highest pressure as well as the highest efficiency.

5.5.1 Tip clearance

The argument of the tip clearance *tc* is one of the most important and, at the same time, complex of fan engineering. General-purpose axial fans for industrial applications usually feature relevant tip clearances, eventually accounting for manufacturing inaccuracies, vibrations and/or blade elongations due to thermal gradients. A tip-clearance ratio $\frac{tc}{D} \simeq 0.5\%$ is a typical value in the fan industry [17, 58]. Conversely, axial compressors generally feature smaller tip clearances. This difference makes the problem of relevant $\frac{tc}{D}$ ratios a specific argument of the axial fan technology. To author's best

knowledge, a comprehensive treatise on the argument is still missing. As a consequence the subject is still matter of investigation (e.g., [59, 60]).

PERFORMANCE AND EFFICIENCY DROP Treating of the detrimental effects on axial fan characteristics caused by relevant a tip gap is quite complex. In absence of a comprehensive systematic investigation on the subject, some insights are here reported that may suggest further investigations. Particular emphasis is reserved to detrimental effects at design flow-rates.

The detrimental effects with increasing *tc* have been shown by several authors, both at the design flow-rate (e.g., [17, 61]) and along the entire fan characteristic (e.g., [59, 62]). In general:

- there is a reduction of the pressure rise and of the efficiency at any flow-rate higher than the deep stall of the characteristic;
- the peak efficiency is reduced in magnitude and shifts towards lower flow-rates;
- there is a reduction of the fan operational range.

According to Venter & Kröger [62], tip clearance effects depends on the type of fan rotor, size, and type of installation. Size and installation effects are related to the boundary layer relative thickness, that can differ in the actual fan installation from the scaled model testing [62]. Under the assumption of flow similarity however, the following loss relations are suggested for conventional straight blades (i.e., with radial stacking-lines):

$$\begin{aligned}\Delta\Psi &= f'(\frac{tc}{D}; \nu; \Phi_{Des}; \frac{d\Gamma}{dr}) \\ &= f'(tc^*; \Phi_{Des}; \frac{d\Gamma}{dr})\end{aligned} \tag{59}$$

and

$$\Delta\eta = f''(tc^*; \Phi_{Des}; \frac{d\Gamma}{dr}) \tag{60}$$

where $\frac{d\Gamma}{dr}$ indicates the gradient of the aerodynamic circulation Γ along the blade ($\frac{d\Gamma}{dr}$ is equal to zero for free-vortex blades). The reasons behind the formulation of Eq.s 59 and 60 are:

ν At equal $\frac{tc}{D}$ the hub-to-tip ratio plays a role according to Fig. 47.

Φ_{Des} At equal $\frac{tc}{D}$, performance and efficiency drops are expected to rise with the design flow-rate, because of the increase of the air bleed through the clearance gap.

$\frac{d\Gamma}{dr}$ Rotors with non-free-vortex (*NFV*) blades feature higher efficiency losses with increasing *tc* with respect to free-vortex ones [63], [3, p. 416].

It should be remarked that f' and f'' into formulations 59 and 60 are different relations. The effects of increasing *tc* on the two parameters differ substantially and *"[..] are unlikely to respond to a common treatment method"*[3, p. 225]. A general-validity form (i.e., accounting for rotor fan type, size, and installation) for the symbolic correlations 59 and 60 is not available. The formulation in [62] for the estimation of Δp_{sf} represents a valuable indication for rotor-only fans (see also [59]). On the contrary, the relation suggested in [3] for free-vortex rotor fans

$$\Delta\eta_f = 2 \cdot \left(\frac{tc}{\text{blade span}} - 0.01\right) \tag{61}$$

generally underestimates the efficiency drop (see also Fig. 48) and is claimed of limited applicability in the fan community.

The careful reader should have noted that it is not specified whether the pressure and efficiency drops of Eq.s 59 and 60 refer to the fan pressure p_f or to the fan static pressure p_{sf}. According to the position of focusing on tip-clearance effects at the design flow-rate $q_{v_{Des}}$, the fan velocity pressure p_{df} is uniquely defined (for a given fan diameter D and rotational speed). Consequently, pressure and efficiency drops are presented in terms of fan static pressure p_{sf} and efficiency η_{sf}. The conversion into *fan pressure* parameters depends on the p_{df} at design duty and can be easily obtained.

In Fig. 48 drops of the static pressure coefficient and efficiency for several rotor-only machines featuring different loading distributions have been collected together. Further experimental indications are reported in [5, p. 269]

5.5.2 Root clearance

The root clearance rc indicates the gap between the blade root and the rotor hub. Plastic rotors usually feature blades that are molded directly with the hub, with $rc = 0$. However, this solution is constrained to small fans ($D \lesssim 400\,mm$) running at low speed ($n \simeq 1000\,rpm$). On the contrary, general-purpose industrial fans usually feature blades that are manufactured in a single piece and that are installed on the rotor-hub through some sort of mechanism. In this manner, the stagger angle of the blade can be changed, increasing or decreasing the fan performance according to the purchaser's needs. Such machines are called *adjustable pitch* fans. Blade roots must feature a suitable distance from the hub to deal with relevant angular rotations (except when the blade is molded directly on a rotating base, e.g., see Fig. 46).

Wallis [3, p. 226] claims that the aspect of the hub clearance have received little effort, and suggests that no efficiency losses must be accounted for clearances $rc^* < 0.5 - 1\%$. Indications on the losses experienced by two cases of axial fans are reported in Tab. 13.

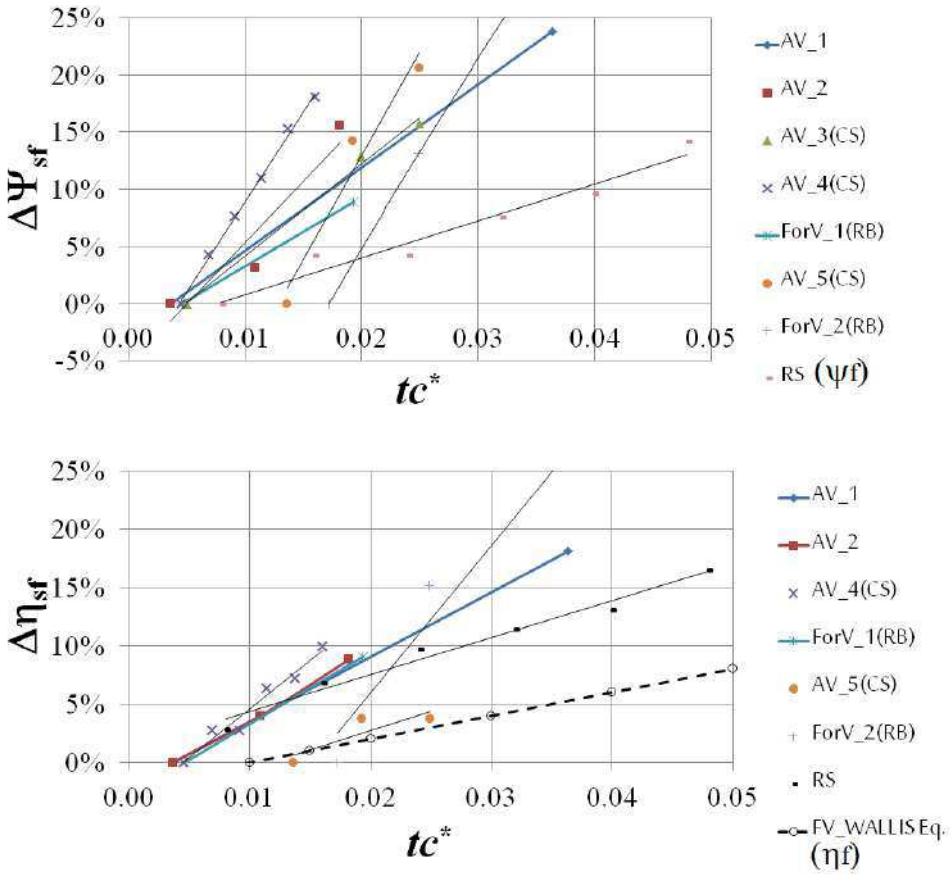

Figure 48: Performance and Efficiency drops with the increase of the dimensionless tip clearance tc^*.

Table 13: Measured Performance and Efficiency losses due to the root clearance.

Config.	ν	rc^*	$\Delta\Psi$	$\Delta\eta$	Ref.
PRS	0.5	$\simeq$ 4.7%	$\simeq$ 0	2%	[3, 27]
RO	0.4	$\simeq$ 2.8%	16%	7%	[19]

5.5.3 End Plates

The concept of plates installed at the blade tip has been investigated in recent years as a tool to reduce fan noise (e.g., [64]). Variations on fan performance and efficiency were recorded as well. Wilkinson and Van der Spuy [59] investigated the effects of metal-sheet end-plates on the the performance of a Rotor-only axial fan with tc^* ranging from approximately 0.4% to 1.3%, recording positive effects, in particular on the fan static efficiency. It seems reasonable expecting further gains from more refined end-plates concepts. Some fan manufacturers include rotors with end-plates in their catalogue (see, for instance, Cofimco®and Wingfan®)

BIBLIOGRAPHY

[1] International Standard Organization. *Fans - Vocabulary and definitions of categories (ISO 13349:2010)*. 2010.

[2] Konrad Bamberger. "Aerodyamic Optimization of Low-Pressure Axial Fans". PhD Thesis. Siegen, Ger: University of Siegen, 2015.

[3] R Allan Wallis. *Axial flow fans and ducts*. Krieger, 1993.

[4] William C Osborne. *Fans*. Vol. 1. Pergamon Press Oxford, 1966.

[5] Bruno Eck. "Fans". In: *1st English ed., Pergamon Press, Oxford* (1973), pp. 139–153.

[6] LE Idel Chick. "Handbook of Hydraulic Resistance Coefficient of Local Resistance and Friction". In: (1966).

[7] Theodore Von Kármán. *Aerodynamics: selected topics in the light of their historical development*. Courier Corporation, 2004.

[8] ADS Carter. "Blade Profiles for Axial-Flow Fans, Pumps, Compressors, Etc." In: *Proceedings of the Institution of Mechanical Engineers* 175.1 (1961), pp. 775–806.

[9] Peter F Pelz and Stefan S Stonjek. "The influence of reynolds number and roughness on the efficiency of axial and centrifugal fans—a physically based scaling method". In: *Journal of Engineering for Gas Turbines and Power* 135.5 (2013), p. 052601.

[10] International Standard Organization. *Industrial fans - Performance testing using standardized airways (ISO 5801:2009)*. 2009.

[11] ESDU. *A guide to fan selection and performance*. Data Item 79037. London, GB: Engineering Sciences Data Unit, Apr. 1980.

[12] Eastman N Jacobs and Albert Sherman. "Airfoil section characteristics as affected by variations of the Reynolds number". In: (1937).

[13] Laurence K Loftin Jr and Hamilton A Smith. "Aerodynamic Characteristics of 15 NACA Airfoil Sections at Seven Reynolds Numbers from 0.7 x 10 (exp 6) to 9.0 x 10 (exp 6)". In: (1949).

[14] JL Koffman. "Fans for Traction Applications". In: *Diesel Railway Traction, March, April* (1951).

[15] Masi Massimo, Castegnaro Stefano, and Lazzaretto Andrea. "Experimental Investigation on the effect of Reynolds Number on the efficiency of Single-stage Axial-flow Fans". In: Under Evaluation for *ASME Turbo Expo 2018: Turbomachinery Technical Conference and Exposition*. American Society of Mechanical Engineers.

[16] Frank Bleier. *Fan Handbook: selection, application, and design*. McGraw-Hill Professional, 1998.

[17] Konrad Bamberger, Thomas Carolus, and Markus Haas. "Optimization of Low Pressure Axial Fans and Effect of Subsequent Geometrical Modifications". In: *Proc. Fan 2015* (2015).

[18] LS Marks and JR Weske. "The Design and Performance of Axial-Flow Fan". In: *ASME Trans., AER-56-13* 56.11 (1934), pp. 807–813.

[19] Francois G Louw et al. "The design of an axial flow fan for application in large air-cooled heat exchangers". In: *ASME Paper No. GT2012-69733* (2012).

[20] Yu Yongsheng QuXiaoli et al. "DESIGN AND TEST OF THE HIGH AERODYNAMIC PERFORMANCE LOW-NOISE FAN FOR 5.5-BY 4-M ACOUSTIC WIND TUNNEL". In: (2016).

[21] Raymond Allan Wallis. *Annular Diffusers of Radius Ratio 0.5 for Axial Flow Fans*. CSIRO, 1975.

[22] Wallace M Schulze, George C Ashby Jr, and John R Erwin. "NACA 65-series compressor rotor performance with varying annulus-area ratio, solidity, blade angle, and Reynolds number and comparison with cascade results". In: (1953).

[23] RJ Downie, MC Thompson, and RA Wallis. "An engineering approach to blade designs for low to medium pressure rise rotor-only axial fans". In: *Experimental thermal and fluid science* 6.4 (1993), pp. 376–401.

[24] I.E. Idel'chick. "Handbook of Hydraulic Resistance Coefficient of Local Resistance and Friction". In: (1966).

[25] J Barrie Graham. "The importance of fan total pressure". In: *Heating, piping and air conditioning* 66.9 (1994), pp. 75–80.

[26] JJ Defoe and DK Hall. "Fan Performance Scaling With Inlet Distortions". In: *ASME Paper No. GT2016-58009* (2016).

[27] RA Wallis. "Development Of The Primary Ventilation System At Mount Isa: II, Aerodynamic Design Of New Fans, Aus. IM & M". In: *Proceedings*. 222. 1967.

[28] Thomas H Carolus and Ralf Starzmann. "An aerodynamic design methodology for low pressure axial fans with integrated airfoil polar prediction". In: *ASME 2011 Turbo Expo: Turbine Technical Conference and Exposition*. American Society of Mechanical Engineers. 2011, pp. 335–342.

[29] N Hay, R Metcalfe, and JA Reizes. "A simple method for the selection of axial fan blade profiles". In: *Proceedings of the Institution of Mechanical Engineers* 192.1 (1978), pp. 269–275.

[30] R Allan Wallis. *Axial Flow Fans: design and practice*. Academic Press, 1961.

[31] RC Turner. *Notes on ducted fan design*. HM Stationery Office, 1966.

[32] Seymour Lieblein, Francis C Schwenk, and Robert L Broderick. *Diffusion factor for estimating losses and limiting blade loadings in axial-flow-compressor blade elements*. Tech. rep. National Advisory Committee for Aeronautics, Cleveland Lewis flight propulsion lab, 1953.

[33] AB McKenzie. "The selection of fan blade geometry for optimum efficiency". In: *Proceedings of the Institution of Mechanical Engineers, Part A: Power and Process Engineering* 202.1 (1988), pp. 39–44.

[34] Stefano Castegnaro. "A Critical Analysis of the Differences Among Design Methods for Low-Speed Axial Fans". In: *ASME Turbo Expo 2017: Turbomachinery Technical Conference and Exposition*. American Society of Mechanical Engineers. 2017, V001T09A008–V001T09A008.

[35] Stefano Castegnaro. "Fan Blade Design Methods: Cascade Versus Isolated Airfoil Approach—Experimental and Numerical Comparison". In: *ASME Turbo Expo 2016: Turbomachinery Technical Conference and Exposition*. American Society of Mechanical Engineers. 2016, V001T09A007–V001T09A007.

[36] Michael H Vavra. "Aero-thermodynamics and Flows in Turbomachines". In: (1960).

[37] Henry F Schmidt. "SOME SCREW PROPELLER EXPERTMENTS WITH PARTICULAR REFERENCE TO PUMPS AND BLOWERS". In: *Naval Engineers Journal* 40.1 (1928), pp. 1–26.

[38] Robert Jorgensen. *Fan engineering: An engineer's handbook*. Buffalo Forge Company, 1970.

[39] MG Beiler and TH Carolus. "Computation and measurement of the flow in axial flow fans with skewed blades". In: *Transactions-american society of mechanical engineers journal of turbomachinery* 121 (1999), pp. 59–66.

[40] A Corsini and F Rispoli. "Using sweep to extend the stall-free operational range in axial fan rotors". In: *Proceedings of the Institution of Mechanical Engineers, Part A: Journal of Power and Energy* 218.3 (2004), pp. 129–139.

[41] János Vad, Gábor Halász, and Tamás Benedek. "Efficiency gain of low-speed axial flow rotors due to forward sweep". In: *Proceedings of the Institution of Mechanical Engineers, Part A: Journal of Power and Energy* 229.1 (2015), pp. 16–23.

[42] Massimo Masi, Stefano Castegnaro, and Andrea Lazzaretto. "Forward sweep to improve the efficiency of rotor-only tube-axial fans with controlled vortex design blades". In: *Proceedings of the Institution of Mechanical Engineers, Part A: Journal of Power and Energy* 230.5 (2016), pp. 512–520.

[43] Massimo Masi, Manuel Piva, and Andrea Lazzaretto. "Design guidelines to increase the performance of a rotor-only axial fan with constant-swirl blading". In: *ASME paper GT2014-27176* (2014).

[44] M Masi, A Lazzaretto, and S Castegnaro. "Effectiveness of blade forward sweep in a small industrial tube-axial fan". In: Under Evaluation for *Proceedings of FAN 2018 Conference. Germany*. 2018.

[45] Jason J Moses, George Serovy, et al. "Effect of Blade-surface Finish on Performance of a Single-stage Axial-flow Compressor". In: (1951).

[46] Hermann Schlichting et al. *Boundary-layer theory*. McGraw Hill, 1968.

[47] L Joseph Herrig et al. "Systematic two-dimensional cascade tests of NACA 65-series compressor blades at low speeds". In: *NACA Rep* 1368 (1958).

[48] M. Tamiozzo. "Analisi e riprogettazione di un ventilatore assiale". PhD thesis. 2011.

[49] RA Wallis. "The F-series aerofoils for fan blade sections. The Institute of Engineers Australia". In: *Mechanical Engineering Transactions* (1977), pp. 12–20.

[50] RA Wallis. "The development of blade sections for axial flow fans". In: *mechanical and chemistry engineering". Trans IE August, vol MC8 (2)* (1972), pp. 111–116.

[51] L Joseph Herrig, James C Emery, and John R Erwin. "Effect of section thickness and trailing-edge radius on the performance of NACA 65-series compressor blades in cascade at low speeds". In: (1951).

[52] Alexey Joakim Stepanoff. *Turboblowers: theory, design, and application of centrifugal and axial flow compressors and fans*. Wiley, 1955.

[53] Eastman N Jacobs. *Preliminary report on laminar-flow airfoils and new methods adopted for airfoil and boundary-layer investigations*. Tech. rep. NATIONAL AERONAUTICS and SPACE ADMIN LANGLEY RESEARCH CENTER HAMPTON VA, 1949.

[54] Henry V Borst. "A new blade element method for calculating the performance of high and intermediate solidity axial flow fans". In: (1978).

[55] Hermann Glauert. *The elements of aerofoil and airscrew theory*. Cambridge University Press, 1926.

[56] S Castegnaro. "Effects of NACA 65-blade's Trailing Edge Modifications on the Performance of a Low-speed Tube-axial Fan". In: *Energy Procedia* 82 (2015), pp. 965–970.

[57] Harriet E Bogdonoff. "Blade design data for axial-flow fans and compressors". In: (1945).

[58] Eleftherios Andreadis. *Design of a low speed vaneaxial fan*. MS Thesis,Cranfield, UK University of Higher Education. 2011.

[59] Michael B Wilkinson and J Sybrand. "The effect of fan tip configuration on air-cooled condenser axial flow fan performance". In: *Proceedings of FAN 2015 Conference. France* (2015).

[60] Alexej Pogorelov, Matthias Meinke, and Wolfgang Schröder. "Effects of tip-gap width on the flow field in an axial fan". In: *International Journal of Heat and Fluid Flow* 61 (2016), pp. 466–481.

[61] A Kahane. "Investigation of axial-flow fan and compressor rotors designed for three-dimensional flow". In: *NACA TN* 1652 (1947).

[62] SJ Venter and DG Kröger. "The effect of tip clearance on the performance of an axial flow fan". In: *Energy conversion and management* 33.2 (1992), pp. 89–97.

[63] János Vad et al. "Comparative investigation on axial flow pump rotors of free vortex and non-free vortex design". In: *Periodica Polytechnica. Engineering. Mechanical Engineering* 46.2 (2002), p. 107.

[64] Alessandro Corsini, Franco Rispoli, and A Geoff Sheard. "Development of improved blade tip endplate concepts for low-noise operation in industrial fans". In: *Proceedings of the Institution of Mechanical Engineers, Part A: Journal of Power and Energy* 221.5 (2007), pp. 669–681.

6 PROPOSED DESIGN METHOD FOR ROTOR-ONLY FANS

The method developed to design Rotor-Only Axial Fans is here presented. On the basis of the information reported in Chapt. 4, the procedure starts with the evaluation of the suitability of the Rotor-only configuration as well as on the selection of the design vortex criteria. A mean-line model is then used to estimate the fan performance and efficiency in case of free-vortex (*FV*) and constant-swirl (*CS*) distributions. The blading design method that allows to achieve the target performance at the peak fan efficiency in then presented.

Only the most important equations are reported to provide a fluid reading of the chapter, relegating the entire mathematical development of the model in Appendix C. The procedure assumes fan operation at chord Reynolds number above $\simeq 80000$.

6.1 ROTOR-ONLY CONFIGURATION EVALUATION; PRELIMINARY SELECTION OF THE VORTEX CRITERION

In this first section the global fan parameters are selected. It is preliminary evaluated whether the Rotor-only configuration is suitable for the requirements. If this is the case, or if the Rotor-only configuration is mandatory, the following step is the selection of the blade loading distribution. The fan performance and efficiency are then estimated in Par. 6.2.

6.1.1 Requirements and evaluation of the Rotor-Only Configuration

The operational requirements of a new design are usually:

the flow-rate q_v $[\frac{m^3}{s}]$

the fan pressure p_f [Pa]

In case of fans operating as *exhaust* machines, the fan static (total-to-static) pressure p_{sf} is the requirement, instead of p_f.

In the fan industry, the diameter of the machine D as well as the rotor speed can be imposed by factors that are not immediately connected with aerodynamics such as space limitations, direct coupling with the electric motor and acoustic reasons. Whether the fan diameter is not constrained, D can be estimated using the Cordier-diagram for rotor-only fans of Fig. 32, after the computation of σ according to Eq.35, with p_f and the assumed rotor speed n (e.g., the electric motor speed). Entering the diagram of Fig. 32,

the fan diameter D can be estimated from the corresponding δ (that is computed with Eq. 35). Whether p_{sf} is required, (*exhaust* case) a preliminary D' value can be assumed, allowing the computation of the fan dynamic pressure $p'_{df} = \frac{q_v}{\pi \frac{D'^2}{4}}$. This, in turn, allows to estimate the fan pressure according to Eq. 12 ($p'_f = p_{sf} + p'_{df}$). With q_v, p'_f, n, the specific speed σ' can be computed (Eq. 35, using p'_f). Entering the Rotor-only-Cordier-line (Fig. 32) with σ', a corresponding specific diameter δ can be obtained with Eq. 35 (using p'_f) and a new D value extrapolated from δ. Such D is compared with the first D' value and the process iterated until convergence. The definitive fan diameter should normally respect the ISO standard indications (e. g., 315, 400, 630 mm, [1, p. 302]), however.

Once q_v, p_f, D and n are defined, the flow and pressure coefficients Φ and Ψ_f can be computed (see Par. 2.4), along with the specific speed σ and diameter δ. According to the $\Phi - \Psi_f$ and $\sigma - \delta$ values, the graphs within Fig.s 25, 26 and Tab. 6 are used to evaluate if the rotor-only configuration is suitable or, conversely, a vane-axial one is more indicated for such operation. Whether the required duty relies within the Rotor-only high-efficiency range, or if the use of the *RO* configuration is mandatory (e.g., because of constraints on the axial length of the machine), the design procedure continues with the evaluation of the suitable vortex criterion.

6.1.2 Preliminary Selection of the Design Vortex criterion

When the Rotor-only configuration has been decided, the design vortex criterion shall be selected. A rapid preliminary evaluation of which vortex class will permit the achievement of the required operation ($\Phi - \Psi_f$ and $\sigma - \delta$) is obtained referring to the graphs 28 and 29. Such graphs provide a first indication of which swirl distribution can be applied among:

- Free-vortex *FV*: $c_u = \frac{const}{r}$;
- Arbitrary-vortex *AV*: $c_u \in \ ]\frac{const}{r}, c_u = const]$ (i.e., free-vortex excluded, constant-swirl *CS* included);
- Forced-vortex *ForV*: c_u increasing along the radius (e.g., $c_u = k \cdot r + b$).

The selection of the vortex criteria entails the related hub-to-tip ratio ν (see e.g., Fig. 31), as reported in the following.

6.2 FAN PERFORMANCE AND EFFICIENCY ESTIMATION, DEFINITION OF THE ν RATIO AND OF THE VELOCITY TRIANGLES

The definitive selection of the vortex criteria is performed after estimating the fan performance and efficiency. The selected vortex criterion (i.e., the

swirl distribution) identifies the hub-to-tip ratio ν as well as the axial velocity distribution $c_{a2}(r)$ at the rotor exit and thus, the span-wise velocity triangles.

The fan performance and efficiency are estimated with a simple *mean-line* model based on the equations and correlations presented in Chapt. 5, and applied differently for two swirl distributions: the free-vortex *FV* and the constant-swirl *CS* one. The model relies on the basic idea of estimating the fan performance and efficiency on the basis of:

$$\begin{aligned}\Psi_f &= f(\Phi, \Psi_{tt_{th}})_{tc=0} - \Delta\Psi_{f_{tc}} \\ &= \Psi_{f_{tc=0}} - \Delta\Psi_{f_{tc}}\end{aligned} \tag{62}$$

$$\begin{aligned}\eta_f &= f(\Phi, \Psi_{tt_{th}})_{tc=0} - \Delta\eta_{f_{tc}} \\ &= \eta_{f_{tc=0}} - \Delta\eta_{f_{tc}}\end{aligned} \tag{63}$$

meaning that Ψ_f and η_f are given by the values estimated in absence of the tip clearance ($\Psi_{f_{tc=0}}$ and $\eta_{f_{tc=0}}$) less the decrements due to the actual tip clearance (right-hand side terms into formulations 63,62).

The development of the model is reported in Appendix C for the *FV* case; the entire development of the analogous *CS* model is presented in [2], while the differences with respect to the *FV* one are highlighted in the Appendix C.

If the estimated Ψ_f and η_f values satisfy the requirements, the swirl distribution is defined and, in turn, the velocity triangles. Therefore, the blade geometry that is able to actually *induce* such flow field (i.e., the *Prescribed Velocity Distribution* approach [3]) can be designed in accordance with the indications presented in the next paragraph 6.3.

The estimation model has been applied satisfactorily on *FV* and *CS* rotor-only fans. It is therefore expected to be successfully applicable to any kind of arbitrary-vortex distribution *AV*. On the contrary, this *mean-line* approach is considered less applicable to *Forced-Vortex* rotor-only machines because of: *i)* the higher radial motion within the blade passage with respect to the other vortex classes, and *ii)* the fact that several *ForV* rotor-only industrial machines actually operates under back-flow conditions at hub and "*[..] there is no analytical treatment capable of dealing with the associated complex flow*"[1, p. 392]. The author has only limited experience with designing such *Forced-vortex* machines; a design method has been proposed in [4].

6.3 BLADING DESIGN

Designing a blade geometry that induces the required flow field (i.e., the required flow deflection) in correspondence of the fan peak efficiency is not immediate. Several design actions have to be performed and sometimes the indications from the literature are not unanimous [5]. The following blade design procedure has been validated against several numerical and experimental cases of *FV* and *CS* rotor-only fans.

ASSUMPTIONS The main assumptions are:

- A limited number of blade sections is considered along the span to build the blading geometry, with the blade surface being *draped* around them. The extreme sections rely at the root radius r_r and at the casing (internal) radius R, respectively.

  Lewis [6] suggests a minimum number of blade sections equal to 8. However, it is suggested to insert additional sections in proximity of marked geometry variations.

- Only the bulk flow is considered, neglecting: *i)* the blade-surface boundary layer, *ii)* secondary flows at the rotor hub and tip.

- Flow angles β and velocities at the same radius (both for *FV* and *CS* cases) are considered for the computation of the local *loading factor* and the staggering of the blade elements. This is strictly correct in the free-vortex case, in which the flow develops along cylindrical surfaces; it is sufficiently accurate for engineering purposes also in case of arbitrary-vortex blades (see also [7–9]).

  Relating velocity triangles at equal radius might not be applied in case of low ν ratio Forced-vortex rotors. In such conditions in fact, the radial motion within the blade passage can be relevantly higher with respect to the other vortex cases.

- The blade-section lift coefficient C_L is substantially identified by the airfoil mean-line, the camber magnitude θ_{cam} and the angle of attack α (provided that the leading-edge sufficiently rounded to prevent any separation).

- The isolated airfoil approach can be used directly up to root solidities $\sigma_{bl_r} = 1.2$, without any correction as the multiplane interference factor in [1].

- The hub and casing are cylindrical.

- The stacking-line is radial.

- Flow conditions at the rotor inlet (section 1) are considered homogeneous and purely axial ($c_{a1} = c_a = \frac{q_v}{\pi R^2(1-\nu^2)}$)

PROCEDURE The sequential blading design procedure is presented as follows:

1. Computation of the velocity triangles at sections 1 and 2 (inlet and outlet rotor sections) according to the selected swirl distribution ($c_u(r) = c_{u2}(r)$). In case of *NFV* design, the axial velocity distribution at the ro-

tor outlet $c_{a2}(r)$ shall be computed according to the radial equilibrium equation (Par. 2.6).

$$\tan\beta_1 = \frac{\omega r}{c_{a1}}$$
$$\tan\beta_2 = \frac{\omega r - c_{u2}}{c_{a2}}$$

At the blade root, the minimum axial velocity ratio shall respect $\frac{c_{a2_r}}{c_a} \leqslant 0.4$ [9] to ensure a sufficient margin from back-flow operation.

2. Considering velocity triangles at the same radius r, computation of the mean velocity triangle as

$$c_{a_m} = \frac{c_{a1} + c_{a2}}{2}$$
$$w_m = \|\vec{c_{a_m}} + (\vec{\omega r} - \frac{\vec{c_{u2}}}{2})\|$$
$$\tan\beta_m = \frac{\omega r - \frac{c_{u2}}{2}}{c_{a_m}}$$

3. Calculation of the span-wise blade solidity according to Lieblein et al [10, p. 9] with

$$DF = (1 - \frac{\cos\beta_1}{\cos\beta_2}) + \frac{\cos\beta_1}{2\sigma}(\tan\beta_1 - \tan\beta_2) \tag{64}$$

for the free-vortex case, while for the general *NFV* one using:

$$DF = (1 - \frac{w_2}{w_1}) + \frac{c_{u2}}{2\sigma w_1} \tag{65}$$

A linear span-wise variation of the diffusion factor can be taken, ranging from $DF_r = 0.55 - 0.6$ at the blade root to $DF_{tip} = 0.4 - 0.45$ at the blade tip. The DF magnitudes at hub and tip can be tuned to provide a lift coefficient distribution (see the following item) as close as possible to the use of a single C_L along the blade-span.

In case of constant-swirl blade design, the assumption of a single lift coefficient C_L along the blade-span results into a chord length that is almost constant along the span [11].

The maximum solidity at the blade hub is imposed as $\sigma_{bl_h} = 1.2$. If such magnitude cannot be respected, an increase of the hub diameter shall be evaluated.

4. Preliminary calculation of the lift coefficient distribution along the blade-span with

$$C_L = \frac{2\cos\beta_m}{\sigma}(\tan\beta_1 - \tan\beta_2) - C_D \tan\beta_m$$

for the free-vortex case. The drag coefficient C_D from two dimensional airfoil tests shall be used. For the arbitrary-vortex case the following approximate form is used:

$$C_L \simeq \frac{2}{\sigma} \frac{c_{u_2}}{w_m}$$

5. Assuming a number of blades nr_{bl} with the equation (5.4.4)

$$nr_{bl} = \frac{6\nu}{1-\nu} \tag{66}$$

6. The Equations at step 4 generally provide a span-wise distribution of the lift coefficient $C_L(r)$ with several decimal digits. However, it is more practical using coefficients with a single decimal (i.e., $C_L = 0.7, 0.8$, etc.). Accordingly, a new lift coefficient distribution is assumed, considering one-decimal-digit C_L, proximal to the one computed at step 4 (e.g., $C_L = 0.82$ is rounded to 0.8).

7. With the one-decimal-digit lift coefficient distribution, a new solidity $\sigma(r)$ distribution is computed according to the loading factor equation (step 4). The slight difference with the first solidity distribution does not affect significantly the blade element efficiency.

8. The required blade-element lift coefficient C_L can be performed considering C4 airfoils at the angle of attack α of maximum $\frac{C_l}{C_d}$ ratio (see Tab. 12).

9. Each blade-element is staggered according to

$$\xi = \beta_m - \alpha \tag{67}$$

10. The blade-elements are positioned at the intersection between the radial stacking-line and the circumference of the reference radius r.

11. In case of free-vortex swirl distributions, the airfoils (blade-elements) shall be projected on the reference cylindrical surface. Conversely, the airfoils shapes can be left bi-dimensional in case of arbitrary-vortex blades.

12. The blade is generated with a drape (*loft*) operation through the blade-elements.[1]

13. The tip clearance *tc* is generated by the intersection of a cylindrical surface and the blade (keeping the blade at the design stagger angle).

This procedure can be automated, for instance with the Rhinoceros®modeling software, together with a Python™script.

1 It shall be ensured that the *loft* operation is performed by the CAD software respecting the original blade-elements shapes.

6.4 COMPENDIUM: ROTOR-ONLY DESIGN PROCEDURE

1. From the requirements q_v and p_f/p_{sf} and assuming/computing the fan diameter D and rotor speed n (see Par. 6.1.1), computation of the dimensionless parameters

$$\Phi \qquad \Psi_f \qquad \sigma \qquad \delta$$

2. Evaluation of the suitability of the Rotor-Only configuration, entering the graphs 25, 26 and Tab. 6 with the $\Phi - \Psi_f$ and $\sigma - \delta$ couples computed at item 1.

3. Whether the Rotor-only configuration is decided, preliminary selection of the vortex criterion that achieves the required operation among free-vortex *FV*, arbitrary-vortex *AV*, and forced-vortex *ForV*, with Fig.s 28 and 29.

4. Estimation of the fan performance and efficiency with Eq.s (see Appendix C):

$$\Psi_f = \left[\overline{\eta_{tt}} \cdot \Psi_{tt_{th}} - (1-\eta_{n,c_u}) \cdot \Psi^2_{tt_{th}} \cdot f_1(\nu) - (1-\eta_{nTc}) \cdot \Phi^2 \cdot f_2(\nu)\right]_{tc=0} - \Delta\Psi_{f_{tc}}$$

$$\eta_f = \left[\overline{\eta_{tt}} - (1-\eta_{n,c_u}) \cdot \Psi_{tt_{th}} \cdot f_1(\nu) - (1-\eta_{nTc}) \cdot \frac{\Phi^2}{\Psi_{tt_{th}}} \cdot f_2(\nu)\right]_{tc=0} - \Delta\eta_{f_{tc}}$$

for different swirl-distributions $c_u(r)$. The distribution (i.e., the vortex-criterion) that achieves the Ψ_f requirement with the highest estimated efficiency shall be selected. The optimum hub-to-tip ratio ν is implicitly defined by the required operation and the selected vortex criterion (see Appendix C) and [2]. The detrimental terms related to the tip clearance $\Delta\Psi_{f_{tc}}$ and $\Delta\eta_{f_{tc}}$ can be estimated from Fig.s 48; *tc* shall be kept as low as possible to achieve an accurate performance and efficiency prediction.

5. Blading design according to the indications reported in Chapter 5. C4 airfoils are suggested; blade elements shall be staggered according to

$$\xi = \beta_m - \alpha$$

with α the angle of attack at highest $\frac{C_l}{C_d}$ ratio, for airfoil polars obtained at Reynolds number $Re_c \simeq 200 - 400 \cdot 10^3$. Maximum loading factor magnitudes $C_L\sigma \simeq 1.2$ are suggested. Whether the design involves chord Reynolds numbers $Re_c \lesssim 50000 - 80000$, substantial performance and efficiency drops shall be expected (see [12]). A reduction of the number of blades nr_{bl} would increase Re_c in that case, whether available.

BIBLIOGRAPHY

[1] R Allan Wallis. *Axial flow fans and ducts*. Krieger, 1993.

[2] Massimo Masi, Stefano Castegnaro, and Andrea Lazzaretto. "A Criterion for the Preliminary Design of High-Efficiency Tube-Axial Fans". In: *ASME Turbo Expo 2016: Turbomachinery Technical Conference and Exposition*. American Society of Mechanical Engineers. 2016, V001T09A006–V001T09A006.

[3] JH Horlock and JD Denton. "A review of some early design practice using computational fluid dynamics and a current perspective". In: *Transactions of the ASME-T-Journal of Turbomachinery* 127.1 (2005), pp. 5–13.

[4] Thore Bastian Lindemann, Jens Friedrichs, and Udo Stark. "Development of a new design method for high efficiency swept low pressure axial fans with small hub/tip ratio". In: *ASME Turbo Expo 2014: Turbine Technical Conference and Exposition*. American Society of Mechanical Engineers. 2014, V01AT10A017–V01AT10A017.

[5] Stefano Castegnaro. "A Critical Analysis of the Differences Among Design Methods for Low-Speed Axial Fans". In: *ASME Turbo Expo 2017: Turbomachinery Technical Conference and Exposition*. American Society of Mechanical Engineers. 2017, V001T09A008–V001T09A008.

[6] RI Lewis. *Turbomachinery performance analysis*. Butterworth-Heinemann, 1996.

[7] A Kahane. "Investigation of axial-flow fan and compressor rotors designed for three-dimensional flow". In: *NACA TN* 1652 (1947).

[8] Thomas H Carolus and Ralf Starzmann. "An aerodynamic design methodology for low pressure axial fans with integrated airfoil polar prediction". In: *ASME 2011 Turbo Expo: Turbine Technical Conference and Exposition*. American Society of Mechanical Engineers. 2011, pp. 335–342.

[9] RJ Downie, MC Thompson, and RA Wallis. "An engineering approach to blade designs for low to medium pressure rise rotor-only axial fans". In: *Experimental thermal and fluid science* 6.4 (1993), pp. 376–401.

[10] Seymour Lieblein, Francis C Schwenk, and Robert L Broderick. *Diffusion factor for estimating losses and limiting blade loadings in axial-flow-compressor blade elements*. Tech. rep. National Advisory Committee for Aeronautics, Cleveland Lewis flight propulsion lab, 1953.

[11] Massimo Masi, Manuel Piva, and Andrea Lazzaretto. "Design guidelines to increase the performance of a rotor-only axial fan with constant-swirl blading". In: *ASME paper GT2014-27176* (2014).

[12] Masi Massimo, Castegnaro Stefano, and Lazzaretto Andrea. "Experimental Investigation on the effect of Reynolds Number on the efficiency of Single-stage Axial-flow Fans". In: Under Evaluation for *ASME Turbo Expo 2018: Turbomachinery Technical Conference and Exposition*. American Society of Mechanical Engineers.

CONCLUSIONS

An investigation on the aerodynamics of low-speed axial fans for industrial applications has been performed, with the aim of providing an innovative and effective design method for this type of machines. The research has been based on theoretical, numerical, and experimental approaches, and both global (i.e., fan pressure and efficiency) and local (i.e., blade design) aerodynamic aspects have been investigated. Two data-bases of fan performance and efficiency (a general one and another specific for the Rotor-only configuration) have been constructed collecting relevant data from the available literature and from more than 100 experimental tests performed on two ISO 5801 test rigs, with the second rig having been specifically designed and built.
The main results of the investigation are:

- The two data-sets have been summarized into $\Phi - \Psi_f$ (flow and fan pressure coefficients) and $\sigma - \delta$ (specific speed and diameter) graphs, that provide a *panorama* of the axial fan operational field. The general graphs (i.e., those for any axial fan configuration) show a relevant extension of the axial-fan range towards higher flow and pressure coefficients with respect to similar previous indications from the literature.
- Three operational ranges have been identified to guide the selection of the single-stage axial-fan configuration, on the basis of the information provided by a simple inviscid model and the general fan data-set:
  - *Rotor-Only fans*: low-pressure rises ($\Psi_f \lesssim 0.2$)
  - *Rotor-Straightener fans*: medium-to-high-pressure rises ($0.2 \lesssim \Psi_f \lesssim 0.5$) at $\Phi \lesssim 0.27$
  - *Preswirler-Rotor fans*: medium-to-high-pressure rises ($0.2 \lesssim \Psi_f \lesssim 0.5$) at $\Phi \gtrsim 0.27$
- Ducted Rotor-only machines (i.e., Tube-axial fans) feature appreciable efficiencies for specific speeds $1.5 \lesssim \sigma \lesssim 2.6$. Fan efficiencies up to $75 - 78\%$ are achieved, featuring magnitudes substantially lower with respect to vane-axial machines.
- Vane-axial (i.e., with fixed blades) and Contra-rotating machines operative duties extend the axial fan range down to specific speeds $\sigma \gtrsim 0.6$. Maximum efficiencies up to $90 - 94\%$ have been measured.
- In the $\sigma - \delta$ graph, where both Rotor-only and Vane-axial fans operate, data pertaining to the first category show higher specific diameters δ at equal σ, indicating that a *Cordier-line* specific for Rotor-only fans relies at higher δ with respect to a diagram for Vane-axial (and Contra-rotating) machines.

- When the Rotor-only *RO* configuration is mandatory (e.g., due to dimensional constraints on the axial length of the machine) and in presence of constraints on the fan diameter (e.g., due to space limitations) and on the rotor-speed (e.g., for acoustical reasons), *arbitrary* and *forced* vortex designs allow to achieve demanding pressure-rise requirements with acceptable efficiencies; in particular:
  - *Free-vortex RO fans* of low hub-to-tip ratios ($\nu = 0.2 - 0.3$) achieve the highest fan total efficiency (up to 77%) at low pressure-rise coefficients ($\Psi_f \sim 0.1$);
  - *Arbitrary-vortex RO fans* with span-wise decreasing swirl distribution achieve relevant efficiency ($\sim 72\%$) at pressure-rises higher than free-vortex design for corresponding flow-rate coefficient ($\Psi_f \sim 0.18$);
  - *Forced-vortex RO fans* are suitable for high flow coefficients ($\Phi > 0.2$) and high pressure coefficient ($\Psi_f > 0.2$). Fan efficiencies up to 62% are achievable, suggesting that forced-vortex rotors are an effective solution for applications where the available axial length of the fan is limited (e.g. air-conditioner external units);

An effective procedure to design Rotor-only fans of the free-vortex and arbitrary-vortex type has been presented. The procedure is based on the information deriving from the fan data-sets, as well as on an analytic model of performance and efficiency estimation and the related blading design methodology. In addition, a specific definition of the axial-flow fan, an actuator-disk model and a Bernoulli-equation model have been developed for didactic purposes. The Bernoulli model allows to relate the axial-fan aerodynamic operation to the parameters that result from a Standard experimental testing.

The results herein presented successfully provide innovative information within the discipline of aerodynamic design of axial fans. Such information, that have been here applied to the Rotor-only fan case with imposed fan diameter and rotor speed, can be conveniently applied to machines with fixed vanes, to provide a comprehensive design methodology for low-speed industrial axial-flow fans.

A DEVELOPMENT OF ANALYTIC EQUATIONS ACCORDING TO THE FAN CONFIGURATION

The analytic Eq.s 14-16 are here developed. It is important to remark that these equations are obtained at the blade mid-span:

$$x_{MS} = \frac{r_{MS}}{R} = \frac{1+\nu}{2} \tag{68}$$

The ratio between the tangential velocity at the blade tip U and the one at mid-span is given by:

$$u_{MS} = U \cdot x_{MS} \tag{69}$$

ROTOR–ONLY

$$\begin{aligned} p_{t_{RO}} &= \rho u c_{u2} - \frac{1}{2}\rho c_{u2}^2 \\ &= \rho u \cdot (u - c_a \cdot \tan\beta_2) - \frac{1}{2}\rho \cdot (u - c_a \cdot \tan\beta_2)^2 \\ &= \rho u^2 \cdot (1 - \frac{c_a}{u} \cdot \tan\beta_2) \\ &-\frac{1}{2}\rho u^2 \cdot \left(1 + (\frac{c_a}{u})^2 \cdot (\tan\beta_2)^2 - 2c_a u \cdot \tan\beta_2\right) \\ &= \frac{1}{2}\rho u^2 \left[1 - (\frac{c_a}{u})^2 \tan\beta_2^2\right] \\ &= \frac{1}{2}\rho U^2 x_{MS}^2 \left[1 - (\frac{c_a}{u})^2 \frac{1}{x_{MS}^2} \tan\beta_2^2\right] \end{aligned} \tag{70}$$

In the dimensionless form:

$$\begin{aligned} \Psi_{RO} &= \frac{p_{t_{RO}}}{0.5 \cdot \rho U^2} \\ &= x_{MS}^2 (1 - \frac{\Lambda^2}{x_{MS}^2} \tan\beta_2^2) \\ &= \left(\frac{1+\nu}{2}\right)^2 \left[1 - (\frac{\Phi}{1-\nu^2})^2 (\frac{2}{1+\nu}^2) \tan\beta_2^2\right] \\ &= (1+\nu)\left[\frac{1+\nu}{4} - \left(\frac{\Phi}{1-\nu^2}\right)^2 \frac{\tan\beta_2^2}{1+\nu}\right] \end{aligned} \tag{71}$$

ROTOR–STRAIGHTENER

$$\begin{aligned} p_{t_{RS}} &= \rho u c_{u2} \\ &= \rho u^2 \cdot (1 - \frac{c_a}{u} \cdot \tan\beta_2) \\ &= \rho U^2 x_{MS}^2 \cdot (1 - \frac{c_a}{U}\frac{1}{x_{MS}} \cdot \tan\beta_2) \end{aligned} \tag{72}$$

In the dimensionless form:

$$\begin{aligned}\Psi_{RS} &= \frac{p_{t_{RS}}}{0.5 \cdot \rho U^2} \\ &= 2x_{MS}^2\left(1 - \frac{\Lambda}{x_{MS}}\tan\beta_2\right) \\ &= 2\left(\frac{1+\nu}{2}\right)\left[1 - \frac{\Phi}{1-\nu^2}\frac{2}{1+\nu}\tan\beta_2\right] \\ &= (1+\nu)\left[\frac{1+\nu}{2} - \frac{\Phi}{1-\nu^2}\tan\beta_2\right]\end{aligned} \tag{73}$$

PRESWIRLER–ROTOR

$$\begin{aligned}p_{t_{RS}} &= \rho u c_{u1} \\ &= \rho u^2 \cdot \left(\frac{c_a}{u} \cdot \tan\beta_1 - 1\right) \\ &= \rho U^2 x_{MS}^2 \cdot \left(\frac{c_a}{U}\frac{1}{x_{MS}} \cdot \tan\beta_1 - 1\right)\end{aligned} \tag{74}$$

In the dimensionless form:

$$\begin{aligned}\Psi_{PR} &= \frac{p_{t_{PR}}}{0.5 \cdot \rho U^2} \\ &= 2x_{MS}^2\left(\frac{\Lambda}{x_{MS}}\tan\beta_1 - 1\right) \\ &= 2\left(\frac{1+\nu}{2}\right)^2\left[\frac{\Phi}{1-\nu^2}\frac{2}{1+\nu}\tan\beta_1 - 1\right] \\ &= (1+\nu)\left[\frac{\Phi}{1-\nu^2}\tan\beta_1 - \frac{1+\nu}{2}\right]\end{aligned} \tag{75}$$

B AXIAL FAN DATA

B.1 DATA-SET FOR ALL AXIAL-FAN CONFIGURATIONS

A selection of fan performance and efficiency data is here reported. Almost only experimental data have been considered within the following table. A conversion of the original data into ISO 5801 standard parameters (and into related dimensionless coefficients) has been necessary in few cases.

Table 14: Performance and Efficiency data for each axial fan configuration.

Config.	Ref.	Φ	ν	Ψ_f	η_f	σ	δ	NOTE
RO	[1]	0.141	0.4	0.123	74%	1.806	1.578	B1-Fan
	[2]	0.140	0.45	0.170	71%	1.416	1.715	Opt_Constrained
	[3]	0.195	0.45	0.201	72%	1.471	1.516	US17
	[4, p. 151]	0.244	0.5	0.155	78%	1.997	1.271	D1
	[4, p. 151]	0.170	0.25	0.110	(84%)	2.153	1.398	D2-excessive η
	[5]	0.253		0.179	69%	1.826	1.293	Tube-Axial
	[6, p. 270]	0.182	0.4	0.169	71%	1.620	1.503	No diffuser
	[7, 8]	0.221	0.2*	0.101	77%	2.633	1.198	full-scale
	[9]	0.215	0.3	0.116	74%	2.329	1.259	DP3
	[10]	0.231	0.4	0.146	71%	2.038	1.286	Fan 1
	[9]	0.108	0.7	0.370	56%	0.693	2.373	DP1
	[11, p. 70]	0.2		(0.1)		2.515	1.257	Original misp. on Ψ
RS	[12, p. 4.37]	0.195	0.64	0.304	74%	1.078	1.682	22° Design
	[12, cap.6-14]	0.179	0.52	0.223		1.301	1.627	
	[12, cap.6-14]	0.141	0.68	0.330		0.863	2.017	
	[12, cap.6-14]	0.234	0.618	0.324		1.127	1.560	
	[12, p. 5.9]	0.232	0.618	0.317	83%	1.140	1.558	
	[4, p. 151]	0.277	0.45	0.38	86%	1.085	1.496	C1
	[4, p. 151]	0.268	0.5	0.52	85%	0.845	1.641	C2
	[4, p. 151]	0.145	0.55	0.25	86%	1.075	1.858	E
	[4, p. 151]	0.225	0.55	0.24	79%	1.384	1.475	F
	[5]	0.253		0.192	80%	1.735	1.315	Vane-axial
	[13]	0.272	0.676	0.40	78%	1.036	1.526	BUP-26
	[13]	0.272	0.676	0.48	80%	0.904	1.597	BUP-29
	[13]	0.272	0.676	0.52	74%	0.851	1.630	BUP-103
	[14]	0.258	0.55	0.279	83%	1.323	1.431	
	[15]	0.265	0.6	0.180	90%	1.867	1.264	
	[16, p. 312]	0.154	0.356	0.042	<80%	4.255	1.151	B not exp.
	[17, 18]	0.343	0.431	0.280	93%	1.522	1.242	
	[11, p. 70]	0.300		0.500		0.921	1.535	

	[11, p. 300]	0.210	0.690	0.715	88%	0.589	2.008	stage efficiency
PR	[4, p. 155]	0.190	0.5	0.265	85%	1.179	1.647	exp. ?
	[4, p. 151]	0.198	0.33	0.044	78%	4.633	1.029	A1
	[4, p. 151]	0.180	0.33	0.086	79%	2.663	1.278	A2
	[4, p. 151]	0.230	0.47	0.160	84%	1.896	1.319	A3
	[4, p. 151]	0.365	0.7	0.500	77%	1.016	1.392	A4
	[4, p. 151]	0.250	0.5	0.300	85%	1.234	1.480	B
	[19]	0.298	0.46	0.180	53%	1.977	1.192	
	[16, p. 399]	0.185	0.4	0.200		1.437	1.556	
	[20]	0.230	0.69	0.446	88%	0.878	1.705	
	PR800 [21]	0.150	0.4	0.166	>50%	1.489	1.648	
PRS	[16, p. 336]	0.200	0.5	0.216	88%	1.412	1.524	
	[22]	0.246	~0.58	0.382		1.021	1.585	
CR	[23]	0.235	0.5	0.507	94%	0.807	1.741	
	[11, p. 317]	0.312	0.5	0.266	90%	1.510	1.285	
	[4, p. 151]	0.203	0.5	0.49	75%	0.769	1.857	
	[24]	0.233	0.29	0.451	74%	0.878	1.697	
	[25]	0.254	0.45	0.4	85%	1.002	1.578	
	[26]	0.243	0.69	0.77	86%	0.600	1.900	

B.2 DATA FOR ROTOR-ONLY FANS

The geometrical specifications and the performance and efficiency data of rotor-fans are reported in Tab. 15. To avoid misunderstandings some clarifications are necessary: i) Whether the chord length at the tip was not declared this value has been estimated by analyzing the pictures of the rotors. Because of the high stagger angles at the tip, c_{tip} is considered approximately equal to the projected length estimated from the front picture of the rotor. This approach introduces uncertainty on the solidity values σ_{tip}, blade aspect-ratio AR and Reynolds number Re_c; ii) the Blade aspect-ratio AR was arbitrary computed on the chord length at the blade tip; iii) the Reynolds number Re_{tip} was computed on c_{tip} and on the tip rotational speed ωR. According to Carter et al. (1960) most of the fans performance reported in Table 1 are not significantly affected by Reynolds number effects. However, for those fans that feature $Re_c < 10^5$ some penalties in terms of efficiency are expected (see also [21]).

Fans were easily classified when the swirl distribution was indicated. When *quasi-* is reported in front of the vortex distribution it is meant that the blade design mostly resembles the related one (e.g., *quasi*-CS means that the swirl distribution is approaching the span-wise constant one). Whenever the vortex-design-criteria is not declared in the original reference, different approaches have been taken (i.e., observation of the velocity distributions at rotor outlet and along the blade span, cross-reference with other

articles of the same author, CFD analysis, and, eventually, analysis of the blade shape). However, some degree of uncertainty in distinguishing free-vortex rotors from arbitrary-vortex ones with span-wise decreasing $c_u(r)$ must be accepted. Whether not specified, air density was assumed equal to 1.2 kg/m^3

Table 15: Rotor-only experimental data at design point or best efficiency, [27]. (*) Estimated.

Ref.	Vortex	Φ	ν	Ψ_f	η_f	σ	δ	Ψ_{sf}	η_{sf}	$Re_{c_{tip}}$	$\frac{tc}{D}$ [%]	NOTE
Peck & Ross, in [6]	FV(*)	0.182	0.4	0.169	71%	**1.620**	**1.503**	0.136	57%	-	-	Rotor-only case
[7, 8]	FV	0.221	~ 0.2*	0.101	77%	**2.633**	**1.198**	0.052	40%	3.86e5	0.1	constant-chord
[9]	*quasi*-FV	0.215	0.3	0.116	74%	**2.329**	**1.259**	0.07	44%	~ 2.00e5	0.1	DP3 rotor
[9]	*quasi*-FV	0.173	0.4	0.236	68%	**1.229**	**1.676**	0.206	59%	2.64e5	0.1	DP2 rotor
FV-1	FV	0.23	0.44	0.187	60%	**1.686**	**1.371**	0.133	41%	5.20e4	0.5	low Re_{tip}
FV-2	FV	0.2	~0.64	0.2	42%	**1.495**	**1.495**	0.145	36%	1.25e5	0.5	no inlet spinner
FV-3	FV	0.23	0.33	0.092	61%	**2.871**	**1.148**	0.04	25%	3.09e4	0.5	low Re_{tip}
[28]	AV(*)	0.141	0.15	0.120	68%	**1.845**	**1.565**	0.100	57%	4.93e5	0.2	GH-fan
[1]	AV	0.141	0.4	0.123	74%	**1.806**	**1.578**	0.103	62%	4.44e5	0.2	B1-fan
[2]	*quasi*-CS	0.14	0.45	0.170	71%	**1.416**	**1.715**	0.15	63%	2.64e5	0.1	constrained design
[9]	*quasi*-CS	0.108	0.7	0.370	56%	**0.693**	**2.373**	0.358	54%	~ 2.00e5	0.1	DP1 rotor
[3]	AV	0.195	0.45	0.201	72%	**1.471**	**1.516**	0.163	58%	2.14e5	0.1	FV - 30% at hub, FV + 20% at tip
[29]	AV(*)	0.222	0.5	0.229	64%	**1.422**	**1.469**	0.180	51%	2.09e5	0.3	opt. rotor
[30]	CS+FV	0.180	0.4	0.189	64%	**1.478**	**1.555**	0.160	54%	2.01e5	0.15	unswept rotor A
[31]	*quasi*-CS	0.197	0.38	0.139	64%	**1.954**	**1.375**	0.101	47%	2.67e5	0.4	Mark-3 rotor
[32]	AV(*)	0.196	0.4	0.146	59%	**1.869**	**1.398**	0.108	44%	8.84e5	0.34	
[10]	*quasi*-CS	0.231	0.4	0.146	71%	**2.038**	**1.286**	0.092	45%	2.51e5	0.48	Fan 1; $\frac{dc_u}{d0}$ <~ 0 decr.
[33]	*quasi*-CS	0.238	0.69	0.249	45%	**1.382**	**1.449**	0.193	35%	3.29e5	0.07	Fan 1
[28]	CS	0.141	0.15	0.115	67%	**1.899**	**1.550**	0.095	55%	4.80e5	0.2	V-fan
[24]	AV	0.174	0.29	0.147	68%	**1.756**	**1.484**	0.117	54%	2.08e5	0.66	RR-rotor
[34]	AV(*)	0.150	0.34	0.178	46%	**1.416**	**1.676**	0.155	40%	2.00e5	0.48	
CS	CS	0.267	0.44	0.226	59%	**1.576**	**1.334**	0.148	41%	7.72e4	0.38	low Re_{tip}
[35]	ForV (*)	0.230	0.28	0.210	29%	**1.546**	**1.412**	0.157	22%	1.97e5	-	
[24]	ForV	0.222	0.29	0.205	59%	**1.546**	**1.429**	0.156	45%	2.01e5	0.66	relevant *tc*
[36]	ForV	0.240	0.2	0.230	60%	**1.476**	**1.413**	0.175	46%	4.50e5	0.6	Fan1.1; relevant *tc*
[36]	ForV	0.209	0.3	0.267	62%	**1.233**	**1.571**	0.225	52%	4.50e5	0.6	Fan2.2; relevant *tc*
[37]	Parabolic	0.185	0.53	0.274	53%	**1.134**	**1.684**	0.240	46%	9.95e5	0.18	ν constrained
[33]	RB	0.238	0.69	0.353	47%	**1.065**	**1.580**	0.296	39%	3.29e5	0.07	Fan 2
RB	RB	0.314	0.337	0.210	62%	**1.710**	**1.230**	0.127	35%	1.12e5	0.6	tip affected

BIBLIOGRAPHY

[1] Francois G Louw et al. "The design of an axial flow fan for application in large air-cooled heat exchangers". In: *ASME Paper No. GT2012-69733* (2012).

[2] Konrad Bamberger, Thomas Carolus, and Markus Haas. "Optimization of Low Pressure Axial Fans and Effect of Subsequent Geometrical Modifications". In: *Proc. Fan 2015* (2015).

[3] Thomas Carolus, Tao Zhu, and Michael Sturm. "A low pressure axial fan for benchmarking prediction methods for aerodynamic performance and sound". In: *FAN2015-International Conference on Fan Noise, Technology and Numerical Methods, Lyon, France*. 2015.

[4] William C Osborne. *Fans*. Vol. 1. Pergamon Press Oxford, 1966.

[5] Eleftherios Andreadis. *Design of a low speed vaneaxial fan*. MS Thesis,Cranfield, UK University of Higher Education. 2011.

[6] Alexey Joakim Stepanoff. *Turboblowers: theory, design, and application of centrifugal and axial flow compressors and fans*. Wiley, 1955.

[7] Enrico Pistolesi. *Il problema dell'elica intubata e le sue applicazioni.* 11. Tipografia editrice cav. F. Mariotti, 1924.

[8] Ten. Castellazzi Ing. Giacomo Arturo. "Impianto Aerodinamico a Circuito Continuo tipo Crocco". In: *Rendiconti Istituto Centrale Aeronautico n.16* (1917).

[9] Konrad Bamberger. "Aerodyamic Optimization of Low-Pressure Axial Fans". PhD Thesis. Siegen, Ger: University of Siegen, 2015.

[10] Massimo Masi, Manuel Piva, and Andrea Lazzaretto. "Design guidelines to increase the performance of a rotor-only axial fan with constant-swirl blading". In: *ASME paper GT2014-27176* (2014).

[11] Bruno Eck. "Fans". In: *1st English ed., Pergamon Press, Oxford* (1973), pp. 139–153.

[12] Frank Bleier. *Fan Handbook: selection, application, and design*. McGraw-Hill Professional, 1998.

[13] János Vad and Ferenc Bencze. "Three-dimensional flow in axial flow fans of non-free vortex design". In: *International journal of heat and fluid flow* 19.6 (1998), pp. 601–607.

[14] Daniel Giesecke et al. "Aerodynamic and Acoustic Performance of a Single Stage Axial Fan With Extensive Blade Sweep Designed to Limit Noise Emissions". In: *ASME Turbo Expo 2016: Turbomachinery Technical Conference and Exposition*. American Society of Mechanical Engineers. 2016, V001T09A004–V001T09A004.

[15] Yu Yongsheng QuXiaoli et al. "DESIGN AND TEST OF THE HIGH AERODYNAMIC PERFORMANCE LOW-NOISE FAN FOR 5.5-BY 4-M ACOUSTIC WIND TUNNEL". In: (2016).

[16] R Allan Wallis. *Axial flow fans and ducts*. Krieger, 1993.

[17] David B Signor. "An experimental investigation of two 15 percent-scale wind tunnel fan-blade designs". In: (1988).

[18] David B Signor and Henry V Borstt. "Aerodynamic performance of two fifteen-percent-scale wind-tunnel drive fan designs". In: *NASA Contr. Report* 3063 (1986).

[19] Jesús Manuel Fernández Oro et al. "On the structure of turbulence in a low-speed axial fan with inlet guide vanes". In: *Experimental Thermal and Fluid Science* 32.1 (2007), pp. 316–331.

[20] E Barton Bell. "Test of Single-Stage Axial-Flow Fan". In: *NACA Rep.* 729 (1942).

[21] Masi Massimo, Castegnaro Stefano, and Lazzaretto Andrea. "Experimental Investigation on the effect of Reynolds Number on the efficiency of Single-stage Axial-flow Fans". In: Under Evaluation for *ASME Turbo Expo 2018: Turbomachinery Technical Conference and Exposition*. American Society of Mechanical Engineers.

[22] Racheet Matai and Savas Yavuzkurt. "Evaluation of Effects of Different Design Parameters on Axial Fan Performance Using CFD". In: *ASME Turbo Expo 2015: Turbine Technical Conference and Exposition*. American Society of Mechanical Engineers. 2015, V001T09A012–V001T09A012.

[23] Alain Godichon. *FAN DESIGN: Past, Present and Future*. Keynote at FAN 2015 Conference. 2015.

[24] Hussain Nouri et al. "Experimental investigation on ducted counter-rotating axial flow fans". In: *Proceedings of Fan Conference, Lyon France* (2015).

[25] M Heinrich, C Friebe, and R Schwarze. "Experimental and numerical investigation of a gearless one-motor contra-rotating fan". In: *FAN 2015 - International Conference*.

[26] E Barton Bell and Lucas J DeKoster. *Test of a Dual-Rotation Axial Flow Fan*. Tech. rep. NATIONAL ADVISORY COMMITTEE FOR AERONAUTICS LANGLEY FIELD VA LANGLEY AERONAUTICAL LABORATORY, 1942.

[27] Stefano Castegnaro, Massimo Masi, and Andrea Lazzaretto. "Preliminary experimental assessment of the performance of rotor-only axial fans designed with different vortex criteria". In: *Proceedings of the XII European Turbomachinery Conference ETC12, Stockholm, Sweden*. 2017.

[28] Sarel Jacobus Venter and DG Kroger. "The effectiveness of axial flow fans in A-frame plenums". PhD thesis. Stellenbosch: University of Stellenbosch, 1990.

[29] Konrad Bamberger and Thomas Carolus. "Optimization of axial fans with highly swept blades with respect to losses and noise reduction". In: *Noise Control Engineering Journal* 60.6 (2012), pp. 716–725.

[30] MG Beiler and TH Carolus. "Computation and measurement of the flow in axial flow fans with skewed blades". In: *Transactions-american society of mechanical engineers journal of turbomachinery* 121 (1999), pp. 59–66.

[31] RJ Downie, MC Thompson, and RA Wallis. "An engineering approach to blade designs for low to medium pressure rise rotor-only axial fans". In: *Experimental thermal and fluid science* 6.4 (1993), pp. 376–401.

[32] Alessandro Corsini et al. "Experimental investigation on double anti-stall ring effects on reversible ventilation fan performance". In: *ASME Turbo Expo 2016: Turbomachinery Technical Conference and Exposition*. American Society of Mechanical Engineers. 2016, V001T09A012–V001T09A012.

[33] A Kahane. "Investigation of axial-flow fan and compressor rotors designed for three-dimensional flow". In: *NACA TN* 1652 (1947).

[34] A Guedel, M Robitu, and V Chaulet. "CFD Simulations to Predict the Energy Efficiency of Fan Axial Fan for Various Casing Configurations". In: *Proceedings of FAN* (2012), pp. 18–20.

[35] Matjaž Eberlinc et al. "Modification of axial fan flow by trailing edge self-induced blowing". In: *Journal of Fluids Engineering* 131.11 (2009), p. 111104.

[36] Thore Bastian Lindemann, Jens Friedrichs, and Udo Stark. "Development of a new design method for high efficiency swept low pressure axial fans with small hub/tip ratio". In: *ASME Turbo Expo 2014: Turbine Technical Conference and Exposition*. American Society of Mechanical Engineers. 2014, V01AT10A017–V01AT10A017.

[37] Maria Teodora Pascu. "Modern Layout and Design Strategy for Axial Fans". PhD thesis. Ph. D. Thesis at Erlangen University, 2009.

C ESTIMATION OF PERFORMANCE AND EFFICIENCY. ROTOR-ONLY FANS

An explicit form of the formulations

$$\Psi_{f_{tc=0}} = f(\Phi, \Psi_{tt_{th}})_{tc=0} \qquad \eta_{f_{tc=0}} = f(\Phi, \Psi_{tt_{th}})_{tc=0} \tag{76}$$

is here developed. It is remarked that the following equations are obtained without tip clearance *global* losses (which are considered empirically in a second instance with indications of Par. 5.5.1). For sake of graphical clearness, subscripts $tc = 0$ are omitted. All the equations that follows can be easily implemented in a *MATLAB*®code (or similar) to provide a rapid estimation of the rotor-only fan performance and efficiency.

The *useful* mechanical pressure delivered to the air by a rotor-only fan is

$$p_f = \textit{what the rotor is able to provide} - \textit{swirl related losses} - \textit{annulus-to-duct axial-velocity related losses} \tag{77}$$

This formulation can be translated into the following Equation:

$$p_f = \overline{\eta_{tt}} \cdot \overline{\Delta p_{th}} - \frac{1}{2}\rho\overline{c_{u2}}^2 \cdot (1 - \eta_{n,c_u}) - \frac{1}{2}\rho(c_a^2 - v_m^2) \cdot (1 - \eta_{nTc}) \tag{78}$$

under the assumption $tc = 0$ (tip clearance detrimental effects are accounted in a second instance) and where the over-lined terms represent integral values on the mass-flow rate. In particular:

η_{tt} is the rotor total-to-total efficiency;

$\Delta p_{th} = \rho(u_2 \cdot c_{u2})$ is the inviscid total pressure rise. Note that $\Delta p_{th} = \epsilon \cdot \Delta p_{th\infty}$, being the last one the inviscid total pressure rise for an infinite number of blades [1, p. 30];

$\frac{1}{2}\rho\overline{c_{u2}}^2$ represents the swirl pressure losses that cannot be directly converted into static pressure due to the absence of the straightener;

η_{n,c_u} is the efficiency of slight natural diffusion of the swirl velocity that occurs even if guide vanes are not installed. According to Marcinoswky; [2, p. 19] $0.15 \leqslant \eta_{n,c_u} \leqslant 0.25$

$c_a = \frac{q_v}{\pi R^2(1-\nu^2)}$ is the mean annulus velocity;

$v_m = \frac{q_v}{\pi R^2}$ is the mean duct velocity at the fan exit;

$\eta_{n,Tc}$ is the efficiency of the natural diffusion of the axial velocity from the mean annulus value to the duct one, as reported in Par. 5.3.2.

Equation 78 can be expressed in the dimensionless form dividing each term for $\frac{1}{2}\rho(\omega R)^2$. In particular the following convenient form is obtained:

$$\Psi_f = \overline{\eta_{tt}} \cdot \Psi_{tt_{th}} - (1 - \eta_{n,c_u}) \cdot \Psi^2_{tt_{th}} \cdot f_1(\nu) - (1 - \eta_{nTc}) \cdot \Phi^2 \cdot f_2(\nu) \tag{79}$$

where each term is derived explicitly in the Par. C.1 for the free-vortex case. Equation 79 is the explicit form of the first of Eq.s 76. In fact:

- functions $f_1(\nu)$ and $f_2(\nu)$ depend on the ν ratio that, in turn, depends on the flow and pressure coefficient (see Par. 5.1 for the *FV* case): $\nu = f(\Phi, \Psi_{tt_{th}})$;
- η_{nTc} also depends on the hub-to-tip ratio (see Eq. 49);
- η_{n,c_u} can be conveniently assumed equal to 0.2;
- $\overline{\eta_{tt}}$ is estimated at the blade mean-span (see Par. C.1.1), resulting dependent on Φ, $\Psi_{tt_{th}}$ and on the airfoil mean characteristics. Nonetheless, whether the indications on the airfoil selection reported in Par. 5 are followed, $\overline{\eta_{tt}} \simeq 0.9$ are typically achieved.

Dividing Eq. 79 by $\Psi_{tt_{th}}$ the second explicit equation is obtained:

$$\eta_f = \overline{\eta_{tt}} - (1 - \eta_{n,c_u}) \cdot \Psi_{tt_{th}} \cdot f_1(\nu) - (1 - \eta_{nTc}) \cdot \frac{\Phi^2}{\Psi_{tt_{th}}} \cdot f_2(\nu) \tag{80}$$

The detrimental terms $\Delta\Psi_f$ and $\Delta\eta_f$ must be then be subtracted to the terms obtained with Eq.s 79 and 80. Such decrements can be preliminary estimated using the indications reported in Par. 5.5.1.

A similar expression of Form. 77 and the consequent development can be obtained for the fan static pressure p_{sf} including the exhaust losses [3, p. 408].

C.1 DIMENSIONLESS FORMULATION. FREE-VORTEX FLOW

For a free-vortex flow, we can write for the swirl velocity at the generic radius r:

$$c_u = \frac{K}{r} = \frac{c_{u_h} \cdot r_h}{r} = \frac{c_{u_h} \cdot (\nu R)}{r} \tag{81}$$

where c_{u_h} is the velocity in proximity of the rotor hub. This velocity can be expressed in function of the inviscid pressure rise:

$$\Delta p_{th} = \rho(u_2 c_u) = \rho(\omega \nu R \cdot c_{u_h}) \tag{82}$$

due to the constancy of the total pressure along the radius. Introducing now the dimensionless coefficient $\Psi_{tt_{th}} = \frac{\Delta p_{th}}{\frac{1}{2}\rho(\omega R)^2}$ we obtain the convenient expression:

$$c_{u_h} = \Psi_{tt_{th}} \cdot \frac{1}{2} \frac{\omega R}{\nu} \tag{83}$$

C.1.1 Rotor efficiency

A *mean-line* estimation of the rotor efficiency $\overline{\eta_{tt}}$ develops as follows:

$$\overline{\eta_{tt}} = 1 - \frac{\overline{p_{loss}}}{\Delta p_{th}} \tag{84}$$

where $\overline{p_{loss}} = \overline{k_r} \cdot \frac{1}{2}\rho c_a^2$, with k_r a loss coefficient defined according to [3, p. 191]:

$$k_r = \frac{C_D \cdot \sigma}{(\cos\beta_m)^3} \tag{85}$$

Assuming now $\overline{k_r} \simeq k_{r_{MS}}$ we write

$$k_r = \frac{\overline{C_D} \cdot \sigma_{MS}}{(\cos\beta_{m_{MS}})^3} \tag{86}$$

In particular:

$$\sigma_{MS} \simeq \sigma_h \cdot \frac{2\nu}{1+\nu} \tag{87}$$

The drag coefficient is estimated according to [4, p. 150]

$$\overline{C_D} = \frac{C_L}{E} + 0.018 \cdot C_L^2 + 0.02\frac{\pi}{n r_{bl}}\frac{1+\nu}{1-\nu} + 0.029 \cdot tc^* \cdot C_L^{1.5} \tag{88}$$

where E is the two-dimensional airfoil efficiency $E = \frac{C_l}{C_d}$ and tc^* is the dimension-less tip clearance defined in Par. 5.5.1.[1]
The β_m angle is computed at the mid-span as follows:

$$\begin{aligned} tan\beta_{m_{MS}} &= \frac{\omega r_{MS} - \frac{c_{u_{MS}}}{2}}{c_a} \\ &= \frac{\omega R\frac{1+\nu}{2} - \frac{1}{2}\frac{2\cdot c_{u_h}\nu R}{1+\nu}}{c_a} \\ &= \frac{\omega R\frac{1+\nu}{2} - \frac{1}{2}\Psi_{tt_{th}}\frac{\omega R}{\nu}\frac{\nu}{1+\nu}}{c_a} \\ &= \frac{1}{2}\left(\frac{\omega R}{c_a}\right)(1+\nu-\frac{\Psi_{tt_{th}}}{1+\nu}) \end{aligned} \tag{89}$$

Recalling now that $\Lambda = \frac{c_a}{\omega R} = \frac{\Phi}{1-\nu^2}$ we obtain the convenient form

$$\begin{aligned} tan\beta_{m_{MS}} &= \frac{1}{2}\left(\frac{1-\nu^2}{\Phi}\right)(1+\nu-\frac{\Psi_{tt_{th}}}{1+\nu}) \\ &= \frac{1}{2}\frac{1-\nu}{\Phi}(\nu^2+2\nu+1-\Psi_{tt_{th}}) \end{aligned} \tag{90}$$

Finally Eq. 84 can be written as

$$\overline{\eta_{tt}} \simeq 1 - \frac{\sigma_{MS}}{(\cos\beta_{m_{MS}})^3}\overline{C_D} \cdot \frac{\frac{1}{2}\rho c_a^2}{\rho\omega\nu R c_{u_h}} \tag{91}$$

1 This *tip-clearance* drag term shall be included in this $tc = 0$ computation.

that substituting c_{u_h} with Eq. 83 finally gives:

$$\begin{aligned}\overline{\eta_{tt}} &\simeq 1 - \frac{\sigma_{MS}}{(\cos\beta_{m_{MS}})^3}\overline{C_D}\cdot\left(\frac{c_a}{\omega R}\right)^2\frac{1}{\Psi_{tt_{th}}} \\ &= 1 - \frac{\sigma_{MS}}{(\cos\beta_{m_{MS}})^3}\overline{C_D}\cdot\left(\frac{\Phi^2}{\Psi_{tt_{th}}}\right)\frac{1}{(1-\nu^2)^2}\end{aligned} \tag{92}$$

Typically used values are $C_L = 0.9$, $E = 50$, $\sigma_h = 1.2$.

C.1.2 Swirl Pressure term

$$\begin{aligned}\frac{1}{2}\rho\overline{c_u}^2 &= \frac{1}{q_\nu}\int_{r_h}^{R} 2\pi c_a\cdot r\cdot\frac{1}{2}\rho c_u^2\,dr \\ &= \frac{\pi c_a}{q_\nu}\rho\int_{r_h}^{R} r\cdot\frac{(c_{u_h}\nu R)^2}{r^2} \\ &= \frac{\pi c_a}{q_\nu}\rho(c_{u_h}\nu R)^2\ln\left(\frac{R}{r_h}\right) \\ &= \frac{\pi}{q_\nu}\frac{q_\nu}{\pi R^2(1-\nu^2)}\rho(c_{u_h}\nu R)^2\ln\left(\frac{1}{\nu}\right) \\ &= \rho c_{u_h}^2\cdot\frac{\nu^2}{1-\nu^2}\ln\left(\frac{1}{\nu}\right)\end{aligned} \tag{93}$$

using then Eq. 83

$$\begin{aligned}&= \rho\left(\Psi_{tt_{th}}\cdot\frac{1}{2}\frac{\omega R}{\nu}\right)^2\cdot\frac{\nu^2}{1-\nu^2}\ln\left(\frac{1}{\nu}\right) \\ &= \frac{1}{2}\rho\Psi_{tt_{th}}^2(\omega R)^2\left[\frac{1}{2(1-\nu^2)}\ln\left(\frac{1}{\nu}\right)\right] \\ &= \frac{1}{2}\rho\Psi_{tt_{th}}^2(\omega R)^2\cdot f_1(\nu)\end{aligned} \tag{94}$$

where

$$f_1(\nu) = \frac{1}{2(1-\nu^2)}\ln\left(\frac{1}{\nu}\right) \tag{95}$$

C.1.3 Annulus-to-Duct axial Velocity term

$$\begin{aligned}\frac{1}{2}\rho(c_a^2 - \nu_m^2) &= \frac{1}{2}\rho\nu_m^2\left[\left(\frac{\frac{q_\nu}{\pi R^2(1-\nu^2)}}{\frac{q_\nu}{\pi R^2}}\right)^2 - 1\right] \\ &= \frac{1}{2}\rho\nu_m^2\left[\frac{1}{(1-\nu^2)^2} - 1\right] \\ &= \frac{1}{2}\rho\nu_m^2\left[\frac{\nu^2(2-\nu^2)}{(1-\nu^2)^2}\right] \\ &= \frac{1}{2}\rho\nu_m^2\cdot f_2(\nu)\end{aligned} \tag{96}$$

where

$$f_2(\nu) = \frac{\nu^2(2-\nu^2)}{(1-\nu^2)^2} \tag{97}$$

C.2 CONSTANT-SWIRL FORMULATION

The estimation model for the Constant-swirl distribution is developed in [5] and follows a similar procedure. The reader is referred to [5] for the complete description; only the peculiarities that distinguish the model from the *FV* one are here reported.

The main differences between the model are related to the distribution c_{a2} at the rotor exit, that in the *CS* case depends on the magnitude of the swirl component c_u. Consequently:

- An explicit formulation $\nu = f(\Phi, \Psi_{tt_{th}})$ is not directly available for the *CS* case. Consequently, the efficiency estimation is performed for several hub-to-tip ratios and the ν values that allows for the highest estimated efficiency has to be selected.
- The estimation is not performed at the mid-span but rather at the radius that ideally gives the required rotor-work assuming that the entire flow-rate q_v crosses the blade at this radial coordinate. This radial coordinate is easily computed as function of the ν ratio.
- The $\eta_{nTc} = f(\nu)$ relation is slightly different with respect to the one suggested for the *FV* case and, in particular, provides lower η_{nTc} magnitudes.

BIBLIOGRAPHY

[1] Bruno Eck. "Fans". In: *1st English ed., Pergamon Press, Oxford* (1973), pp. 139–153.

[2] Konrad Bamberger. "Aerodyamic Optimization of Low-Pressure Axial Fans". PhD Thesis. Siegen, Ger: University of Siegen, 2015.

[3] R Allan Wallis. *Axial flow fans and ducts*. Krieger, 1993.

[4] William C Osborne. *Fans*. Vol. 1. Pergamon Press Oxford, 1966.

[5] Massimo Masi, Stefano Castegnaro, and Andrea Lazzaretto. "A Criterion for the Preliminary Design of High-Efficiency Tube-Axial Fans". In: *ASME Turbo Expo 2016: Turbomachinery Technical Conference and Exposition*. American Society of Mechanical Engineers. 2016, V001T09A006–V001T09A006.

PUBLICATIONS BY THE AUTHOR

1. S Castegnaro, M Masi, and A Lazzaretto. "Design and Testing of an ISO 5801 Inlet Chamber Test Rig and Related Issues with the Standard". In: Under Evaluation for Proceedings of FAN 2018 Conference. Germany. 2018.

2. M Masi, A Lazzaretto, and S Castegnaro. "Effectiveness of blade forward sweep in a small industrial tube-axial fan". In: Under Evaluation for Proceedings of FAN 2018 Conference. Germany. 2018.

3. Masi Massimo, Castegnaro Stefano, and Lazzaretto Andrea. "Experimental Investigation on the effect of Reynolds Number on the efficiency of Single-stage Axial-flow Fans". In Press, ASME Turbo Expo 2018: Turbomachinery Technical Conference and Exposition. American Society of Mechanical Engineers.

4. Stefano Castegnaro, Massimo Masi, and Andrea Lazzaretto. "Preliminary experimental assessment of the performance of rotor-only axial fans designed with different vortex criteria". In: (to be published) Proceedings of the XII European Turbomachinery Conference ETC 12, Stockholm, Sweden. 2017.

5. Stefano Castegnaro. "A Critical Analysis of the Differences Among Design Methods for Low-Speed Axial Fans". In: ASME Turbo Expo 2017: Turbomachinery Technical Conference and Exposition. American Society of Mechanical Engineers. 2017, V001T09A008–V001T09A008.

6. S Castegnaro et al. "A bio-composite racing sailboat: Materials selection, design, manufacturing and sailing". In: Ocean Engineering 133 (2017), pp. 142–150.

7. Massimo Masi, Stefano Castegnaro, and Andrea Lazzaretto. "A Criterion for the Preliminary Design of High-Efficiency Tube-Axial Fans". In: ASME Turbo Expo 2016: Turbomachinery Technical Conference and Exposition. American Society of Mechanical Engineers. 2016, V001T09A006– V001T09A006.

8. Stefano Castegnaro. "Fan Blade Design Methods: Cascade Versus Isolated Airfoil Approach—Experimental and Numerical Comparison". In: ASME Turbo Expo 2016: Turbomachinery Technical Conference and Exposition. American Society of Mechanical Engineers. 2016, V001T09A007– V001T09A007.

9. Massimo Masi, Stefano Castegnaro, and Andrea Lazzaretto. "Forward sweep to improve the efficiency of rotor-only tube-axial fans with con-

trolled vortex design blades". In: Proceedings of the Institution of Mechanical Engineers, Part A: Journal of Power and Energy 230.5 (2016), pp. 512– 520.

10. S Castegnaro. "Effects of NACA 65-blade's Trailing Edge Modifications on the Performance of a Low-speed Tube-axial Fan". In: Energy Procedia 82 (2015), pp. 965–970.

11. M Masi, S Castegnaro, and A Lazzaretto. "Increase the Efficiency of Rotor-Only Axial Fans with Controlled Vortex Design Blading". In: Proceedings of the Fan 2015 Conference. 2015.

12. Stefano Castegnaro. "Incremento delle prestazioni di pale a vortice arbitrario per ventilatori assiali a sola girante: verifica sperimentale e numerica". In: MS Thesis-University of Padova (2014).

13. S Castegnaro and M Masi. "S. Castegnaro and M. Poli and M. Basile and P. Barucco and C. Gomiero and C. Battisti and U. Pizzarello and A. Lazzaretto". Galileo Jour. 214 (http://www.galileomagazine.com/?portfolio_item=galileo-214) (2014).

14. S Castegnaro and M Masi. "Validazione di un modello CFD semplificato per analisi dele prestazioni globali di ventilatori assiali a sola girante". Analisi & Calcolo Jour. (http://aec-analisiecalcolo.it/static/media/articoli/Versione62_b_pag14.pdf), (2014).